High Repetition Rate Laser Shock Peening on Biodegradable Magnesium Alloys

Hossein Kamkarrad

A Thesis

In the Department

Of

Mechanical and Industrial Engineering

Presented in Partial Fulfillment of the Requirements

For the Degree of

Doctor of Philosophy (Mechanical and Industrial Engineering) at

Concordia University

Montreal, Quebec, Canada

January 2016

Concordia University

SCHOOL OF GRADUATE STUDIES

This is to certify that the thesis prepared

By: **Hossein Kamkarrad**

Entitled: **High repetition rate laser shock peening on biodegradable magnesium alloys**

and submitted in partial fulfillment of the requirements for the degree of

Doctor of Philosophy (Mechanical Engineering)

Complies with the regulations of the University and meets the accepted standards with respect to originality and quality.

Signed by the final Examining Committee:

---------- Chair
Chair's name

---------- External Examiner
External Examiner's name

----------Examiner
Dr. Muthukumaran Packirisamy

----------External
Dr. Javad Dargahi

----------External to the Program
Dr. Lucia Trica

----------Supervisor
Dr. Sivakumar Narayanswamy

Approved by ----------
Dr. Ali Dolatabadi, Graduate Program Director

---------- ----------
2016 Dr. Asif Amir, Dean
Faculty of Engineering and Computer Science

ABSTRACT

High repetition rate laser shock peening on biodegradable magnesium alloys
Hossein Kamkarrad, Ph.D.
Concordia University, 2016

Recently, Magnesium based alloys have been identified as a potential bio-degradable material for implants. While the biggest advantage of magnesium based implants is that it eliminates the need for additional surgery for removal, magnesium corrodes within human body much faster than the cure of broken bones. Hence, reduction of corrosion rate in magnesium surface is important to successful implementation. Laser Shock Peening (LSP) as mechanical treatment has been used successfully on implant surfaces to reduce the corrosion rate. Having reviewed the literature in LSP, it can be seen that the lasers used are low repetition rate high power lasers. Owing to cost of low repetition lasers, high repetition laser shock peening (HRLSP) is introduced in this work.

The general objective of this thesis dissertation is to develop HRLSP for low mechanical strength metals/alloys like Magnesium. To this end, a feasibility study of HRLSP was performed and pertinent laser parameters for successful peening of magnesium were evaluated. The finite element analysis using Abaqus Dynamic/Static was performed in both single shot mode as well as in multi shot mode. The simulation was used to predict the surface deformation on the peened area, magnitude of Compressive Residual Stress (CRS), and the propagation of CRS along the depth from the surface. The effect of laser parameters and scanning parameters on these values have been analyzed by Finite Element Analysis (FEA).

Based on the results from the feasibility study, an experimental setup involving both optical as well as scanning arrangement was performed and design of experiment was done for peening. From the experiments, with two laser intensities at 0.91GW/cm^2 and 2GW/cm^2, peening was possible only at 2GW/cm^2. The magnitude of peening was varied by changing the %overlap between subsequent spots, and the total number scans. Increasing the number of peened shots within the specimen surface area of 10 X 10 mm, increases the magnitude of CRS that was shown by Finite Element Analysis. Comparison of peened samples to unpeened samples showed

significant improvements in the mechanical attributes, comparable to that seen in the literature. The hardness increased from 45 HV to 103 HV; Surface roughness (R_a) increased from 0.35 μm to 3.3 μm; surface wettability measured as function of contact angle reduced from 68.5° to 44.4°; and wear resistance improved from $5.5E^{-4}$ gr/s to $1.8E^{-4}$ gr/s. The results mentioned above clearly indicate the relationship between improvements in mechanical attributes to the magnitude of peening.

ACKNOWLEDGEMENTS

I am appreciative of Dr. Sivakumar Narayanswamy for supporting me during these past years in my research works. I will forever be thankful for his generous assistance.

I also acknowledge Dr. Muthukumaran Parckinasamy, Dr. Javad Dragahi, and Dr. Lucia Trica for their supportive advice since my first defense at comprehensive exam.

Dr. Mamoun Medraj is another Professors who I appreciate for his hearty support during the work I had in TMG lab.

Also, I cannot forget the assistance of Dr. Mohammad Keshmiri in establishing some sets of experiments.

I trust that a respectable support system is significant to nurture a researcher during his or her period of study, and I was lucky to be a part of such great research teams at Concordia University.

Hossein Kamkarrad

Dedication

Proudly, I dedicate this thesis to

My parents, who are my first teachers

And

My wife and daughter because of their longanimity during my education.

Contributions of Author

In this thesis a novel method of laser shock peening is introduced by high repetition pulsed laser peening (HRLSP). This technique can improve a number of mechanical attributes such as hardness, wettability, wear and corrosion of magnesium alloys similar to common laser shock peening. The outstanding advantage of HRLSP is lower capital of it in laser peening process.

Enhancement of mentioned characteristics can improve abilities of using magnesium as biocompatible/degradable orthopedic implant which is used within human body.

Implementation of metallic biodegradable implants eliminate additional surgery to implant removal which is needed after curing broken bones. Moreover, HRLSP can play a role of advanced technique to enhancement performance of mechanical parts.

A number of participated applications of HRLSP have been stated in two categories of bio and industrial applications:

Industrial points of view:

- Increasing resistance of blades and vanes in turbojet
- Application of HRLSP in production desalination pump impeller for reduction of corrosion.
- Releasing unwanted residual stress which is created in micro welding, casting or machining
- Detection of specimens defect by assessing of mechanical shock wave within composite materials.

Biomedical points of view:

- HRLSP of biodegradable shapes memory alloys like Fe30Mn6Si and its application for production of no need balloon biodegradable cardiovascular stents
- Design of intelligent alloy with predefined changeable corrosion rate
- Maximum corrosion rate control by applying ultra-short pulse duration laser
- Combination of HRLSP and Biodegradable polymeric coating of Magnesium based implants
- Cavity of teeth by laser shock peening instead of drilling which can be painful and long process
- Increasing durability of permanent teeth metallic coating
- HRLSP of biodegradable screws with application of bone-plate fixator

Table of Contents

List of Figures xi
List of Tables xiv
List of Symbols xv
List of Abbreviations xvii
CHAPTER 1. Introduction and Literature Review 1
1.1 Introduction 1
1.2 Background 2
1.3 Biodegradable Mg-Ca Alloys 2
1.3.1 Magnesium alloy application and mechanical, chemical and physical behaviors 2
1.4 Surface Treatment and its importance 4
1.4.1 Spray coating 4
1.4.2 Laser cladding 4
1.4.3 Shot peening 5
1.4.4 Burnishing 5
1.4.5 Polymer coating 5
1.5 Laser Shock Peening 6
1.5.1 Effect of Confining Medium on Plasma Pressure 9
1.5.2 Effect of Pulse Duration on Plasma Pressure 10
1.5.3 Variations in Scanning Methodology 10
1.5.4 Experimental verification of shock load: 12
1.6 Theories of Laser Shock Peening 13
1.7 Effects of Laser Shock Peening 14
1.7.1 Surface Topography 14
1.7.2 Residual stress 16
1.7.3 Surface Hardness and Wear Volume 19
1.7.4 Corrosion 21
1.8 Motivation for Current Work 24
1.8.1 Challenges to Overcome 25
1.9 Objectives and Scope 27
1.9.1 Scope of the Proposed Work 27

1.10 Anticipated Impact of HRLSP and its Applications 28
1.11 Thesis organization in the manuscript based thesis format 29
CHAPTER 2. Feasibility Study of HRLSP of Biodegradable Magnesium Alloys 33
2.1 Introduction 33
2.2 Theory of High Repetition Laser Shock Peening (HRLSP) 34
2.3 High Repetition Laser Shock Peening Model 36
2.3.1 Laser specification 36
2.3.2 Peening Specifications 40
2.4 Discussion 42
2.5 Conclusion 43
CHAPTER 3. HRLSP on Magnesium Based Biodegradable Alloys 45
3.1 Introduction 45
3.2 High Repetition Laser Shock Peening (HRLSP) 46
3.2.1 Design of laser scanning system/specifications 47
3.2.2 Peening specifications: 49
3.3 Design of Experiments (DOE) 51
3.4 Results and Discussion 53
3.4.1 Peening depth evaluation 53
3.4.2 Hardness 55
3.4.3 Surface topography and roughness 57
3.5 Conclusions 60
CHAPTER 4. FEA of Residual Stress and Surface Displacement of a Single Shot in HRLSP on Biodegradable Magnesium Implant 61
4.1 Introduction 61
4.2 HRLSP theory and principles of induced CRS 62
4.3 Proposition of the simulation diagram 63
4.3.1 Pressure-Time-distance functions 64
4.3.2 Geometric model and material definition 67
4.3.3 Element Sizes 68
4.3.4 Solver tools 69
4.3.5 Optimization period of ADE 70

4.4 Compressive residual stress (CRS) 71
4.5 Surface displacement 75
4.6 Conclusions 76
CHAPTER 5. FEA of HRLSP on magnesium by multiple and overlapped techniques. 77
5.1 Introduction 77
5.2 Theory of Multiple HRLSP and CRS induction 78
5.3 Solver Tools 79
5.3.1 Shock pressure 80
5.3.2 Overlap calculation 82
5.3.3 Element size 83
5.3.4 Adjustment sequence of pressure pulse 84
5.4 Results 86
5.4.1 Surface topography 86
5.4.2 Verification of FEM by experimental results 88
5.4.3 Compresive residual stress (CRS) 88
5.5 Conclusion 92
CHAPTER 6. Improvement in Attributes of Magnesium Surface by HRLSP 93
6.1 Introduction 93
6.2 High Repetition Laser Shock Peening (HRLSP) 94
6.3 Setup and design of experiments 95
6.4 Results and discussions 97
6.4.1 Hardness 97
6.4.2 Surface topography 98
6.4.3 Wettability 100
6.4.4 Wear 103
6.5 Conclusions 105
CHAPTER 7. Conclusions and Future Work 106
7.1 Conclusions 106
7.2 Future Work 108
References: 110

List of Figures

Figure 1-1 Schematic of shield stress in the bone 3
Figure 1-2 Schematic of confined LSP 6
Figure 1-3 Impact of confining medium on pressure.....9
Figure 1-4 Impact of pulse duration on pressure 10
Figure 1-5 Schematic of LSP Experiment movement of specimen by robot 11
Figure 1-6 LSP Experiment movement of specimen by X-Y table 11
Figure 1-7 LSP Experiment laser scanning by Galvo-scanner.....12
Figure 1-8 Measurement of Shock pressure by Piezoelectric method.....12
Figure 1-9 Schematic of LSP experiment and different overlap peening 15
Figure 1-10 Impact of Overlap and laser power on surface topography.....16
Figure 1-11 Measurement of RS by XRD.....17
Figure 1-12 Demonstration of CRS in different LSP 17
Figure 1-13 Distribution of CRS in different axes.....18
Figure 1-14 Measurement of CRS resulted by different methods 18
Figure 1-15 Peak of shock pressure and CRS in a femtosecond laser peening.....19
Figure 1-16 Impact of laser pulse density on Hardness 20
Figure 1-17 Effect of protective coating on Wear and Hardness 20
Figure 1-18 Schematic of PP corrosion test 21
Figure 1-19 Potentiodynamic Polarization Curve 21
Figure 1-20 Difference in corrosion rate by change in LSP parameters 22
Figure 1-21 Chemical containment on peened and un-peened surfaces 22
Figure 1-22 PP curve for stainless steel 23
Figure 1-23 Distribution of pitting corrosion 24
Figure 1-24 Comparison of energy pulse in low and high repetition rate laser 26
Figure 1-25 Sequence of laser shots in no and overlapped peening 27
Figure 2-1 Schematic of LSP.....34
Figure 2-2 Impact of Repetition rate.....37
Figure 2-3 Impact of spot size on pressure.....38
Figure 2-4 Galvomirror scanning mechanism 39
Figure 2-5 Effect of Protective Coating on shock load.....40

Figure 2-6 Effect of Confining Medium on shock load 41
Figure 3-1 Overlap along the X-axis 47
Figure 3-2 DAQ signals for X and Y axis servo-motors 48
Figure 3-3 Adjustment optical devices for HRLSP 49
Figure 3-4 Impact of confining medium (CM) on shock pressure 50
Figure 3-5 Impact of protective coating (PC) on shock pressure 51
Figure 3-6 Measurement average laser power in different regions 52
Figure 3-7 Fluctuations of peening depth at 60 μm 54
Figure 3-8 Fluctuations of peening depth at 40 μm 54
Figure 3-9 Fluctuations of hardness @ 40 μm 56
Figure 3-10 Fluctuations of hardness @ 60 μm 56
Figure 3-11 HRLSP of magnesium surface @40μm spot size 58
Figure 3-12 HRLSP of magnesium surface @ 60μm spot size 58
Figure 3-13 Fluctuations of roughness @ 40 μm 59
Figure 3-14 Fluctuation of roughness @ 60μm 59
Figure 4-1 Generation of residual stress 62
Figure 4-2 schematic of HRLSP 63
Figure 4-3 The flowchart of FEM 64
Figure 4-4 Fluctuation of shock load pulses 66
Figure 4-5 Relationship of pressure and radial distance 67
Figure 4-6 Design of elements 68
Figure 4-7 Fluctuations internal energy at three pressures 70
Figure 4-8 Fluctuations kinetic energy at three pressures 71
Figure 4-9 FEM Distribution of Von misses along the depth 72
Figure 4-10 Stresses along the surface and Depth 74
Figure 4-11 Plastic/elastic deformation by ADE 75
Figure 4-12 Spring back after ASI 75
Figure 4-13 Measured depth profile of a laser shot 76
Figure 5-1 Flowchart of simulation 79
Figure 5-2 A pulse of shock pressure for a single laser shot 81
Figure 5-3 Radial propagation of shock pressure 81

Figure 5-4 The schematic of HRLSP and Overlap in x-axis during laser shock peening.....82
Figure 5-5 Schematic of meshing technique 83
Figure 5-6 Real time sequential pressure pulses.....84
Figure 5-7 Internal energy at single laser shot.....85
Figure 5-8 Modified pressure/time inputted in model 85
Figure 5-9 Depth of peening at 0%overlap 86
Figure 5-10 Depth of peening at 33%overlap 86
Figure 5-11 Depth of peening at 66%overlap 87
Figure 5-12 SEM of specimen surface at 66%overlap and 3 scans laser peening 87
Figure 5-13 Comparison FEM and experimental results of peening depth 88
Figure 5-14 Residual stress at 0%overlap 89
Figure 5-15 Residual stress at 33%overlap 89
Figure 5-16 Impact of number of scans and %overlap on S_{33} magnitudes and depth 90
Figure 5-17 Residual stress at 66%overlap 90
Figure 5-18 Relation of S33 on the surface and hardness.....91
Figure 6-1 Schematic of HRLSP 95
Figure 6-2 SEM of peened surface a) at 40 μm and b) at 60 μm 97
Figure 6-3 Influence of overlap % on fluctuations of roughness depth (D) at 60 and 40 μm.....98
Figure 6-4 Impact of percentage of overlap on hardness at 60 and 40μm 99
Figure 6-5 Impact of percentage of overlap and number of scans on contact angle at 60 μm....101
Figure 6-6 Impact of percentage of overlap and number of scans on contact angle 101
Figure 6-7 Impact of more peening (increasing in hardness) on contact angle.....102
Figure 6-8 Impact of hardness on wear rate 103
Figure 6-9 Wear rate of specimen 4 and 7 in 25(S) attrition.....104

List of Tables

Table 1-1 Comparison of mechanical properties of several types of implant materials 3
Table 1-2 Laser Shock Peening - Review of Literature 8
Table 1-3 Comparison of different confining medium for LSP: 9
Table 1-4 Comparison of LSP and HRLSP in some performances 28
Table 2-1 Comparison of different confining medium for LSP 42
Table 2-2 comparison of HRLSP and LSP 43
Table 3-1 Laser specifications for 40 and 60 μm spot sizes 49
Table 3-2 List of experiments 53
Table 4-1 Laser specifications 64
Table 4-2 Specimen specification 65
Table 5-1 Laser and Specimen Specifications 79
Table 6-1 Laser Specifications 96
Table 6-2 Peening Specifications 96
Table 6-3 List of experiments and measured hardness 96

List of Symbols

P = shock pressure

Z = Impedance of shock wave

I = Laser intensity

J =Average energy of laser pulse

t = Duration of shock pressure

A = cross sectional area of a laser shot

α = constant of laser absorption

HEL = Hugonoit Elastic Limit

υ = Poisson‘s ratio

Ss = Scan speed

We = Equivalent weight

Ra = surface roughness

Rc = mean amplitude of roughness

dn = spacing between layers before peening

dΨ = spacing between layers after peening

Ψ = Diffraction angle

D_p = Pulse density

D_l = diameter of laser beam

F = force

ω = Pyramid top angle

ds = side of square

ρ = density

P_w = Laser power

τ = Laser pulse duration

f = Repetition rate

U_s = shock velocity within material

σ_y^{Dyn} = Dynamic yield stress

σ_u^{Dyn} = Ultimate dynamic stress

Ct = transparency coefficient of confining medium

σ_{surf} = residual stress upon the surface

σ_0 = Initial residual stress upon the surface before the laser shock peening

λ, μ = lame constant

ε_p = Strain

Lp = Plastic deformation depth

r_0 = Spot radius

PVDF = Polyvinylidene fluoride

φ = Contact angle

H_{vap} = Enthalpy of vaporization at target

E_{vap} = energy of vaporization of the target

λ_w = Wavelength

D = depth of peening

C_{el} = Speed of elastic wave in the material

C_{pl} = Speed of plastic wave in the material

TD = Transient duration

ns = nanosecond

List of Abbreviations

LSP = Laser Shock Peening

HRLSP = High Repetition Rate Laser Shock Peening

CASS = Copper-Accelerated Acetic–Salted Spray

CM = Confining medium

CRS = Compressive residual stress

EDS = Energy Dispersive Spectroscopy

HRLSP = High repetition rate laser shock peening

PC = Protective coating

PGA = Poly glycolide acid

PLA = Poly lactide acid

PP = Potentiodynamic Polarization

RS = Residual stress

XRD = X-Ray diffraction

SEM = Scanning electron microscopy

EDS = Energy Dispersive Spectroscopy

PP = Potentiodynamic polarization

CASS = Copper-Accelerated Acetic–Salted Spray

LSM =Laser surface melting

CA = Contact angle

DOE = Design of Experiment

FEM = finite element modeling

TRS = tensional residual stress

ADE = Abaqus dynamic explicit

ASI = Abaqus Static Implicit

NS = Number of scans

GS = Galvo Scanner

CHAPTER 1. Introduction and Literature Review

1.1 Introduction

Metallic bio-implants like stainless steel & Titanium alloys have had vast applications in orthopedic surgeries. Although use of conventional implants has contributed to the cure of many patients, they have a number of side effects such as reduction of mechanical attributes in the bones and cause inflammation. Moreover, these implants are not bio-degradable, hence requiring additional surgery to remove them. Recently, a number of Magnesium based alloys have been identified as a potential bio-degradable material for implants. On the one hand, these biodegradable implants have similar mechanical strength to that of bones, thereby reducing bone asthenia and helps hold the clamp implant screw. On the other, due to excellent material property, the biocompatibility of these implants increases in comparison with conventional implants. The significant advantage is that since the material is biodegradable, it eliminates the need for additional surgery for removal, thereby reducing pain and risk to the person, and saves cost of additional surgery.

Though biodegradable magnesium alloys (Mg-Ca, Mg-Ca-Zn) offer a superior advantage over conventional alloys (Ti or SS) for bio-implants, the disadvantage of these medical alloys is that they corrode within human body much faster than the conventional implants. Accordingly, these implants may degrade before the broken bones, on which this implants are attached to, have cured completely. This causes the bone to fail again before treatment. Hence, research is being currently concentrated on reduction of surface corrosion rate of these biodegradable implants; mainly on three major directions:

I) Mechanical treatments by shot peening, burnishing and laser shock peening II) Alloying specific amounts of Calcium and Zinc to magnesium. III) Coating by Thermal spray methods or laser cladding of different elements on Mg-Ca Implant.

1.2 Background

Considering the state of the art in this important area, and the problems mentioned earlier, one the goals of this thesis is to indicate the significance of applying biodegradable metallic implants. In this regards, an advanced method for reducing corrosion rate of biodegradable magnesium alloys to an acceptable level is required, so that physicians use these implants with greater confidence that the degradation will happen after the bone has cured and not earlier. A number of researches illustrate Laser Shock Peening (LSP) as a mechanical treatment that has been successfully applied on many areas like airplane spare parts, gas turbine[1] and heavy duty pumps. Since, LSP of biodegradable metallic magnesium implant is the area of this research work, in this chapter, the significance of biodegradable magnesium along with its advantages and challenges is covered. Subsequently, the effect of LSP on various mechanical attributes of various metals including magnesium are surveyed from the literature in the second part of this chapter.

1.3 Biodegradable Mg-Ca Alloys

Magnesium alloys have been introduced as novel metallic alloys in recent years. In the review, particular attention has been paid to mechanical aspects of medical magnesium alloys. Magnesium by itself does not have adequate strength; it must be alloyed with some other metals for improving both strength and elongation.

1.3.1 Magnesium alloy application and mechanical, chemical and physical behaviors

Applying implants that have very high Young's modulus compared to that of bones, leads to 'stress shielding'[2] [3] which means the stresses flow pass through the implant and most proportion of stress will be applied on implant instead of bon Young's modulus of bones is 10-30 GPa and this factor is 100-200 GPa for conventional implant materials. The figure 1-1 shows schematic of shield stress in the bone [3]. Table 1-1 shows general mechanical properties of the magnesium, natural bone and some conventional orthopedic alloys [4]. According to ''Wolff's Law''[5], due to elimination or reduction of applied stresses to the bones, bones' density will decline and this leads to decrease in its mechanical strength.

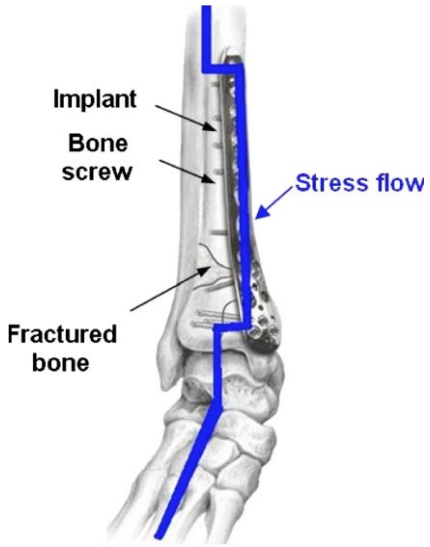

Figure 1-1 Schematic of shield stress in the bone

Properties	**Bone**	**Magnesium**	**Ti alloy**	**Co–Cr alloy**	**S Steel**	**DL/PLA**
Density (g/cm^3)	1.8–2.1	1.74–2.0	4.4–4.5	8.3–9.2	7.9–8.1	1.1
Elastic modulus (GPa)	3–20	41–45	110–117	230	189–205	1.9-2.4
Compressive strength (MPa)	130–180	65–100	758–1117	450–1000	170–310	N/A
Fracture toughness ($MPa.m^{1/2}$)	3–6	15–40	55–115	N/A	50–200	N/A

Table 1-1 Comparison of mechanical properties of several types of implant materials

In this regard, many researchers have been looking for finding appropriate remedies. Even though polymeric implants such as PLA (poly lactic acid) and PGA (poly glycolide acid) have been identified as a second generation bio implants, owing to weak mechanical strength (Table1-1); the polymeric implants are not suitable for orthopedic implantation [6]. Hence, the primary considerations are Young's modulus and degradability or corrosion for implant materials, such as magnesium and its alloys. In order to better degradability, selected alloys must have extreme amount of corrosion within human body without being toxic. Alloying Zinc with Magnesium in particular circumstances is a successful method to enhance mechanical attributes. Particularly, Zn is nontoxic and it can be easily absorbed by the cells in the body [7]. But zinc alloying increases the rate of oxidation; thereby the rate of corrosion [8], therefore Calcium is an appropriate alloying element both from the non-degradability and from the mechanical attributes points of view.

Although calcium alloying increases tensile strength, it will cause reduction in elongation and brittleness of the magnesium alloy will be enhanced. When the calcium content is about 1 weight percentage, optimum mechanical properties can be achieved [8]. In order to control degradability, cold working on surface because of increasing of residual stress [9] on surface could be an effective method. Surprisingly, high level of load for cold working has severe plastic deformation and it cannot be suitable way to conduct permanent residual stresses. In order to obtain permanent residual stress, it should be applied in optimum amount of cold working [10].

1.4 Surface Treatment and its importance

Compatibility [11], desired mechanical behavior and degradability of medical magnesium alloys are factors those highlight merits of magnesium implant compared with conventional ones. However, the challenge is to reduce the corrosion rate by surface treatments that have been primarily based on either alloying or by surface enhancement methods. Spray coating [12], laser cladding [13], shot peening [14], burnishing [15], polymer coating [16] and laser shock peening (LSP) are a number of identified methods for surface enhancement which affect corrosion attributes. Overall, surface treatment, in terms of geometric face and mechanical properties, plays undeniable role on parts performance.

1.4.1 Spray coating

Magnesium alloys, because of low density and acceptable mechanical strength has advantage of using in aerospace industries. However, its high rate of corrosion is the most restriction for the acceptance of magnesium as an alternative [12]. Spray coating can create a protective layer to enhance some poor surface attributes such as resistance to corrosion and reduction of wear [17].

1.4.2 Laser cladding

Laser cladding is one of the advanced coating method that is used for improvement of surface properties. The principle of this technique is based on creation of a protective coating [13]. The protective layer is bonded to surface specimen as in spray coating. The great control on laser parameter leads to have a predicted properties on new created surface [18].

1.4.3 Shot peening

Unlike the coating processes, shot peening is a mechanical surface treatment and no materials would be bonded to specimen. In shot peening the impact of accelerated tiny metallic balls to specimen can create micro surface cold-working. By the mentioned surface displacement, the surface attributes such as hardness , resistance to wear and corrosion can be improved [14][19].

1.4.4 Burnishing

Burnishing is another mechanical surface treatment. In this method strain hardening by cold working on the surface causes increase in surface hardness. In addition, by creation smoother surface and increasing of compressive residual stress beneath the surface, a barrier can be created against the expansion of micro cracks which is can be protected the surface against the early fatigue and corrosion [15][20].

1.4.5 Polymer coating

Polymer coating is one of the methods for improving specimen surface in corrosive conditions [16]. In addition, some polymeric protection such as PLA or Teflon can enhance biocompatibility of metals with poor biocompatibility [21]. However, weak bonding of polymer-metals is a restriction of polymeric coating.

Although each of the methods mentioned above offers surface improvement, the laser shock peening has more substantial advantages. LSP does not require to bonded secondary material as coating. Detachment of coating from the base is the most significant disadvantage of coating usage. Furthermore, excellent adjustable specifications of laser can create controlled attributes on the specimen surface [22].

By the discussions, Magnesium alloys offer excellent biodegradability owing to their degradability within human body. However, their application as an implant without surface treatments is impossible owing high rate of corrosion. In this work, laser shock peening has been proposed as an excellent surface treatment option for biodegradable Magnesium implants.

1.5 Laser Shock Peening

The table 1-2 indicates a number of previous research work in Laser Shock Peening (LSP). The ability of LSP to creation of compressive residual stress and mechanical attributes have been confirmed by mentioned observations. In LSP, a high energy pulse of laser irradiates the sample surface. Upon absorption of laser energy that exceeds the material threshold, ablation will be effected. At that moment, a phase transformation occurs and material is transformed from solid state to vapor. The metallic vapor absorbs adequate energy for converting gas atoms to ions and plasma is resulted [23]. Plasma is able to generate a high-pressure (GPa range) in a few nano seconds or less [24]. The magnitude of shock pressure can be controlled by regulatory of laser density, pulse duration and repetition rate of pulses. As long as this force be greater than yield stress of sample material, micro plastic deformation will occur on the top layer. Figure 1-2 shows the schematic of confined LSP with water medium.

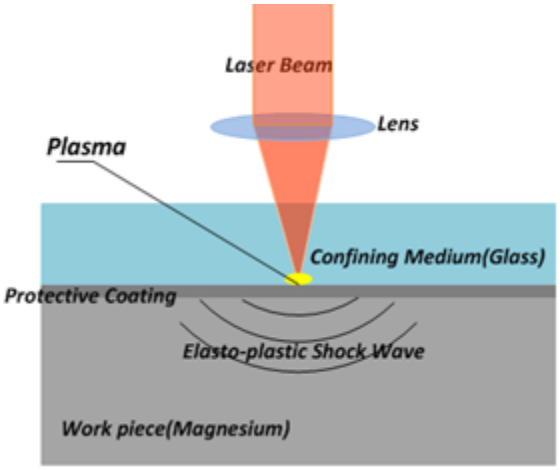

Figure 1-2 Schematic of confined LSP

Spec. materials	Confining medium, protective coating	Laser, Peening specifications	Results, Procedures, Observations	Ref.
12Cr steel, 316L	Water and Al (70–80μm)	Pressure duration 6–50 ns, beam diameter 1.6-5mm	2D-FEM calculation of shock propagation and residual stresses; materials using Johnson–Cook's plasticity model; effects of shock pressure and pressure pulse duration,	P Peyre [25]
35CD4 50 HRC	Water & black paint	30 ns, spot 5 mm, Intensity = 8GW/cm2	*3D-FEM* of single and multiple LSP using Perfectly elastic–plastic and the plastic. Definition of relation of dynamic yield strength and HEL	Hu [26]
Inconel 132 & 182	Water	Nd:YAG, 532 nm, spot size 1mm	1000 MPa compressive residual stress accumulated at 1mm in depth. Corrosion rate has been improved.	Sano [27]
Ti-6Al-4V	Water	I= 9GW/cm2,	700–800MPa were introduced by laser shock peening near surface, With maximum depth of 1.5	King [28]
X12CrNiMo 12-2-2& 316L	Water Al paint	λ =1.064μm, 8–10 ns, spot 3–4 mm 10GW/cm2	Shock pressure = 7 GPa, pressure pulse duration =20 ns The HEL measured experimentally by VSAR A large work-hardening happened on 316	Peyre [29]
Mg-Ca	CM: Water glass, Vac, Quartz PC: Al, Mg Be, Fe	λ =1.064μm, 14 ns, spot 40μm I =1.5-2.1 GW/cm2	Feasibility study of high repetition rate laser shock peening (HRLSP) on biodegradable magnesium alloys has been introduced. Impact of different confining medium and coating have been assessed.	Kamkarrad & S.N [30]
Mg-Ca	1mm glass Without Overlay	λ =1.064μm, 14 ns, spot 40, 60μm GW/cm2	Hardness of magnesium increased up to 105 HV at 40 μm- 57 HV at 60 μm. Maximum change in roughness at 10.8 μm in 40 μm	Kamkarrad & S.N [31]

Table 1-2 Laser Shock Peening - Review of Literature

Fe, Mo, Ti	Water	210 fs &6 ns, I=260Tw/cm^2 & 9Gw/cm^2	A large increase in hardness of just nanosecond peening have been observed. After 6 shots on Fe and Mo, the density of surface have been increased.	Kaspar [32]
AISI304	Flowing of water	Nd:YAG, 532 nm, 5 ns, 10 Hz, spot 0.65 mm	The achieved CRS is 700 MPa 30 μm beneath the surface at 10 000 pulses/cm^2	Schmidt [33]
Al	Water	XeCl, 0,308μm, 50 &150 ns, spot 1×4 mm, 0.1–6Gw/cm^2	Achieved peak pressures at 2.5 GPa were optical breakdown in water happened at I>2GW/cm^2	Berthe [34]
0.55%C steel	Water, Glass	1.06μm, 25 ns, spot 5mm (circle and square), 1.7–10GW/cm2, 25% overlap	Exceeding of CRS over the 350 MPa in depth of 1.1mm	Mass [35]
AISI 316L	Black paint	0.6 ns, spot 7.2 mm I=0.3TW/cm^2	LP has been compared with explosive shock pressure (1–2 GPa,1μs) close results in hardness have been observed The CRS in both case shown stability in fatigue test.	Gerland [36]
Fe–Ni alloy	Vacuum	0.53μm, 1 ns, spot 4.3 mm I=10^{13} W/cm2	Martensitic transformation happened close to surface-the depth of CRS occurred at 150 μm	Grevey [37]

Table 1-3 Laser Shock Peening - Review of Literature

1.5.1 Effect of Confining Medium on Plasma Pressure

In direct ablation, laser irradiates the surface in ambient and no material is used for protecting sample surface, whereas in confined method, transparent liquid or solid medium such water, mixed of water and agar [38], quartz as defined in table 1-3 [20], is used. Use of confining medium causes the shock wave being restricted in plasma region and most portion of shock pressure being reflected to the interaction region. Thereby, confined methods can generate much stronger shock wave compared to direct methods. The figure 1-3 indicates the differences of plasma pressure load in air ambient and in water as confining medium while using the same laser power [25].

Confining medium	Advantages	Disadvantages
Inorganic solids(Quartz, Glass)	Highest pressure(due to highest acoustic impedance)	Not applicable to curved surface-remained glass particles -multiple shock troublesome.
Polymers(acrylic, rubber)	Can be applied to curved surface without wetting	Multiple shocking is time and material consuming
Liquids(water)	Can be applied to curved surface, suits well for multiple shocking	Wet method-Lower pulse pressure.

Table 1-4 Comparison of different confining medium for LSP

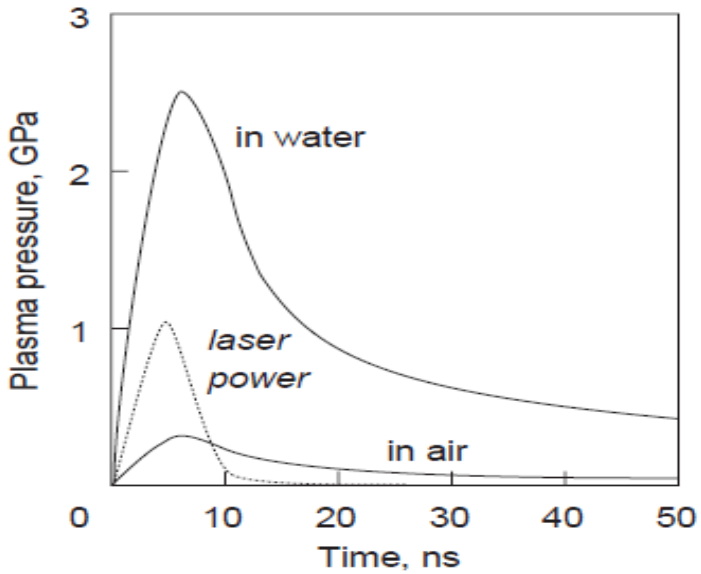

Figure 1-3 Impact of confining medium on pressure [25]

It can be clearly seen that, the created shock pressure by using water as confining medium is 7 times larger than direct peening in air. Utilizing water is a suitable way in order to prevent probable

thermal side effects on surface. Lots of research have been performed to evaluate the role of confining medium. LSP under flowing water [33], use of quartz [30] and glass [35] are some that are prominent.

1.5.2 Effect of Pulse Duration on Plasma Pressure

The figure 1-4 shows that the time to reach peak pressure is increased by increasing pulse duration [26]. The importance of laser pulse duration can be clearly seen when the pulse duration reduces drastically like in femtosecond laser. Considering an average laser power, by reduction of pulse duration, the peak laser intensity can be as high as few Terawatts/cm^2 [32][37]. More explanation has been proposed in Section 1.7.2.

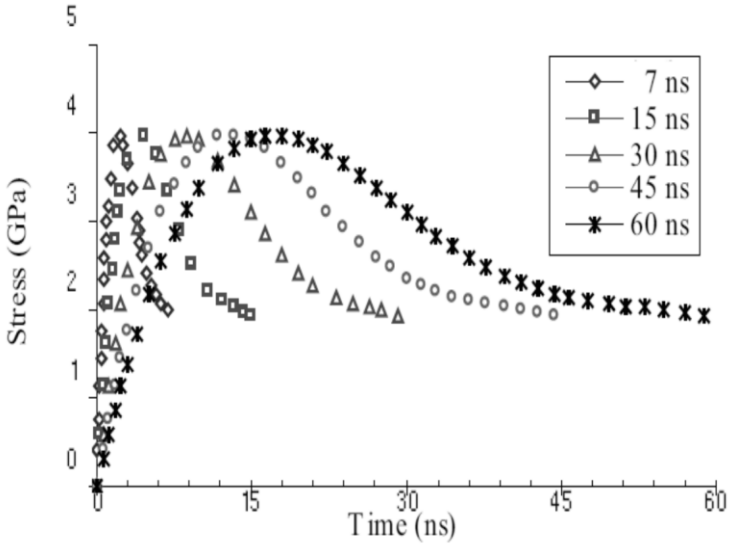

Figure 1-4 Impact of pulse duration on pressure [26]

Another merit of LSP is a number of alloys like austenitic steel or pure metals like magnesium those do not have ability of hardening by conventional heat treatment can be hardened by laser shock peening [39][40].

1.5.3 Variations in Scanning Methodology

One of the significant parts of LSP is set up of laser scanning which is proposed by different techniques. In most researches, the relative motion between the laser beam and specimen is achieved by the precise movement of specimen. Two types of specimen movement have been

presented in figures 1-5 and 1-6. The figure1- 5 shows a schematic of LSP using the robot for movement of specimen [41] and figure 1-6 demostrates a set up of experiment where the specimen movement has been carried out by X-Y table.The advantages of using robot is movement of specimen in more than two axes, which increases the versatality of laser shock peening for complicated shapes.

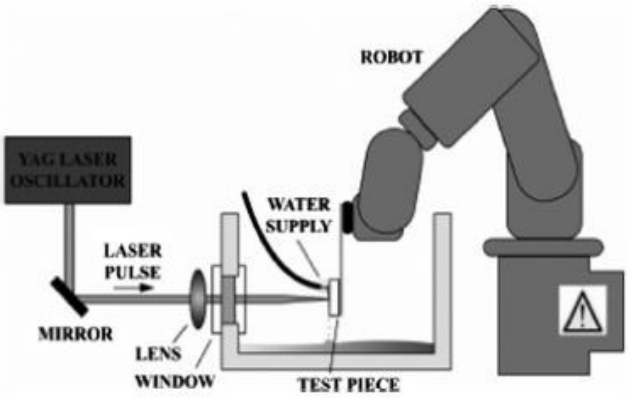

Figure 1-5 Schematic of LSP Experiment movement of specimen by robot [41]

When the repetition rate of laser increase, so as to avoid impact of several shots at the same position, the speed of relative movement should be increased properly. However, in high repetition rate laser shock peening (HRLSP) proposed in this thesis, the X-Y table cannot provide required speed of specimen adequately.

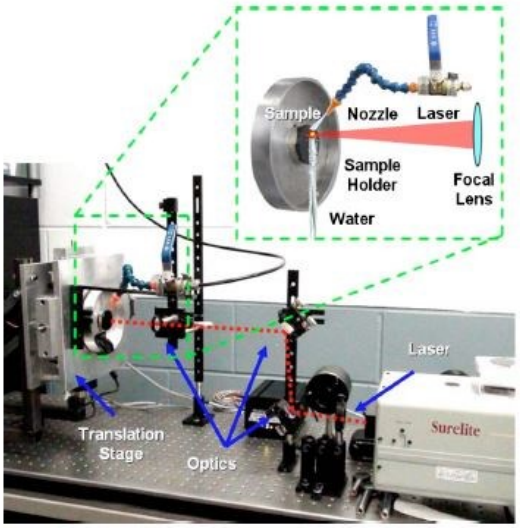

Figure 1-6 LSP Experiment movement of specimen by X-Y table [42]

Application of Galvo scanner for relative movement of laser over a fixed specimen can be an appropriate technique to overcome this challenge. The schematic of this scanning system shown in figure 1-7.

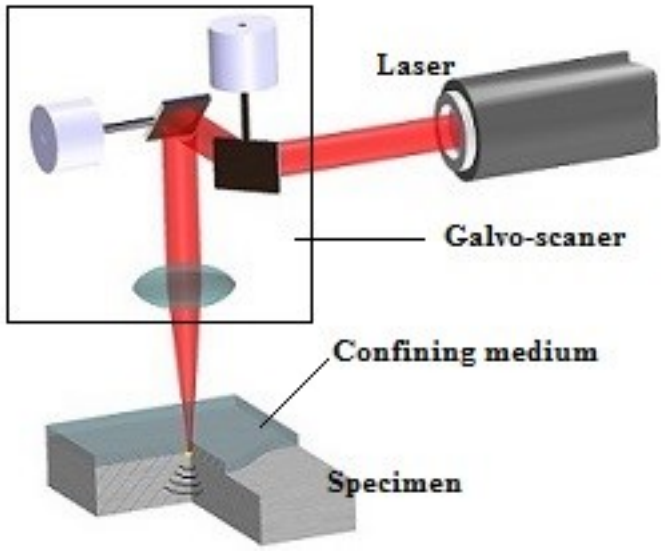

Figure 1-7 LSP Experiment laser scanning by Galvo-scanner

1.5.4 Experimental verification of shock load:

For the measurement of shock load, Polyvinylide Fluride (PVDF) is applied [22] as shown in figure 1-8. The pressure load (P) can be obtained by equation 1-1

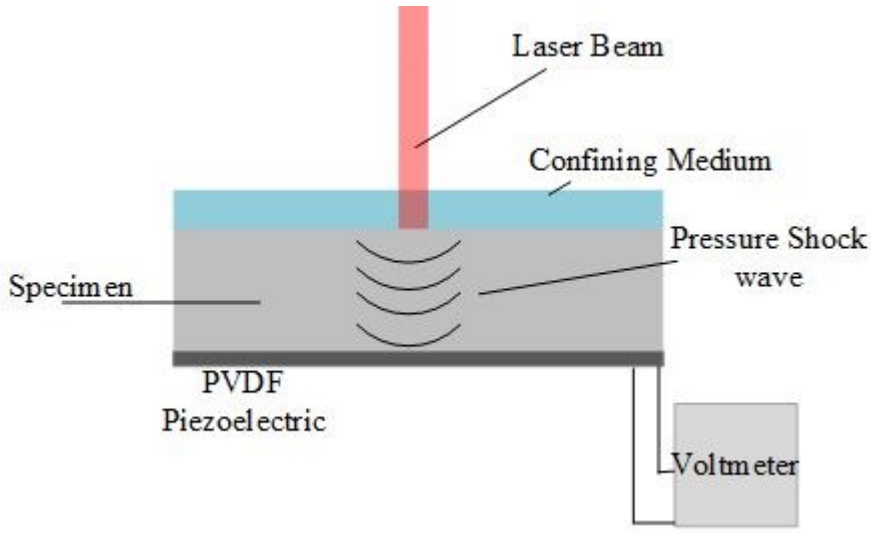

Figure 1-8 Measurement of Shock pressure by Piezoelectric method

$$i = (P - P_0)d_p S/t \quad (1\text{-}1)$$

$$t_p = g/v \quad (1\text{-}2)$$

Where, i is the measured current, d_p is piezoelectric coefficient, S is the effective area of piezoelectric and P_0 primary pressure that crystal has been clamped behind the specimen, g is the thickness of the PVDF, v is the acoustic velocity in PVDF and t_p the time of pressure action through the piezoelectric quartz crystal. In order to conduct a successful LSP experiment, all of the involved factors have to be controlled properly.

1.6 Theories of Laser Shock Peening

There are many presented models for calculation of shock pressure in LSP. However, the most significant works have been stated in this section. The primary calculation of plasma shock pressure in confining medium has been carrried out by the Fairand and Clauer[43] in 1979. The model compares favorably with the experiment when the laser intensity is in the range of 1–4 GW/cm^2. Griffin et al. [44] offered a new mathematical model that its priciples relies on equations of energy balance. In 1994, Peyre and Fabbro [45] presented a model with assumptions close to that of Griffin et al. However, in this model the laser pulse assumed was Gaussian. Also, a number of constants have been modified. Since Peyre and Fabbro model predict accurate results, shock load can be calculated using equations 1-3 to 1-6 [46] [47].

$$P(GPa) = 0.01\sqrt{\frac{\alpha}{2\alpha+3}}\sqrt{Z(\frac{gr}{cm^2 s})}\sqrt{I\left(\frac{GW}{cm^2}\right)} \quad (1\text{-}3)$$

$$\frac{2}{Z} = \frac{1}{Zs} + \frac{1}{Zw} \quad (1\text{-}4)$$

$$I = J/\tau A \quad (1\text{-}5)$$

$$z = \rho U \quad (1\text{-}6)$$

Where P (GPa) is the peak shock load, Z (g/cm^{2}s) is the impedance of shock wave, I($\frac{\mathrm{GW}}{\mathrm{cm}^2}$) is intensity of power, J is average energy of a pulse in jouls, τ(s) is pulse duration and A (cm^2) is the cross sectional area of the generated plasma, α is a constant that is related to efficiency of laser absorption by the material (if most of laser energy absorbed by surface, α will be close to 0.1). Z_W and Z_S are the impedences defined by the density and shock velocity in water and material respectively, ρ is density (kg/m^3) and U is velocity of shock wave within material and it is equal

to sound velocity. Because of short interaction time of each laser pulse, the created shock load is like a strike and this condition is different from static situation.

This has been explained by Hugonoit Elastic Limit in equation 1-7 [48][49], which means greatest elastic stress level above which permenant plastic deformation takes place

$$HEL = \frac{(1-\upsilon)(\sigma_y^{Dyn} - \sigma_0)}{1-2\upsilon} \qquad (1\text{-}7)$$

where υ is Poisson's ratio and σ_y is static yield stress. Knowing the poisson's ratio and the static yield stress of a material, HEL can be computed, and if the HEL is less than the shock wave pressure (equation 1-3), LSP can be effected.

1.7 Effects of Laser Shock Peening

Laser shock peening has different effects on specimen in terms of physical and mechanical attributes. Surface hardening, corrosion rate, fatigue property, wear rate, and change in surface roughness are the attributes that can be improved using LSP. The main reason of enhancing named attributes is increasing compressive residual stresses. In order to conduct accurate analysis of experimentation results, identification of all the involved parameters is important. Wavelength, power density, time duration of each pulse, repetition rate, scanning speed, diameter of laser beam, angle of irradiation, pitch between scan lines, confining medium, coating protector and alloy contaminants are some of the elements that needs to be identified based on the final mechanical properties. In the next sections the effectiveness of LSP on surface topography, creation of compressive residual stress, changes in hardness and wear rate, and corrosion rate have been reviewed.

1.7.1 Surface Topography

In LSP the creation of high plasma shock pressure which is beyond of dynamic yield stress of material surface leads to permanent deformation on the surface resulting changes in surface topography. Hence, both magnitudes of surface roughness R_a and mean amplitude R_c will be changed. The method which is used for laser scanning of the surface consists of percentage of overlap and number of scans have significant impact on surface topography. The impact of LSP on surface topography of implant has been studied by Guo et. al. 2012 [42]. They used a laser

density of 5.1 and 13.6 GW/cm^2 and overlap ratio of 25, 50, and 75%, to control the surface properties and study the effect of corrosion resistance on polished Mg-Ca alloys. Their experimental configuration of LSP is shown in figure 1-9 along with the spot overlap and microscopic images of the peened samples [42].

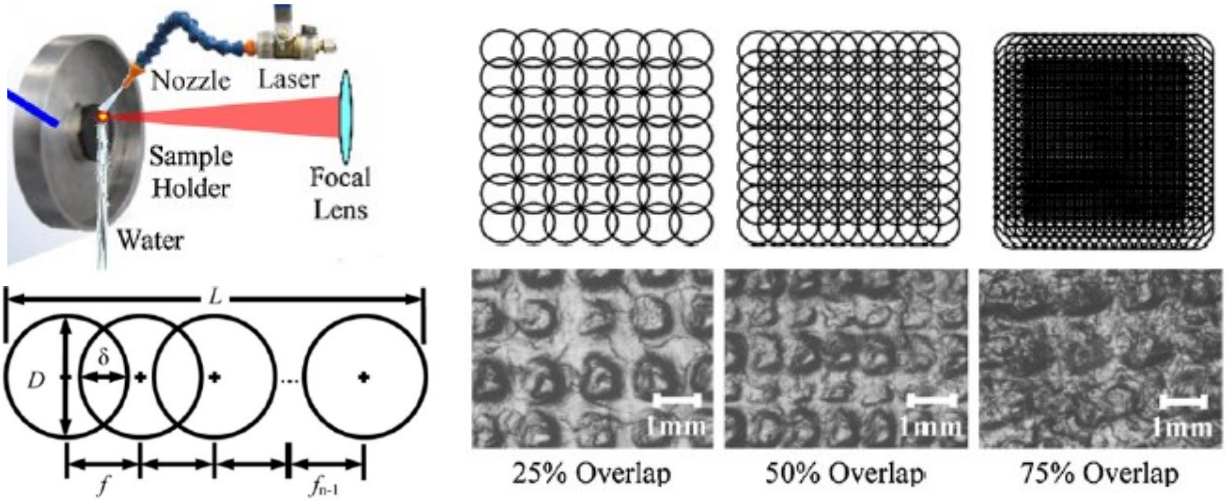

Figure 1-9 Schematic of LSP experiment and different overlap peening [42]

Figure 1-10 displays the R_a of unpeened magnesium were measured at 0.15µm and it can be clearly seen that the increase in both power and overlap ratio increases the R_a. This is an important parameter as bones are found to attach easily to rougher surfaces [50]. R_c which indicates the mean amplitude is another surface parameter that influences biocompatibility as higher R_c means higher surface area favoring cell adhesion. From the figure it can be seen that increasing power increases R_c while increasing the overlap ratio reduces the R_c. When, surfaces with higher R_c is preferred from the cell adhesion point of view, it increases the corrosion rate. Hence, an optimum value R_c needs to be determined taking into account both corrosion resistance and bone adhesion. Surface treatment, whether mechanical or chemical, has a direct impact on biocompatibility of the implant. The porous surface created by laser or other techniques thus become a suitable place for growth of new cells [50]. On the other hand, wettability which is a vital biocompatibility factor could be increased by few methods such as laser pulse irradiation [51].

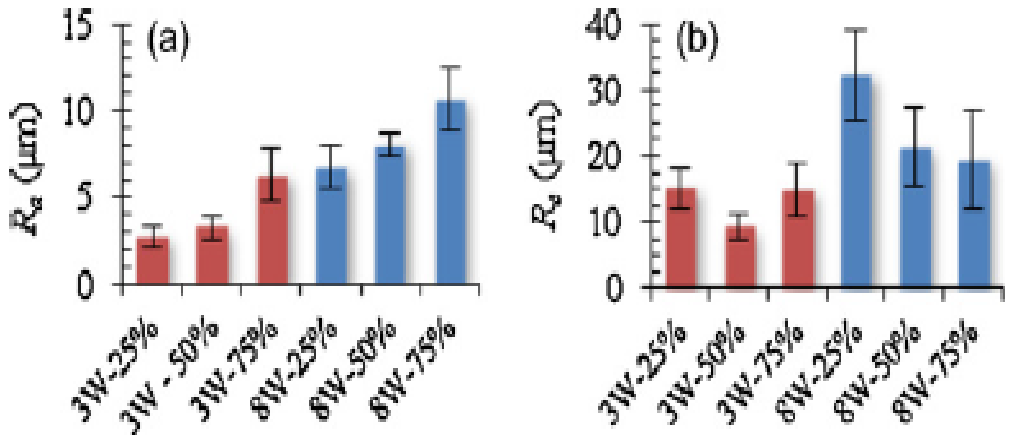

Figure 1-10 Impact of overlap and laser power on surface topography [42]

1.7.2 Residual stress

Determination of compressive residual stress can be carried out by experimental and finite element analysis methods. A number of experimental methods such Neutron diffraction [52], hole drilling [53], Slitting [54], Ultrasonic [55] and Magnetic [56] are used for measurement of CRS. However, X Ray Diffraction (XRD) has been recognized as an accurate experimental method for measuring of CRS[57]. The principle of this method relies on the penetration of X-Ray into atomic layer, and gets diffracted based on the spacing between the layers. The figure 1-11 demonstrates principle of XRD. LSP causes reduction in layer spacing. By knowing the properties of a particular material, the spaces in crystallography structure is known. Thereby, XRD can be used to measure changes in the spacing and the strain is measured; subsequently the residual stress is calculated using equations 1-8 and 1-9. These equations to calculate residual stress relies on diffraction and Bragg's law [57].

$$RS = \left(\frac{d_\Psi - d_n}{d_n}\right) E/[(1+\upsilon) sin^2\Psi] \qquad (1\text{-}8)$$

$$n\lambda_w = 2\mathrm{d}.\sin\theta \qquad (1\text{-}9)$$

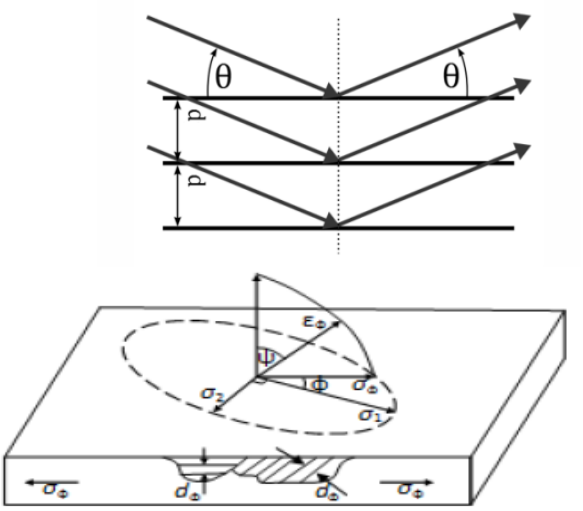

Figure 1-11 Measurement of RS by XRD[57]

Where RS is residual stress, d_n and d_Ψ are the spacing between layers before and after peening, Ψ is diffraction angle, E is Young's Modulus, λ_w is wavelength, and υ is Poisson's ratio. Figure 1-12 indicates residual stress magnitude as measured by XRD at different depths for two steel sapmles that were peened with two different laser intensities and one sample is unpeened. It can be clrearly seen that, laser peening could increase residual stresses three times more than the unpeened sample.

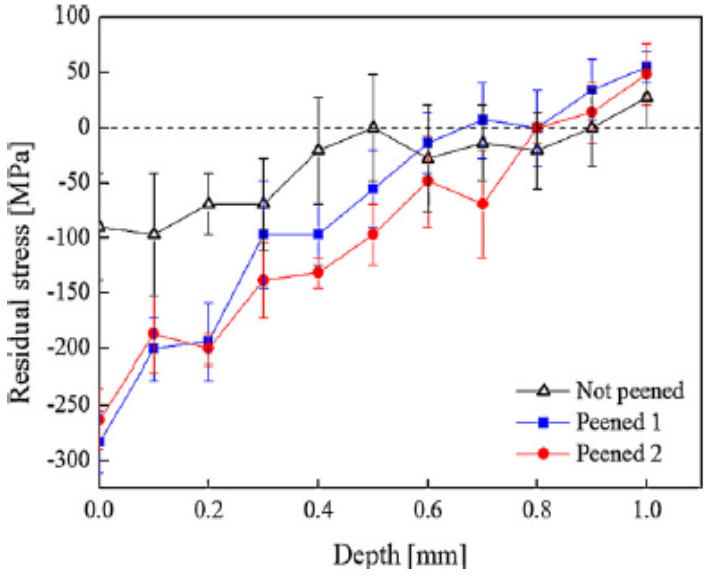

Figure 1-12 Demonstration of CRS in different LSP [58]

From the figure, it can be seen that, compressive residual stresses can be deposited upto a depth of about 0.8 mm from the surface with LSP [58]. Mg-Ca alloys subjected to LSP were then studied for imparted residual stress and the results shown in figure 1-13 [42] where the residual stress concentrates at about 80μm beneath the surface.

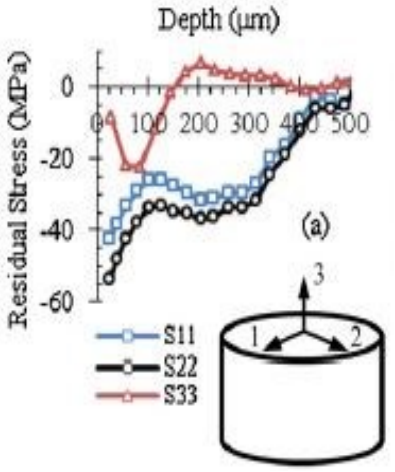

Figure 1-13 Distribution of CRS in different axes[42]

In figure 1-14 [42], advantages of LSP to creation of CRS have been demonstrated. Even though burnishing and shot peening have the ability to create greater magnitude of residual stress compared to LSP, the residual stress with LSP is closer to the surface, leading to better corrosion resistance.

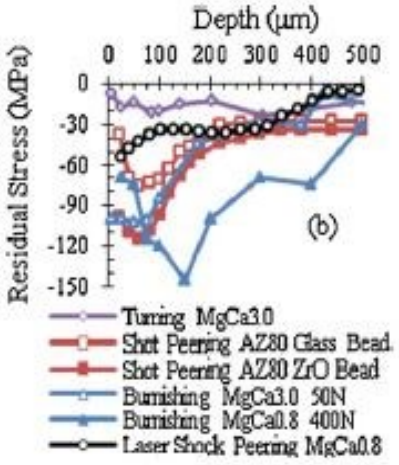

Figure 1-14 Measurement of CRS resulted by different methods [42]

Applying laser with shorter pulse duration as in picosecond or femtosecond laser leads to accumulation large magnitudes of the CRS be occurred closer to the surface and greater protection

will be happened versus corrosion [59]. The peak power of femtosecond lasers reach a much higher value compared to nanosecond lasers because of the shorter time duration, because of which both the shock pressure increases to 10^{10}Pa compared to GPa in nanosecond pulses. This creates a higher amount of CRS. When the duration of the peak is 2 picoseconds as in figure1-15 [59] the residual stress stored less than 5μm below the surface.

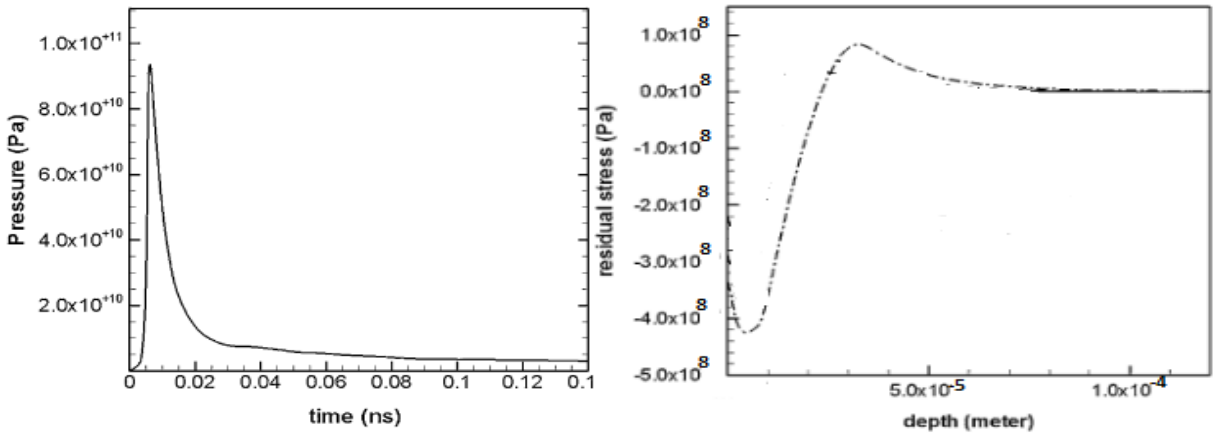

Figure 1-15 Peak of shock pressure and CRS in a femtosecond laser peening[59]

As long as use of lower duration pulse laser such as picosecond and femtosecond laser, interesting results can be achieved. Due to reduction in pulse duration, the peened region cannot absorb laser energy in an ultra-short time and this reduces the undesirable heat affected zone. In this circumstance, residual stresses accumulate close the surface [59]. The ability to control the depth where the maximum residual stress occurs within the material has lot of applications for LSP. In order to enhance the fatigue life of a metallic part, deep residual stresses can be more helpful [60]. Whereas in metal forming, particularly in thin sheet metal [59], it is important that the residual stresses are accumulated closer to the surface.

1.7.3 Surface Hardness and Wear Volume

LSP has significant effect on surface hardness and wear rate. The measurement of surface hardness was compared between unpeend samples and samples peened with different laser densities. Figure1-16 shows relationship between LSP and hardness in an experiment on duplex stainless steel [61]. It can be clearly seen that, increase in peening has caused enhancement of hardness. The figure 1-17 shows, as the surface hardness increases, there is a significant reduction in wear

volume, measured using pin-on-disc methods. The wear volume is defined by measuring of specimens' mass before and after conducting tests based on ASTM standard [62].

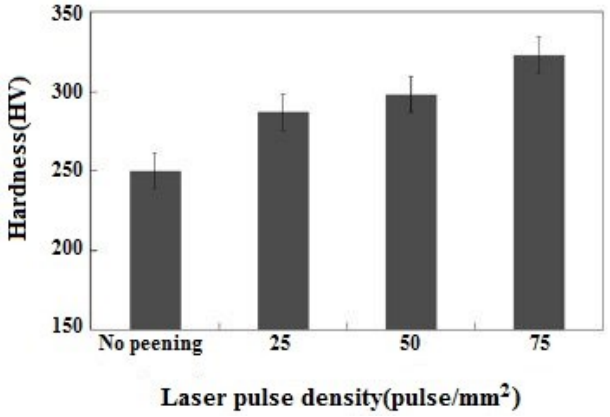

Figure 1-16 Impact of laser pulse density on hardness [61]

The importance of protective coating has been highlighted by figure 1-17, as well. experiment indicates effectiveness peening on wear volume and surface hardness. Based on test results, it can be seen that, samples peened under Aluminuim foil as the confining medium achieves maximum hardness and mininmum wear.

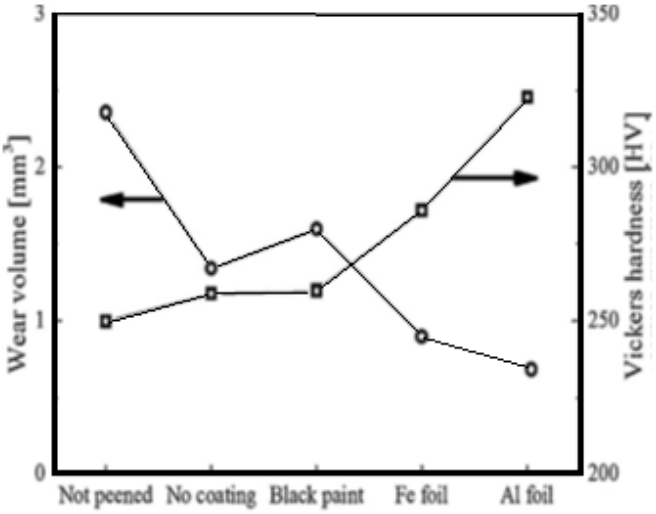

Figure 1-17 Effect of protective coating on wear and hardness[61]

This is owing to notable difference between density of the Al coating ($2700 kg/m^3$) Fe coating ($7700 kg/m^3$) and stainless steel ($7800\ kg/m^3$) [61][63]. Though the density of the black paint is smaller than Al coating, high laser power leads to protective coating damage and shock load reduces. The coating material and its thickness thereby restrict the increase in laser power density.

1.7.4 Corrosion

Further to residual stress and surface topography, Guo et al also studied the effectiveness of LSP on corrosion rate in their research [42]. In order to evaluate impact of LSP on corrosion rate, Potentiodynamic polarization (PP) test was performed in Lonza Hanks solution, which is a simulated biological solution [60]. In PP test, three electrodes are mounted in the electrolyte which is consists of a corrosive solution as shown in figure 1-18. While the counter electrode is carbon and the reference electrode is saturated calomel, the specimen is mounted with epoxy resin as the corroding electrode. The electrolyte can be Hank's Solution [64] which is a simulated organic electrolyte. In order to analyze the corrosion rate, PP curve is shown in figure 19[65]. Passivity of specimens' surface against corrosion is a characteristic of some metals.

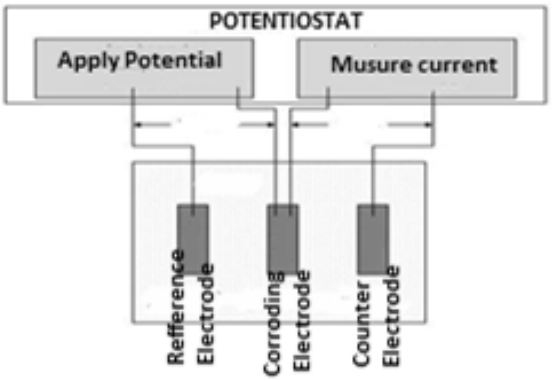

Figure 1-18 Schematic of PP corrosion test

This resistance to corrosion is due to strong oxidizing situations or anodic polarization. E_{corr} shows the passivity level of a particular material and the corresponding I_{corr} indicates the rate of corrosion, as indicated in figure 1-19 and in equation 1-10 [61][66]

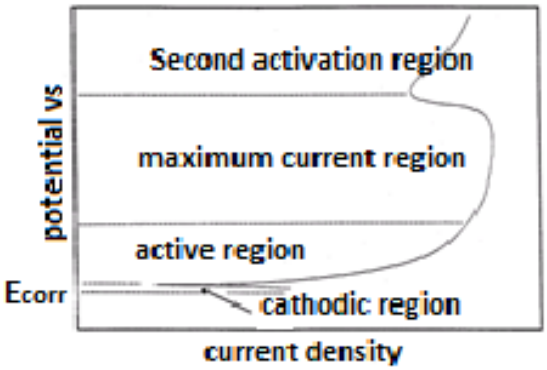

Figure 1-19 Potentiodynamic Polarization Curve [65]

$$\text{Corrosion rate}\left(\frac{\text{mm}}{\text{year}}\right) = \frac{3.27\times10^{-3}\times i_{corr}\left(\frac{\mu A}{cm^2}\right)\times w_e(gr)}{\rho\left(\frac{gr}{cm^3}\right)} \quad (1\text{-}10)$$

Where, W_e and ρ are the equivalent weight and density of the material. In the following section, the effect of LSP on the control of corrosion is studied by comparing the pp curves between peened and unpeened samples. The result of corrosion test of peened specimens has been illustrated in figure 1-20 [42]. The corrosion rate was computed using the polarization resistance method.

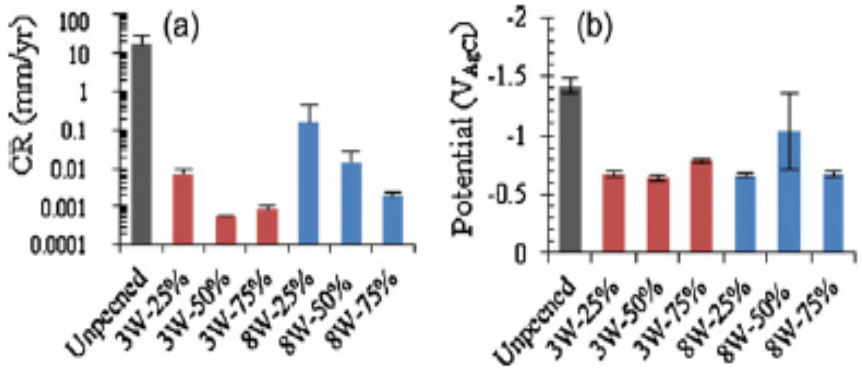

Figure 1-20 Difference in corrosion rate by change in LSP parameters [42]

It can be seen from figure 1-20 that, peened samples have significant drop in the corrosion rate, and also that the effect of power and overlap ratio is similar to the R_c values. Higher R_c leads to higher corrosion rate and vice versa. The right hand side of figure 1-20 shows that the unpeened samples have more potential to corrode compared to peened samples. The figure 1-21 [42] shows a comparison between surface contaminants of peened and un-peened specimens, studied using Energy Dispersive Spectroscopy (EDS).

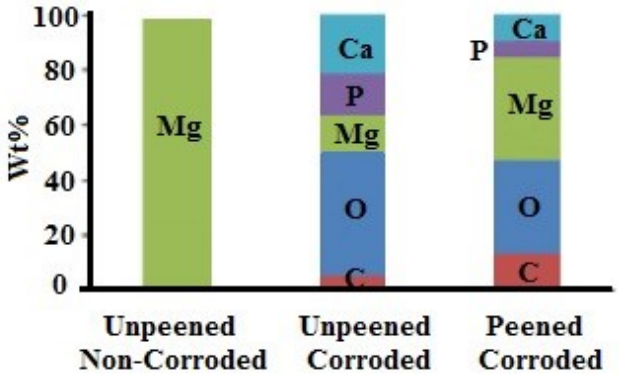

Figure 1-21 Chemical containment on peened and un-peened surfaces [42]

The results compare the surface elements of unpeened sample before and after corrosion, and peened sample after corrosion. It can be clearly seen that the magnitude of oxygen contaminant in the peened corroded surface is less compared to un-peened corroded surface. This effectively concludes that the peened surface has lesser tendency towards corrosion. In figure 1-22 another example on duplex stainless steel shows reduction of corrosion after LSP [61]. This figure shows the anodic (in positive voltage area) and the cathodic (in negative voltage area) corrosion reaction in PP test. It can be clearly seen that there is a reduction in I_{corr} in the peened sample compared to unpeened ones.

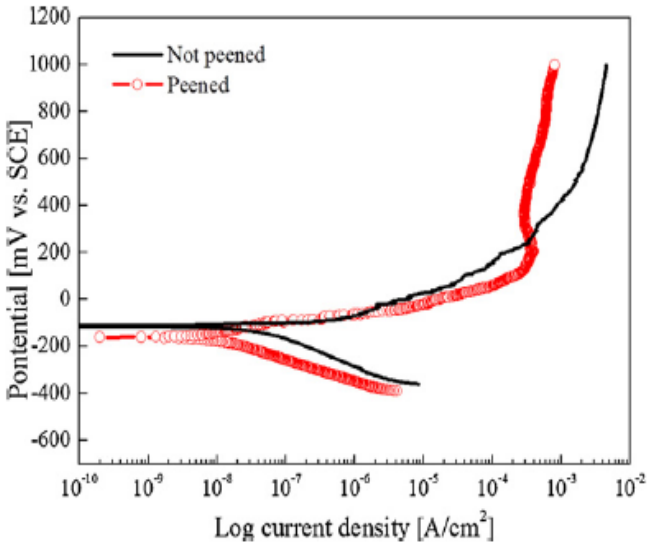

Figure 1-22 PP curve for stainless steel[61]

Applying the equation 1-10 shows that 75% reduction in corrosion rate. The potentiodynamic polarization test for corrosion was followed by Copper-Accelerated Acetic–Salted Spray (CASS) test for pitting corrosion. This test is an accelerated corrosion test which generates a corrosive environment to the treated surface samples. CASS is performed as per ASTM B 117 and ISO 9227 standard. Since pure samples did not have sufficient pits in both peened and unpeend situation, tests were done on the samples that were tested for wear. CASS results in Figure 1-23 [33] shows that the number of pits on peened specimen reduces by 50%, and there are no larger pits in comparison to unpeened specimen.

This concludes that laser peening effectively reduces the rate of corrosion. Considering the advantage of Mg alloys from biodegradability point of view, and the advantage of LSP from the

surface treatment point of view, the last section of this chapter, forms the motivation and the objectives of the current work.

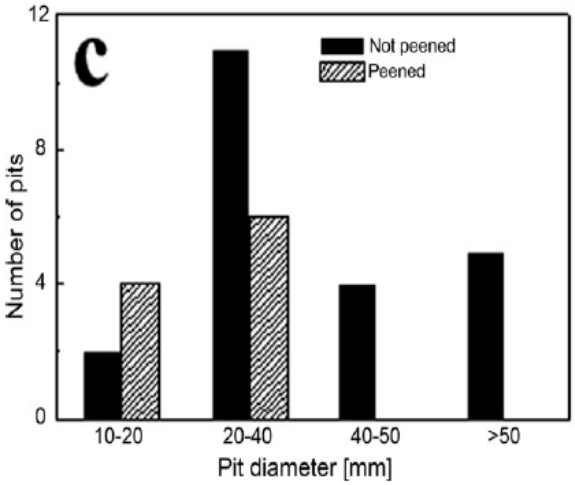

Figure 1-23 Distribution of pitting corrosion[33]

1.8 Motivation for Current Work

From the critical review of literature, it is clear that, biodegradable metallic implants and application of LSP for tuning their properties is a novel area which needs lots of research work. The advantage of Mg-Ca bio-implants are: I) mechanical strength comparable to that of bones II) increased biocompatibility III) biodegradability. Since the implants are biodegradable, the need for additional surgery for removing the implant is eliminated, thereby saving cost and time, in addition to patient safety and reducing complications. However, the disadvantage of Magnesium medical alloys is that they corrode within human body, faster than the conventional implants requiring surface treatment methods to retard corrosion. Review of literature suggest different methods Mechanical treatments like shot peening, burnishing and laser shock peening; or by alloying with different metals to Mg; or Cladding.

One of the common methods for reduction of surface corrosion is increasing compressive residual stresses on the surface of the material. And mechanical treatments are capable to perform this. LSP as mechanical treatment has been used successfully on implant surfaces on many materials to reduce the corrosion rate. In addition LSP is a capable way to modify other useful attributes such as fatigue resistance, durability, reduction in wear volume and also be able to provide greater

biocompatible surface. In recent years, enhancement of mechanical attributes of medical magnesium alloys by LSP has been noticed. The effects of LSP on corrosion resistance, micro-hardness, residual stress and surface topography have been studied.

Having reviewed the literature, it can be seen that the lasers used are low repetition rate high power lasers. In this work, use of low power but high repetition rate lasers is proposed so the predictive modeling and the material laser interaction will have to be worked out. Owing to cost of low repetition laser machines, it is valuable to evaluate the possibility of applying high repetition laser for LSP. Meanwhile, due to applying high energy pulse laser, physical damage of tiny specimen without adequate mechanical strength is possible. In these cases HRLSP with lower energy pulses would be more effective. The other significant merit of HRLSP is high speed shock peening process. Superior control on corrosion rate which is important in performance of biodegradable metallic implant is another important advantage of HRLSP. This is primarily because of reduction of spot size diameter [49] the CRS accumulates closer to the surface thereby providing better resistance to corrosion.

1.8.1 Challenges to Overcome

Although HRLSP has notable positive points, the main difficulty of HRLSP is that, the lack of adequate energy in each pulse causes to reduce the required laser power density. In addition, due to high frequency pulse, speed of scanning must be increased by several orders of magnitude compared to low repetition ones. Even though LSP and HRLSP rely on the same principle from most of technical angles, substantial differences are hidden in their laser pulse modalities and speed of scanning. The figure 1-24 shows power-time graphs of low and high repetition rate laser. It can be clearly seen that, even though average power are equal, the energy of each pulse in low repetition ones is several times more than high repletion ones. Note that, the laser with repetition rate less than 100 Hz can be classified in range of low repetition rate and more than 1000 Hz can be assumed in range of high repetition rate lasers.

When frequency comes down from 10 KHz to 10 Hz it means, the energy of each pulse increases by thousand times more. In normal circumstance, the energy of each pulse in high repletion pulse laser is not adequate for shock peening. The equation 1-11 illustrates that; the energy of each pulse (J) in joule has a reverse linear relation with repetition rate.

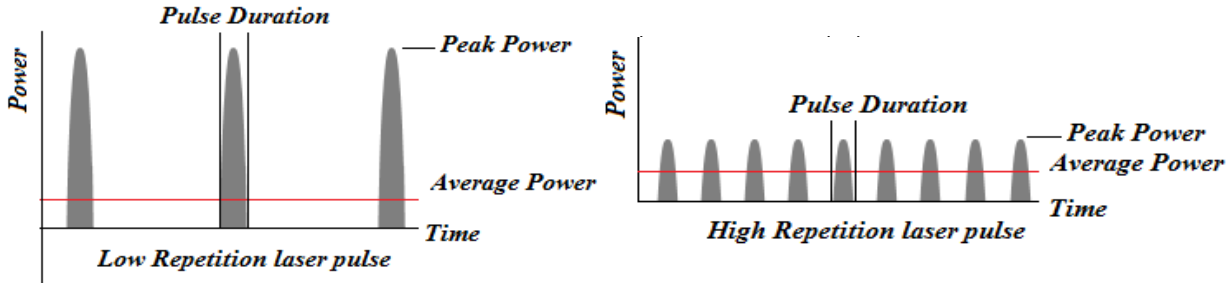

Figure 1-24 Comparison of energy pulse in low and high repetition rate laser

$$J = P_w / f \qquad (1\text{-}11)$$

Where, P_w is laser power in Watt and f is laser repetition rate in Hertz. Depends on increasing of pulse number, the energy of each pulse will be declined. In regular low repetition laser peening the energy of each pulse is between 1-5 joules. Meanwhile, in regular high repetition laser, the energy of each pulse will be several milli-joules. Based on LSP theory and by applying equations 1-3, 1-4 and 1-6, the importance of laser intensity will be distinguished. In order to applying successful laser peening in low mechanical strength metals such Magnesium, intensity magnitude must exceed than 0.11 GW/cm^2 necessarily (it is calculated by assumption no protective coating, water is confining medium and HEL is 0.28 GPa for magnesium). This is possible by focusing low energy laser pulse into a smaller area. Laser scanning speed is another fundamental difference in HRLSP.

Due to high repetition pulses, for avoiding repeated laser spots at the same position, the speed of scanning should be increased by thousandths of times compare to normal LSP. In addition, it is necessary to make sure subsequent spots in a scanning sequence are at an adequate distance for prevention of thermal effect. It is necessary to recognize effective factors in LSP process and then, how these effective parameters can be manipulated. Laser spot size (laser beam diameter), confining medium (CM), protective coatings (PC), scan speed, overlapping in terms of time and spot position and laser types are significant factors which are important to HRLSP.

Providing this amount of speed is the first difficulty and the second one is inadequate time to releasing heat for prevention of thermal side effects when laser shots applied continues in identical area. In order to increase speed of laser scan, Galvo-scanner could be a proper method. A probable sequence of laser shots is shown in figure 1-25.

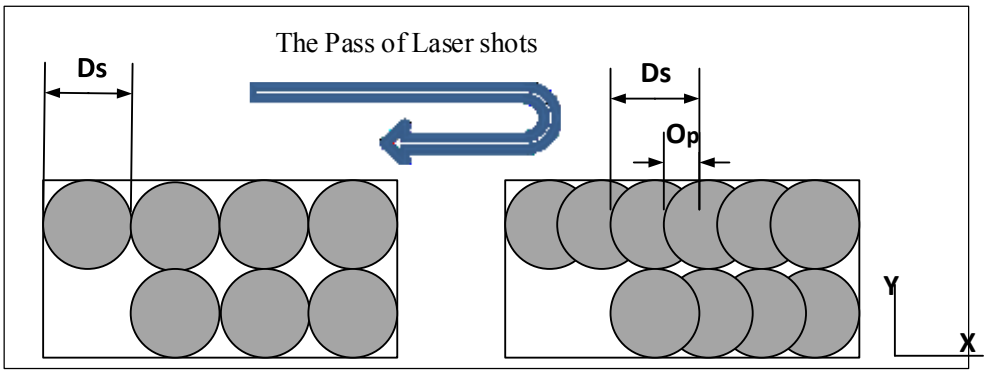

Figure 1-25 Sequence of laser shots in no and overlapped peening

1.9 Objectives and Scope

The general objective of this thesis aims to develop HRLSP for low mechanical strength metals/alloys like Magnesium and the specific goals of the thesis are:

1- Theoretical objectives:

a) Feasibility of high repetition rate laser shock peening

b) FEA of single shot of high repetition rate laser for evaluation of HRLSP occurrence

c) FEA of multiple HRLSP for assessment effects of peening on magnesium

2- Experimental setup and performance verifications

a) Effect of HRLSP on surface topography and Hardness

b) Effect of HRLSP on wear rate and wettability which are important for biocompatibility

Considering the state of the art in this important area, and the problems mentioned earlier, the goal of this proposal is to identify the possibility of HRLSP on surface modification in terms of mechanical (increasing hardness, growing fatigue and wear reduction, corrosion rate) and biological aspects. These issues have been included in two main areas: optimization of laser parameters such as laser density, pulse duration and frequency of pulses. The second area is predictive modeling of CRS and corrosion rate.

1.9.1 Scope of the Proposed Work

The table 1-4 compares the two types of laser peening with low repetition and high repetition lasers. The laser characteristics such as intensity, pulse energy, pulse repletion rate, laser beam diameter, overlapping, scan speed and pulse duration have fundamental impact on HRLSP. Combination of mathematical equations and experimentations contribute to finding a realistic

model towards identifying best laser characteristics for HRLSP. The scope of this work also include experimental setup; peening of mg samples and verification of peening by measuring wear resistance, surface roughness, hardness and wettability of samples that are unpeened as well the samples that are peened with different laser parameters.

Materials	Scan speed	Spot Size Diameter	Repetition Rate	Power Intensity	Average Power	Peak Pressure
S.S (LSP)	1 cm/s	1-8 mm	10–30 Hz	5 GW/cm^2	15 W	6.5GPa
Mg (HRLSP)	800cm/s	10-100µm	10-20KHz	0.8GW/cm^2	4 W	2.4GPa

Table 1-5 Comparison of LSP and HRLSP in some performances

1.10 Anticipated Impact of HRLSP and its Applications

HRLSP can have vast application in medical, aerospace and other area, where corrosion control would be significant. HRLSP is able to modify implant surface in terms of biocompatibility by increase in surface roughness and wettability. The contact angle between water drop and work piece surface changes with the surface morphology that can be controlled by controlling the laser parameters. Increasing of surface roughness, contributes towards creation of suitable conjunction between implant and surrounding tissues.

Additionally, HRLSP can modify mechanical attributes such as wear and corrosion resistance of metallic implants. Some other applications that can benefit from HRLSP are:

- Shapes memory alloys and their application in biodegradable cardiovascular stents
- Design of intelligent alloys with predefined changeable corrosion rate
- Biodegradable polymeric coating of Magnesium based implants
- Increasing durability of permanent teeth metallic coating
- Biodegradable screws with application in bone-plate fixator
- Increasing erosion resistance of blades in turbojet, and in desalination pump impellers
- Releasing unwanted residual stress created in micro welding, casting or machining
- NDT by assessing mechanical shock wave within composite materials.

1.11 Thesis organization in the manuscript based thesis format

The proposed manuscript-based thesis is consisted of 7 chapters. In the first chapter indicates a critical review of literature on biodegradable mg alloys and on laser shock peening was performed. The basic principle and theory of laser peening have been discussed from literature. Also, the motivation, scope and objectives have been stated. The specific objectives of the thesis as listed in section 1.9 are covered in chapters 2 through 6. The chapters 2 through 6 are duplicated from 2 published journal articles and 1 journal article under revision, and 2 other journal articles under review. The chapters themselves are organized in a cohesive manner and formatted as stated in "Thesis Preparation and Thesis Examination Regulations (version 2013), of the School of Graduate Studies, Concordia University. In the duplicated articles, the sections, figures, tables and equations are numbered as per the Thesis Guidelines. A single comprehensive reference list is presented at the end in the Reference section of the thesis, in lieu of the individual manuscript references at the end of each chapters. Conclusions of this research work, and recommendation for future work are presented in Chapter 7.

Chapter 2: Duplicated from article published in International Journal of Advanced Manufacturing Technology

H. Kamkarrad, S. Narayanswamy, and X. S. Tao*, "Feasibility study of high-repetition rate laser shock peening of biodegradable magnesium alloys,"* Int. J. Adv. Manuf. Technol., V 74 (9–12), pp. 1237–1245, Jun. 2014.

Recently, a number of Magnesium based alloys have been identified as a potential bio-degradable material for implants. The challenge in the application of medical alloys is that, these medical alloys corrode within human body much faster than duration of broken bones conglutination. In this regards, laser shock peening by increasing compressive residual stress upon biodegradable metallic implant surface had been proposed as a capable method for corrosion reduction. Laser shock peening is currently performed by high power low repetition rate lasers. Its high cost for applying on low-priced and light mechanical strength specimen is the main restrictions for its performance. This research is an attempt to theoretically ascertain the feasibility of LSP by high repetition rate pulsed laser. Lower cost, more processing speed and accumulation of compressive residual stress closer to the surface by high repetition rate laser, combined with better corrosion

control is the primary motivator for evaluation of the possibility Due to increasing wettability, HRLSP can increase efficiency of surface coating.

Chapter 3: Duplicated from article published in Journal of Laser Micro/Nanoengineering

Kamkarrad, H., Narayanswamy, S., & Keshmiri, M.*" High Repetition Laser Shock Peening on Magnesium Based Biodegradable Alloys".* Journal of Laser micro/Nanoeng., Vol. 10, No. 3, 2015, pp.261-267, Dec.2015

New generation of metallic implants through capability of absorption within biological environment has been introduced in recent researches. Although, magnesium implant with proper biocompatibility has been proposed as biodegradable metallic implant, its insufficient mechanical attributes must be enhanced for implantation within human body. Laser shock peening has been successfully conducted for modification of magnesium implant. Overall, laser shock peening can be performed by low repetition rate (less than 30 Hz) and high power pulsed laser which needs expensive devices. In order to laser shock peen magnesium alloys that have a lower mechanical strength, it is better to use high repetition pulsed laser which is much faster and economical. Recently, high repetition rate laser shock peening of magnesium has been theoretically found feasible in previous research of authors. In order to validate occurrence of high repetition rate laser shock peening, changes in surface topography and hardness are evaluated on the magnesium specimens.

Chapter 4: Presents the article submitted to Journal of Mechanical Science and Technology

Kamkarrad, H., Narayanswamy, S. *"FEM of Residual Stress and Surface Displacement of a Single Shot in High Repetition Laser Shock Peening on Biodegradable Magnesium Implant"* Journal of Mechanical Science and Technology, Manuscript Number: MEST-D-15-00769R1 (*Under revision*)

Laser shock peening (LSP) is being proposed as the surface processing technique to enhance the mechanical characteristics of the induced compressive residual stress on the specimen surface. Generally, LSP is performed using high energy, low repetition pulsed laser. Recently, a novel method of LSP using high repetition rate laser on biodegradable magnesium alloys has been introduced as high repetition laser shock peening (HRLSP). Increased speed of peening and reduced cost when compared to conventional LSP are the key highlights of HRLSP. This research

is aimed to validate the possibility of HRLSP through creation of Compressive Residual Stress and change in surface topography. A finite element method (FEM) has been proposed to show the ability of a focused laser pulse (Nd: YVO4 laser, wavelength of 1064 nm, repetition rate of 10 KHz and pulse duration of 14 ns) for peening magnesium. If increase in CRS can be created by single shot of laser pulse, it can be concluded more shots in real high repetition rate laser can be used for creation of CRS and possibility of HRLSP on magnesium can be validated. To certify results of simulation, the results of CRS have been verified by analytical results where the analytical von misses (σs) is found to be 31.5 MPa, which is similar to the value from FEM at 30 MPa. Furthermore, the plastic displacement of FEM at 4.02 μm is substantiated by experimental result at 3.698μm and analytical result at 4.01 μm.

Chapter 5: Presents the following article submitted to Journal of Laser Micro/Nanoengineering

Kamkarrad, H., Narayanswamy, S., *"FEM of high repetition rate laser shock peening on magnesium by multiple and overlapped techniques* "Journal of Laser micro/Nanoeng, Manuscript number: JLMN-15-076*(Under review)*

Laser shock peening (LSP) has been identified as an advanced method of improvement mechanical attributes of metallic specimen by deposition of Compressive Residual Stress (CRS) under the peened surface. Recently high repetition rate laser shock peening is introduced as high repetition rate laser shock peening (HRLSP). This novel method with low energy pulse can be applied on low mechanical strength metals such as magnesium. In order to assess success of HRLSP, measurement of CRS is a reliable technique. This study is a finite element analysis to demonstrate creation of CRS and plastic deformation of a magnesium specimen using a high repetition rate nanosecond laser. Moreover, influence of increase in number of laser shots on the CRS has been evaluated. In order to estimate accuracy of the model, the results of plastic deformation on the peened surface has compared to experimental results.

Chapter 6: Presents the following article submitted to Materials Characterization

Kamkarrad, H., Narayanswamy, *"Improvement of attributes in Magnesium surface by high repetition rate laser shock peening* "Journal of Materials Engineering and Performance, Manuscript Number: JMEP-15-12-9637*(Under review)*

The biodegradability of magnesium can provide the privilege of avoiding the second surgery required to remove the implant. However, mechanical attributes such as hardness and wear resistance should be improved; otherwise failure of magnesium implants within the human body may occur faster than a broken bone conglutination. This research is aimed to substantiate the possibility of laser shock peening on magnesium by high repetition rate pulsed laser(Nd: YVO4 laser, wavelength of 1064 nm, repetition rate of 10 KHz and pulse duration of 14 ns). It is evident that conventional laser shock peening enhances the attributes required for implants. However, the present research attempts to validate HRLSP by demonstrating modification in hardness, wear rate, and wettability of magnesium. Fast processing and economical equipment are two major merits of high repetition rate laser shock peening. The high repetition rate laser shock peening can enhance hardness of peened surface from 45 HV to 103 HV. Furthermore, the wear resistance can be increased more than three times from 5.5E-4 gr/s (unpeened specimen) to 1.7E-4 gr/s (3 scans and 66% overlap peening). In addition, variation in grain size and surface morphology leads to enhancement of wettability, which is valuable for biocompatibility.

Chapter 7: Presents conclusions, Summary and anticipated work

CHAPTER 2. Feasibility Study of High Repetition Rate Laser Shock Peening of Biodegradable Magnesium Alloys

This chapter is based on an article published in Journal of Advanced Manufacturing Technology[30]. This chapter covers the objective '1a' of the "Objectives and Scope of the Thesis" in section 1.9

2.1 Introduction

Metallic bio-implants like stainless steel & Titanium alloys have had vast applications in orthopedic surgeries. Although use of conventional implants has contributed to the cure of many patients, they have a number of side effects such as reduction of mechanical attributes in the bones and cause inflammation. Moreover, these implants are not bio-degradable, hence requiring additional surgery to remove them. Recently, a number of bio-degradable metallic alloys have been identified for implants with ability of absorption. These biodegradable implants have similar mechanical strength to that of bones, thereby reducing bone asthenia [1] and helps hold the clamp implant screw. In addition, due to excellent material properties, the biocompatibility of these implants increases when compared with conventional implants. The biggest of the advantage is that since the material is biodegradable, it eliminates the need for additional surgery for removal, thereby reducing pain and danger to the person, and saves cost of additional surgery. Though biodegradable Magnesium alloys (Mg-Ca, Mg-Ca-Zn) [2] offer a superior advantage over conventional alloys (Ti or SS) for bio-implants, these implants may degrade before the broken bones have cured completely, causing the bone to fail again. Hence, reduction of corrosion rate in magnesium surface is important to applying this new implant type [3]. This modification mainly is performed by different methods such as coating and increasing compressive residual stress on implant surface. LSP with low repetition and high energy pulse has been identified as a probable method for corrosion rate control by increasing compressive residual stress (CRS) upon implant surface [4]. Owing to cost of low repetition laser machines, the research regarding possibility of applying high repetition laser for LSP would be valuable. Meanwhile, due to applying high energy pulse laser, physical damage of tiny medical specimen without adequate mechanical strength is possible. In these cases HRLSP with lower energy pulses would be more effective. However, Performance of HRLSP faces two main restrictions. The first one is that the energy of each pulse

cannot provide adequate intensity for peening. The second difficulty is, in order to avoid repeated laser shots at the same point, the required scan speed should be increased drastically.

2.2 Theory of High Repetition Laser Shock Peening (HRLSP)

Although there are notable differences in energy and repetition rate in high and low repetition rate laser, the principle of HRLSP and LSP relies on an identical concept. Under certain circumstances upon absorption of laser energy exceeds the certain magnitude, ablation will be affected. In this process, a phase transformation occurs and material is transformed from solid state to vapor. The metallic vapor absorbs adequate energy and its temperature increases drastically. Then, free electrons can be moved out atoms [5] and gas atoms will be converted to ions and plasma is resulted. Plasma is able to generate a high-pressure (GPa range) over a course of few nanoseconds. Figure 2-1 demonstrates schematic of laser shock peening. Short time plasma shock action is similar to impact. As long as generated laser shock load exceeds of Hugonoit Elastic Limit (HEL) in equation 2-1 [6] shock peening will be effected.

$$\mathrm{HEL} = \frac{(1-\vartheta)\sigma_Y^{Dyn}}{1-2\vartheta} \qquad (2\text{-}1)$$

Provided that pulse duration is adequately [67]small, it is proved by equilibrium 2-2

$$\tau \ll r_0\sqrt{\frac{\rho(\lambda+2\mu)}{4\mu(\lambda+\mu)}} \qquad (2\text{-}2)$$

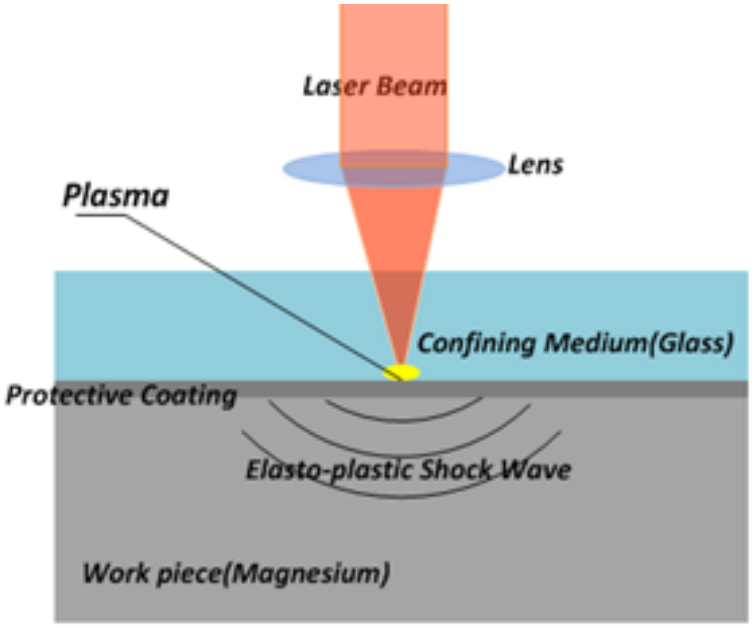

Figure 2-1 Schematic of LSP

Where υ is Poisson's ratio and σ_Y^{Dyn} is dynamic yield stress, τ is pulse duration in nanosecond, ρ is density in gr/cm^3, r_0 is the radius of the laser spot and λ, μ are Lamé constants. HEL is computed by knowing the Poisson's ratio and the dynamic yield stress of specimen's material. On the other hand, the shock pressure can be computed through equations 2-3 to 2-7 [9].

$$P = 0.01\sqrt{\frac{\alpha.Z}{2\alpha+3}} \times \sqrt{(A.I - E_{vap}/\tau)} \quad (2\text{-}3)$$

$$E_{vap} = m\Delta H_{vap} \quad (2\text{-}4)$$

$$\frac{2}{Z} = \frac{1}{Zs} + \frac{1}{Zw} \quad (2\text{-}5)$$

$$I = E/tA \quad (2\text{-}6)$$

$$z = \rho U \quad (2\text{-}7)$$

Where P (GPa) is the peak shock load, Z (g/cm^2.s) is the impedance of shock wave, E (Jules) is average energy of a pulse, τ is laser pulse duration, t is time of pressure and D is diameter of laser beam, α is a constant that is related to efficiency of laser absorption by the material (if most of laser energy absorbed by surface, α will be close to 0.1), A is spot size area, E_{vap} is energy of vaporization of the target in J/cm^2, m is mass of ablated material (protective coating material), ΔH_{vap} is enthalpy of vaporization target, I is laser power density in Gw/cm^2, Z_C and Z_S are the impedances of confining medium and specimen, respectively and U is velocity of shock wave which is equal to sound velocity in m/s within the material. The above mentioned equations indicate the significance of a number of peening parameters such as confining medium, protective coating and mechanical strength of specimen material. The equations 2-5 and 2-7 illustrate the material with high density and inner acoustic speed will be able to build more amount of acoustic impedance. Simply equation 2-3 shows that higher impedance materials contribute to more powerful shock load. In this regards, confining medium must have lowest light absorption and adequate mechanical strength against the plasma pressure. However, in protective coating, high acoustic impedance itself is not determinant factor for increasing resulted pressure in specimen. This situation is explained by mismatch theory as per equation 2-8 [10]. This equation shows that, protective coating of lesser density causes shock load reinforcement. Hence this phenomenon is significant that it can be used for amplification of low power shock loads and contributes to realization of HRLSP.

$$\frac{P_2}{P_1} = \frac{4\rho_2}{\left[(\rho_2)^{\frac{1}{2}} + (\rho_1)^{\frac{1}{2}}\right]^2} \quad (2\text{-}8)$$

Where P_1 (peak shock load before the protective coating) is calculated by equation 1, ρ_1 is density of protective coating and ρ_2 is density of work piece in gr/cm^2 and P_2 is resulted pressure at workpiece. However, shock load could be raised by increasing the impedance of protective coating. Hence, it can be stated that proper material for protective coating should have lowest density and highest sound speed as possible. In addition, the thickness of protective coating plays a significant role towards uniform shock propagation. The appropriate thickness can be calculated by equation 2-9 [10].

$$d \leq 2U_s.\tau \qquad (2\text{-}9)$$

The thickness of coating layer (d) is a function of sound speed in protective coating (U_s) and laser pulse duration (τ). For more thickness, attenuation of mechanical shock load and for lower thickness, rupture of coating foil will be expected.

2.3 HRLSP Model

2.3.1 Laser specification

Laser power intensity: Substantial difference of low and high repetition rate laser is the peak power of laser pulses. Hence, providing sufficient power intensity is a significant factor for possibility of HRLSP. When spots become circular, the intensity is calculated by equation 2-10 [11].

$$I = \frac{P/f}{0.78D^2.\tau} = E/tA \qquad (2\text{-}10)$$

Where, P is laser power (W), f is pulse repetition rate (Hz), D is laser beam diameter (mm) and τ is pulse duration (s). In order to effect laser peening, the laser intensity should be beyond the determined magnitude. Zhang and Yu (1998) had optimized this magnitude by proposing a condition as in equation 2-11 [12], where, required power density for peening should be

$$\frac{64\left(\sigma_Y^{Dyn}\right)^2}{\alpha.Z.C_t} < I < \frac{64\left(\sigma_U^{Dyn}\right)^2}{\alpha.Z.C_t} \qquad (2\text{-}11)$$

In equation 2-11, I is laser power density in (GW/cm^2), σ_Y^{Dyn} is dynamic yield stress, σ_U^{Dyn} is ultimate dynamic stress, Z is impedance because of work piece and confining medium interface that is calculated using equation 2-5 and C_t is transparency coefficient of confining medium. With equations 2-1, 2-3, and 2-11 it can be seen that, peening of materials with lower mechanical strength like magnesium needs lower laser intensity compared to materials with higher mechanical

strength. For instance, the threshold intensity for peening magnesium will be 0.013 GW/cm^2, when acrylic has been used as confining medium. Whereas, in identical conditions; the threshold intensity for peening stainless steel should exceed 0.25 GW/cm^2.

Figure 2-2 presents the effects of laser repetition rate and spot size on intensity. In the figure the broken lines indicate the relationship between laser power varied from 5 to 15 watts in the x-axis and the Laser intensity in the left Y axis for pulse repetition rate of 10 KHz. The spot sizes have been assumed as 1 mm and 0.5 mm, for computing the intensity. The confining medium is acrylic. The horizontal solid line at 0.013GW/cm^2 shows the threshold intensity required for peening magnesium. From the figure it is evident that if spot size is selected as 1mm, the intensity is not sufficient to effect peening, even with increasing the laser power up to 15 W.

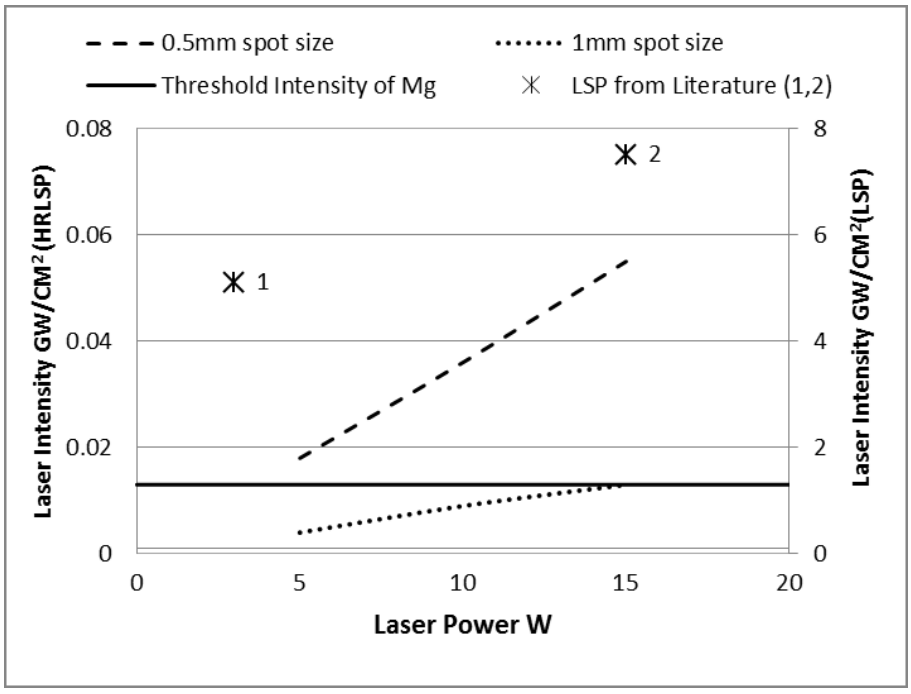

Figure 2-2 Impact of Repetition rate

However, by reducing the spot size to 0.5 mm of lesser, peening can be effected even using 5W of laser power. In order to show significance of repetition rate on intensity, two low repetition peening examples are shown from previous researches [42][61] with Laser power in the x-axis and Laser intensity in the right Y-axis. In first point, the laser power is 3 watts, pulse duration is 7ns, repetition rate is 30 Hz and spot size is 0.6mm which provides laser intensity around 5.5GW/cm^2.

In second point, power is 15 watts, spot size is 1.8mm and pulse duration is 8 ns [13] which provides laser intensity around 7.5GW/cm^2. Although, identical laser power have been applied on the specimens in the literature as well as in the current study, the intensity levels in low repetition rate lasers are at least ten times more than high repetition ones.

In order to achieve adequate intensity for peening, it is significant to define appropriate lens for obtaining required spot size in the order of several microns. The required spot size could be calculated by equation 2-12 [11].

$$d = 2.44 \times f.\lambda/D \qquad (2\text{-}12)$$

Where, f (mm) is focal length and D (mm) is initial beam diameter, λ (mm) is wavelength and *d* (mm) is spot size diameter. The benefit of reduction in spot size is that this causes accumulation of CRS much closer to surface [11]. This phenomenon can have positive effect on better control on corrosion rate, while reducing the fatigue strength of the material. This is more beneficial in terms of biodegradable implants such as Magnesium alloys for which this study is performed.

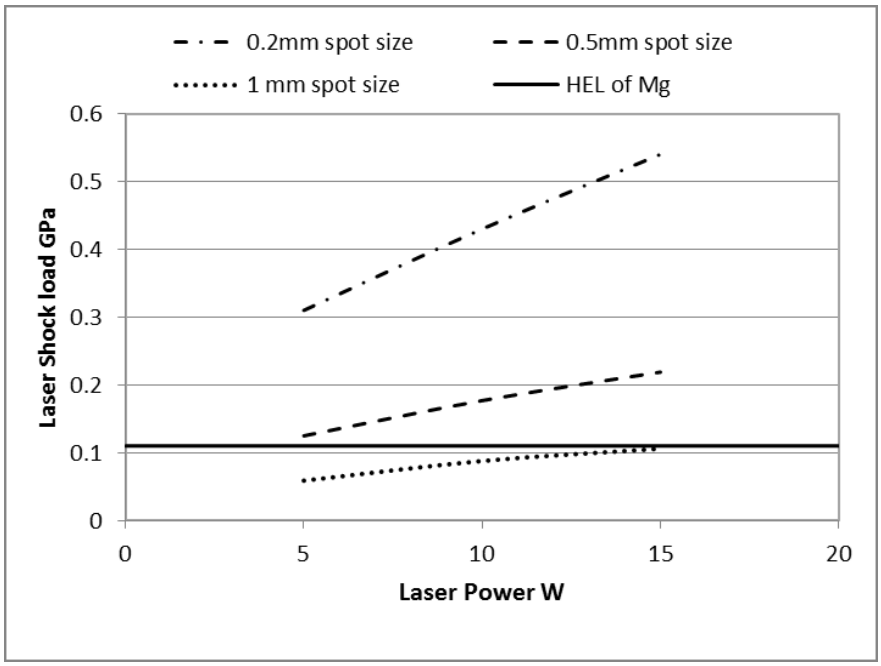

Figure 2-3 Impact of spot size on pressure

Figure 2-3 shows impact of spot size on generated pressure. For this graph magnesium is assumed as the workpiece, pulse duration is 14 ns, repetition rate is 10000Hz and acrylic is the confining medium. The broken lines show the relationship between laser power range in the x-axis varied from 5 to 15 watts and the laser shock load for 0.2, 0.5 and 1 mm spot sizes. The solid line at

0.11GPa shows the HEL of Mg calculated from equation 2-1. It can be clearly seen that, the shock pressure from 0.5 and 0.2 mm spots exceed the HEL of Magnesium, thereby making HRLSP feasible. However for a spot size of 1 mm peening is not possible within the studies laser power range.

Scan speed: Increasing repetition rate of laser leads to increasing number of shots. This is another significant difference between LSP and HRLSP. Consequently, surface engraving or machining might occur instead of peening. In order to avoid this, laser scan speed must be increased corresponding to the increase in repetition rate. Equation 2-13 is able to calculate the required scan speed.

$$S_s = D_s \times [1 + (1 - O_p)(f - 1)] \qquad (2\text{-}13)$$

Where, S_s is scan speed in mm/s, D_s is spot size in mm, f is repetition rate and O_p is overlap percentage. Although, HRLSP is performed by micro spots, X-Y table for scanning will not be sufficient to provide the required scan speed. Galvo-mirror as a high speed optical device contributes to overcoming this difficulty. Determination of spot size is primary factor for proposed appropriate scan speed. The required spot size, focal length and scan speed can be calculated using equations 10-13, which will help design the optical system for peening. For instance 50 μm is an

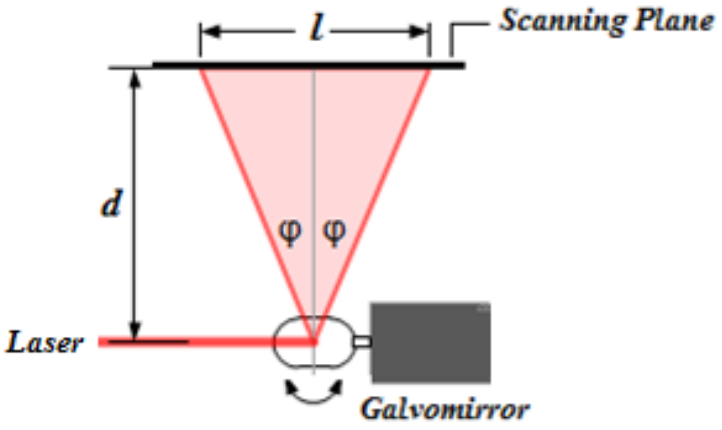

Figure 2-4 Galvomirror scanning mechanism

appropriate size which can be assumed for peening Magnesium. Where, repetition rate is 10000Hz, power is 12W and pulse duration is 14 ns, the appropriate scan speed will be 500mm/s. Figure 2-4 shows a schematic a Galvo-scanner. The laser irradiates on two mirrors respectively to provide scanning in both X and Y direction. The length of scanning could be achieved by equation 2-14

$$L = 2d.\tan\varphi \qquad (2\text{-}14)$$

Where, L is length of scanning and d is distance between scanning plane and second mirror and $\boldsymbol{\varphi}$ is oscillation angle.

2.3.2 Peening Specifications

Protective coating and confining medium are two significant parameters which have critical impact on possibility or improvement of HRLSP.

***Protective coating**:* Protective coating not only protects specimen surface against the direct laser irradiation, but also under particular modality, it can play a role of shock load amplifier. The effectiveness of a number of different protective coatings on pressure reinforcement or attenuation has been shown in figure 2-5. Where, the laser power is 10 watts, pulse duration is 14 ns, repetition

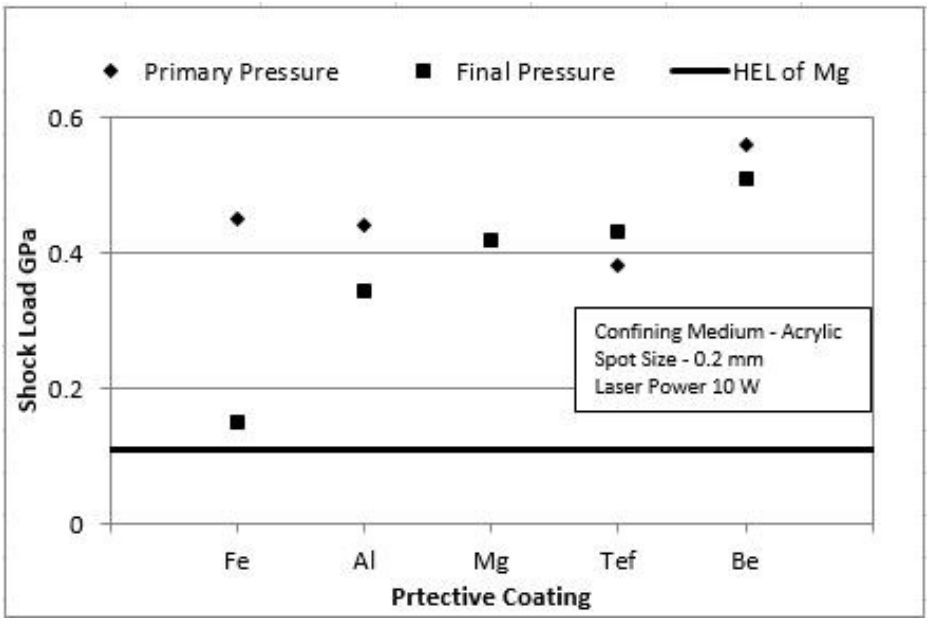

Figure 2-5 Effect of Protective Coating on shock load

rate is 10000Hz, spot size is 200 µm and confining medium is Acrylic. If the density of protective coating is less than the specimen density, the resulted pressure can be amplified. This circumstance can be interpreted by mismatch theory mentioned in equation 2-8. Although, the primary generated pressure (generated pressure before the protective coating by equation 2-3) by iron foil is more than aluminum, the resulted pressure (generated pressure after protective coating by equation 2-8) is less than half of pressure which is created by Aluminum foil. Beryllium with more density

compared to magnesium causes more pressure even in comparison with Teflon with lower density. This is because of sound speed in Beryllium exceeds 12860m/s and highest acoustic impedance (Z) has been achieved. Therefore, the resulted pressure is the highest of all the protective coatings tested in this study. In order to define appropriate protective coating, it should be a material of lowest density and highest acoustic velocity with acceptable level of mechanical strength. The ultimate tensile strength of protective coating should be more than shock pressure, so that the coating rupture can be avoided.

***Confining medium**:* Choosing the appropriate confining medium is another critical factor in HRLSP. Figure 2-6 demonstrates effectiveness of different confining mediums on shock load. In this case, the laser power is 10 watts, pulse duration is 14 ns, repetition rate is 10000Hz, and spot

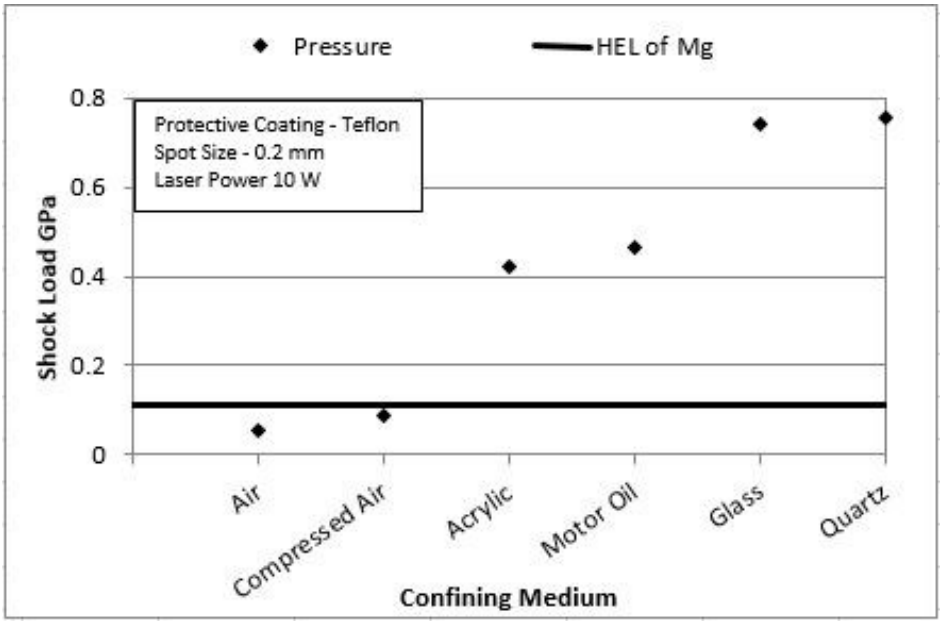

Figure 2-6 Effect of Confining Medium on shock load

size is 200 µm and Teflon is the protective coating. Although Beryllium is able to generate more powerful shock load (figure 2-5), due to its high cost, Teflon has been preferred for this part of the study.

From figure 2-6 it can be understood that glass or quartz as two proper confining mediums, can increase shock load up to 10 times more than air. In case of air and compressed air at 100 Bar, peening cannot be effected because the generated shock load in both cases is less than the HEL of Magnesium. Whereas, applying acrylic and motor oil shows acceptable level of pressure for

successful peening. High acoustic impedance of quartz and glass provide ability to achieve maximum shock load. However, use of hard confining medium for complicated shapes like implants is not convenient. Therefore liquids, particularly water, have vast applications for complex work-piece shapes. Water has similar properties to that of acrylic and the resulted shock load will be similar to that of acrylic in figure 2-6. Owing to probable chemical reaction of water and magnesium, motor oil can be offered as a liquid alterative confining medium for complicated shapes, but motor oil may be combustible and mg is highly inflammable as well. Hence, liquids with high acoustic impedance and low chemical reactivity could be used as confining medium for peening magnesium. The table 2-1 indicates relative merits and demerits of different confining mediums.

Confining medium	Advantages	Disadvantages
Solids: Quartz, Glass, Transparent Spinal Ceramics	-Highest pressure(due to highest acoustic impedance) - High transparency	-Not applicable to complicated shapes -Remained glass dust
Liquids: water, motor oil, High Density organic liquids	-Can be applied to complicated surface, -Suitable for multiple shocking – Cooling	-Wet method -Lower pulse pressure -Probability of chemical Reaction

Table 2-1 Comparison of different confining medium for LSP [12]

2.4 Discussion

The critical point in laser shock peening is HEL magnitude which is a function of material; and the applied laser characteristics. A number of researches that are referred in this study have proved the relationship between increasing CRS and modification in mechanical attributes of work pieces. Based on the literature, mechanical attributes such as fatigue, corrosion resistance, hardness and wear resistance will be enhanced by laser peening. The results of proposed study show the feasibility of HRLSP with a regular nanosecond pulsed laser at 0.2 laser spot size and 10 W power, which is able to generate 0.8 GPa shock pressure.

In first glance, due to the significant difference between generated shock load by LSP and HRLSP, it seems this method cannot be efficient, but while the specimen has low mechanical strength,

HRLSP can be very effective, particularly in terms of corrosion control. Moreover, HRLSP is much faster to perform compared to LSP. For instance, HRLSP by 10 KHz laser and 0.2mm spot size could peen an area of 20×20mm in 2 seconds. Whereas, it takes 10 seconds for LSP with 10Hz and 2mm spot size for the same area. In addition to this, due to the use of Galvo-mirror, selective peening can be performed precisely and peening of tiny workpiece such as biodegradable cardiovascular stents would now be possible. Due to goal of this research, which is to reduce the corrosion rate of magnesium based biodegradable implants, it is better to use HRLSP as a lower capital cost and faster method of peening. The table 2-2 indicates a comparison of HRLSP and LSP performance.

	LSP	HRLSP
Cost of equipment	Expensive	Not expensive
Process speed	Medium	Fast
Fatigue modification	Better performance due to dipper and more CRS accumulation	
Corrosion control		Better due to smaller spot size
Increasing hardness	Better performance due to more CRS accumulation	
Wear reduction	Better performance due to more CRS accumulation	
Precise peening	Medium	High

Table 2-2 Comparison of HRLSP and LSP

2.5 Conclusion

To the knowledge of the authors, high repetition rate laser shock peening is a novel method of laser peening. Due to, low energy of each pulse, in order to carry out of successful HRLSP, spot size reduction, drastic and proper controlled increase in scan speed, applying appropriate protective coating and also use of efficient confining medium are needed and this has been identified in this work. By modification mentioned factors, the required power intensity and pressure can be achieved for a successful peening. It has been recommended, in order to HRLSP Magnesium, the best choice could be: Magnesium foil as protective coating and quartz for flat and motor oil or any proper liquid with low chemical reaction and high acoustic impedance for complicated shapes as confining medium. Low cost equipment, fast performance, and accumulation of compressive residual stress closer to the surface providing better corrosion rate

control are the main reasons for assessing the feasibility of HRLSP as a novel method instead of LSP. This is particularly useful in production of biodegradable magnesium based implants, such as cardiovascular stents.

Having concluded that the High Repetition Rate Laser Shock Peening is theoretically feasible, in chapter 3, the experimental verification of HRLSP will be assessed. Chapter 3 is aimed at peening magnesium samples with different laser parameters, and assessing specific parameters like hardness and roughness. These parameters will then be compared with that of unpeened magnesium to experimentally verify the occurrence of peening.

CHAPTER 3. High Repetition Laser Shock Peening on Magnesium Based Biodegradable Alloys

This chapter is based on an article published in Journal of Laser Micro/Nanoengineering [31]. This chapter covers the objective '2a' of the "Objectives and Scope of the Thesis" in section 1.9

3.1 Introduction

Complications of second surgery for removal of permanent implants were the original idea to propose a new generation of biodegradable implants. Recently, magnesium based alloys have been identified as a potential degradable alloys [8]. These biomaterials could be excellent materials in terms of biomechanical aspects, have comparable mechanical strength to bones and have privilege of avoiding stress shielding [5]. However, in order to fix broken bone, fixators having sufficient mechanical strength are required. Otherwise, subsequent breakage of the treated bone can occur [68]. Increasing compressive residual stress (CRS) is the advanced methods that has been introduced for enhancement of mechanical attributes. Due to numerous exclusive merits, laser shock peening (LSP) has been recommended as a potential method for creation of CRS upon the specimen surface. Deeper and higher magnitude of CRS achieved with LSP [69] has desired performance of specimen in corrosive environment [70]. In addition, LSP has undeniable positive effect on fatigue strength of peened sample [46]. Currently, LSP is performed with high power low repetition pulsed laser[70][46][24]. High cost devices and low speed method are the main restrictions in LSP. Hence, it is appropriate to evaluate the possibility of high repetition laser shock peening (HRLSP) that is more economical and much faster as an alternative to LSP. For HRLSP, tight focusing of laser beam diameter to few micrometers, using appropriate confining medium, utilization of suitable protective coating and highly accurate adjustment of laser scan speed by a Galvo-mirror are proposed works in this thesis. The fact that mechanisms of LSP and HRLSP has been based on the identical principles, similar to LSP the occurrence of HRLSP is recognized by a number of experimental methods such as measurement of changes in surface roughness, peening depth and hardness.

3.2 High Repetition Laser Shock Peening (HRLSP)

As long as the absorption of laser energy exceeds the material threshold, ablation is conducted and the material is transformed from solid to gas state, directly. The metallic gas captures adequate energy and its temperature increases drastically. Consequently, free electrons can be departed atoms and plasma is affected [24]. Plasma can generate a high pressure (GPa range) over the course of few nanoseconds. The achieved shock pressure can be calculated by the equations 3-1 to3-4 [49].

$$P = 0.01\sqrt{\frac{\alpha.ZI}{2\alpha+3}} \qquad (3\text{-}1)$$

$$\frac{2}{Z} = \frac{1}{Zs} + \frac{1}{Zc} \qquad (3\text{-}2)$$

$$I = \frac{P_w/f}{0.78D^2.\tau} = E/\tau A \qquad (3\text{-}3)$$

$$Z = \rho U \qquad (3\text{-}4)$$

Where, P (GPa) is the shock pressure, Z (g/cm^2.s) is the impedance of shock wave, E (J) is average energy of a pulse, τ (nanosecond) is laser pulse duration and D (mm) is the diameter of laser beam or spot size, α is a constant that is proportional to efficiency of laser absorption (if most of laser energy absorbed by surface, α will be close to 0.1), A is spot size area, I is laser intensity in Gw/cm^2, P_w is average laser power in watt, f is repetition rate in Hz and Z_C and Z_S are the impedances of confining medium and specimen, respectively. ρ is density in g/cm^3 and U is velocity of shock wave and it is equal to sound velocity in cm/s within the material. Providing the shock load exceeds the Hugonoit Elastic Limit (HEL) [48], laser shock peening will be effected. HEL is presented by equation 3-5

$$HEL = \frac{(1-\vartheta)\sigma_Y^{Dyn}}{1-2\vartheta} \qquad (3\text{-}5)$$

where υ is Poisson‘s ratio and σ_Y^{Dyn} is dynamic yield stress. Therefore, the principal term for laser peening is $P > HEL$, provided that pulse duration is adequately small and it should be proved by equilibrium in equation 3-6 [22].

$$\tau \ll r_0\sqrt{\frac{\rho(\lambda+2\mu)}{4\mu(\lambda+\mu)}} \qquad (3\text{-}6)$$

Where, μ and λ are lama constants, r_0 is radius of spot size and τ is pulse duration.

Equations 3-1 to 3-5 can reveal reasons of difficulty in HRLSP. Owing to P_w and τ being approximately constant, as long as *f* increases up to 10000 Hz in equation 3-3, the intensity (I) decreases 10000 times. Hence, P in equation 3-1 decreases drastically and required pressure by equation 3-5 cannot be provided. In order to amplify shock pressure, reduction of beam diameter (D) in equation 3-3 and enhancing of Z in equation 3-1 are two possible approaches. The D can be condensed by appropriate lens and Z can be enhanced by choice of proper confining medium (CM) and protective coating (PC). The equations 3-2 and 3-4 indicate impact of CM and PC on Z magnitude.

3.2.1 Design of laser scanning system/specifications

In order to avoid multiple laser shots at the same point, the scan speed should be designed , properly. The required peening scan speed (S_s) without overlap along the y-axis, is achieved by equation 3-7.

$$S_s = D \times [1 + (1 - O_p)\,(f - 1)] \qquad (3\text{-}7)$$

Where, O_p is percentage of overlap as displayed in figure 3-1.

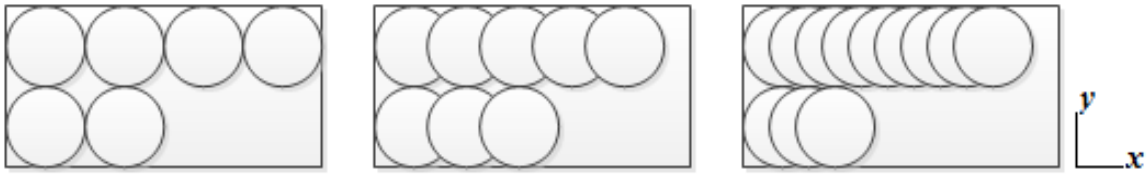

a) 0% overlaps **b) 33% overlap** **c) 66% overlap**

Figure 3-1 Overlap along the X-axis

From equations 3-1 to 3-5, it can state the 40 μm is an appropriate size of D for peening of magnesium specimens where, repetition rate is 10 KHz. The speed calculation of the peening at 40 μm spot size is explained in the next section. The proper scan speed at 40 μm with 0% overlap is 400 mm/s. In order to, provide this high scan speed for LSP, use of galvo-mirror *THORLABS GVS002*, is proposed. The system consists of two galvano mirrors each attached to a servo DC motor. The servo motors are controlled with a *NI6211 USB* DAQ board. This board gets the motor's desired position as an analog voltage and sets the motor's position to an angle proportional to the applied voltage. The range of the analog voltage is between -10 to +10. The range of motion of each motor is between -12° to +12°. Hence, the voltage range between -10 to +10 volts

corresponds to 24° of motion range which provide a resolution 1.2°/V. The DAQ is equipped with two analog outputs which provide the desired set points for motors. A LabView program has been developed to control the output voltage and subsequently the motor position. Each motor is responsible for 1 degree of freedom (DOF) movement of the laser on the work piece. A desired path is produced to cover evenly a 10 mm square on the work piece. For this, one of the motor is controlled using a triangular profile signal (Figure 3-2-a) with a magnitude that covers the 10 mm in the X axis. At each top and bottom peak of the triangular profile the other motor moves forward one step in the Y axis and remains at that position until the next peak of the triangular profile (Figure 3-2-b) covering the square of 10 mm on the workpiece.

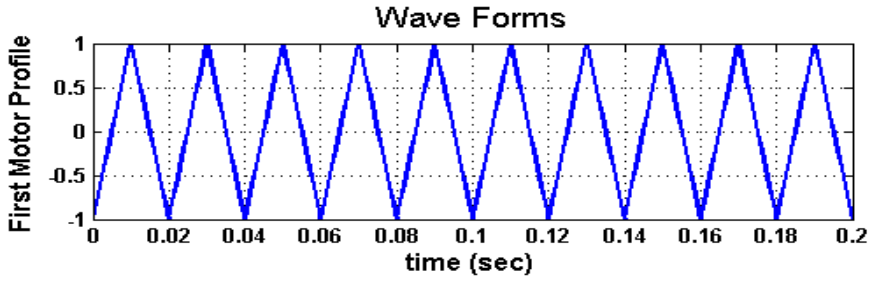

(a)

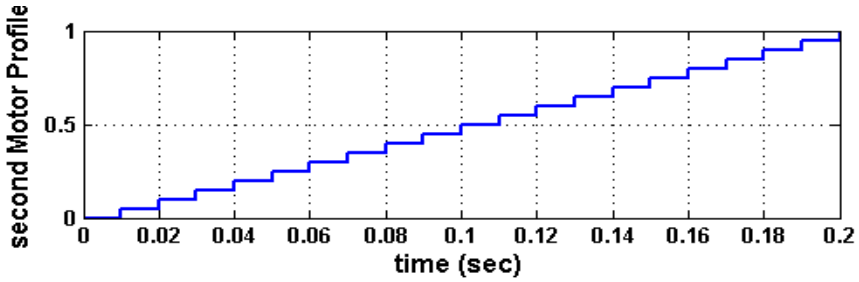

(b)

Figure 3-2 DAQ signals for X and Y axis servo-motors

The laser that is used in this work is PRISMA TM1064-V diode pumped, solid-state laser and its specifications are given in table 3-1. Aforementioned, the scan speed at 40 μm with 0% overlap is 400 mm/s. From figure 3-3, *l*=10 this means 400/10=40 lines need to be scanned in a second. In other words, mirror oscillation frequency (MOF) should be 40 Hz. For spot size of 60 μm, the required scan speed is 600 mm/s according to equation 3-7. Therefore, MOF must be 60Hz. Determination of spot diameter (d) is conducted by equation 3-1 and 3-3 for having a successful HRLSP. Spot size is a function of initial laser beam diameter (D), laser wavelength (λ) and focal

length (f_L) of the lens. By use of equation 3-8, the required initial beam diameter has been determined in table 1.

$$d = 1.27 \times f_l \frac{\lambda}{D} \qquad (3\text{-}8)$$

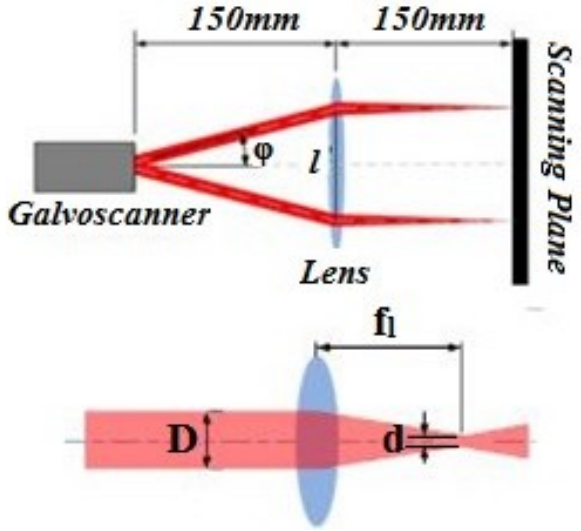

Figure 3-3 Adjustment optical devices for HRLSP

d*	**D***	**MOF$_0$***	**MOF$_{33}$**	MOF$_{66}$	
40	5.06	30	19.8	9.9	
60	3.37	60	39.6	21.78	
d*	**Φ_X°**	**Φ_Y°**	**S$_0$***	**S$_{33}$**	**S$_{66}$**
40	±1.909	0.015	400	266.66	133.33
60	±1.909	0.022	600	400	200

d: Spot size (mm) D: Initial beam diameter (mm)
MOF: Mirrors Oscillation Frequency (Hz)
Φ: Mirrors Oscillation S: Scan speed (mm/s)
The subscript 0, 33 and 66 define the % overlap as in Fig.1

Table 3-1 Laser specifications for 40 and 60 μm spot sizes

3.2.2 Peening specifications:

Excluding of effectivness of laser specifications on HRLSP, peening parameters such as strength of specimen, confining medium (CM) and protective coating (PC) have fundamental influence on occurance of HRLSP.

The equations 3-2 and 3-4 define impact of CM on shock pressure. Quartz and glass with higher impedance (Z) compared with air, water and motor oil can increase Z_c. Increasing of Z_c leads raising Z and enhancement of shock pressure has been resulted. The figure 3-4 demonstrate significance of CM on enhancement of shock pressure, where applying of quartz and glass can creat highest shock pressure compared with other CMs. The figure has been drwan by carrying out of equations 3-1 to 3-5. The figure 3-5 indicates influence of PC on shock pressure. This figure shows that the maximum resulted shock pressure can be generated with beryllium foil as PC. Beryllium with the highest sound speed (12800 m/s), provide higher Z and according to eqaution 3-1, the shock pressure can be increased. Furthermore, lower density of beryllium as PC compared with specimen (magnesium) leads enhancement of shock pressure, as well. This phenomenon can be interpreted by mistmached theory in equation 3-9 [63].

$$\frac{P_2}{P_1} = \frac{4\rho_2}{\left[(\rho_2)^{\frac{1}{2}}+(\rho_1)^{\frac{1}{2}}\right]^2} \qquad 9$$

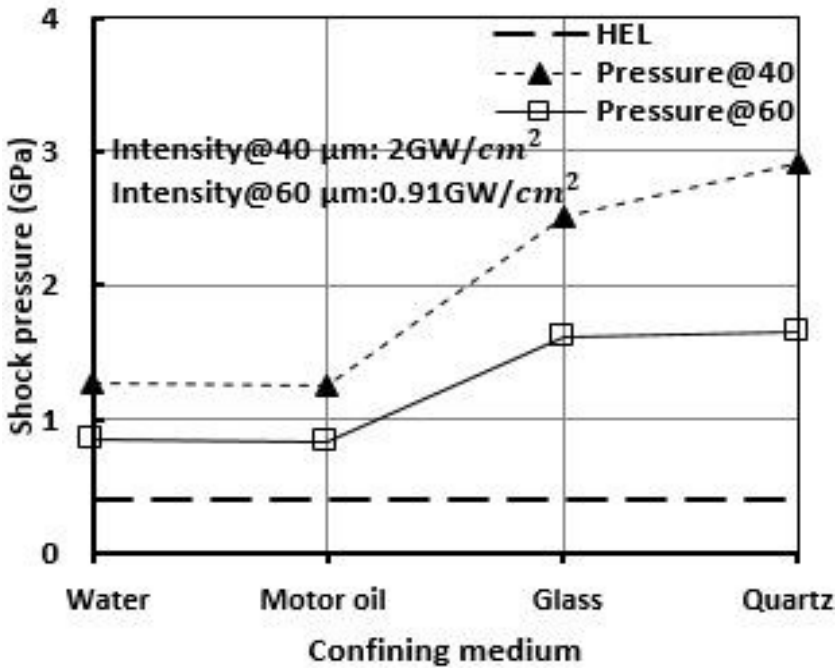

Figure 3-4 Impact of confining medium (CM) on shock pressure

Where P_1 is shock pressure before the protective coating that is calculated by equation 1, ρ_1 is density of PC, ρ_2 is density of specimen and P_2 is resulted pressure. the figure 3-5 has been achieved by equations 3-1 to 3-5 and 3-9. More elaborate explanations, have been proposed in

recent research of this study of author [30]. Even though beryllium can amplify the shock pressure, considering the cost of beryllium, PC has not been used in our experiments.

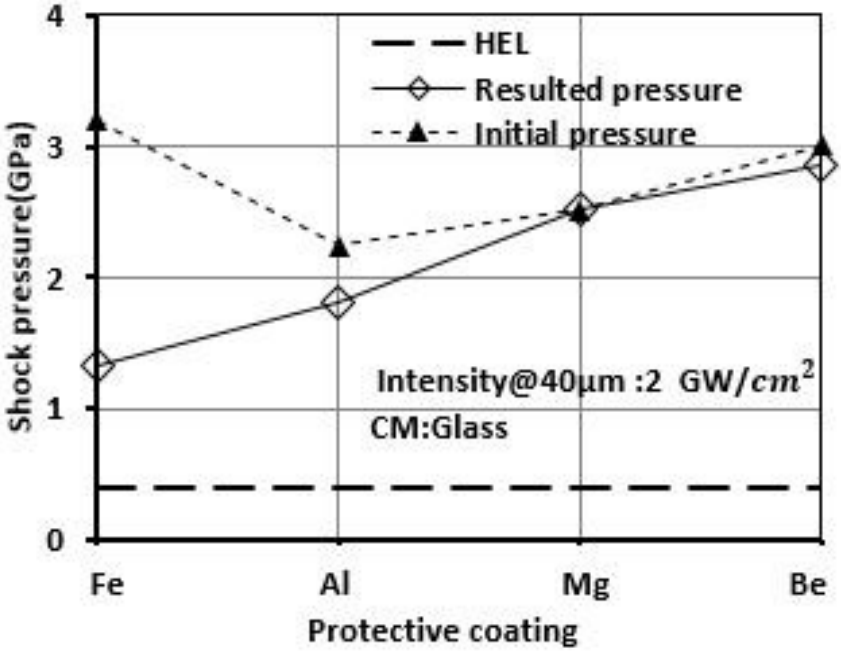

Figure 3-5 Impact of protective coating (PC) on shock pressure

3.3 Design of Experiments (DOE)

In design of experiments, the significant parameters should be cosidered as involved factors. The equation 3-3 indicates the laser intensity (I) is one of important parameters which is varied by beam diameter (D). It must be noted that repetition rate, laser power and pulse duration have been assumed as constant parameters. In addition to D, number of scans (the number of repeating shots at an identical point) and percentage of overlap are other variables in this work. Since, some portion of laser energy is absorbed by through passing of optical devices, the effective laser power should be determined. As shown in figure 3-6,The laser power in A, B, and C is measured by *Gentec UNO* at 4.8W, 3.55 W and 3.52 W, respectively. By having, effective laser power (3.52 W at C) and conduction parameters of table 1at equations 1-5, the proper D for laser peening must be less than 70 μm. Furthermore, some constraints in applied optical devices leads more reduction of D (less than 35 μm) cannot be executable. Thus, two magnitudes of D at 40 (for Evaluation of HRLSP at a perfect peening situation because of more than sufficient intensity which is provided at 40μm) and 60 μm (for evaluation of HELPS occurrence in boundary condition) are used as proper choices.

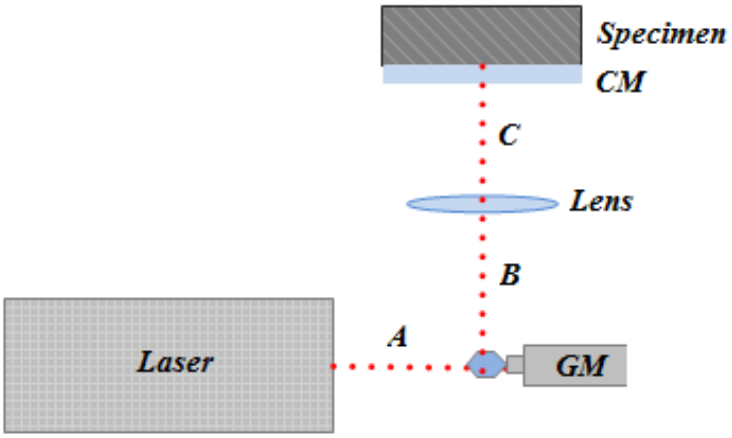

Figure 3-6 Measurement average laser power in different regions

In all experiments the used laser is PRISMA TM 1064-V diode pumped, solid-state laser. The laser power is 3.52 W at 10 KHz repetition rate. Pulse duration is 14 ns, wavelength is 1064 nm and initial beam diameter (D) varied from 5.06 to 3.37 mm for 40 and 60 µm spot sizes, respectively. Therefore, the intensity of 2 GW/cm^2 at 40 µm spot size and 0.91 GW/cm^2 at 60 µm spotsize is available for peening magnesium specimens, where glass with 1 mm as CM are clamped to specimens. To have grater effect of shock pressure, the interface between CM and surface of specimen should be reduced as possible, otherwise air can be considered as CM instead of glass and shock pressure declines, drastically. To reduction thickness of interface between CM and specimen, all specimens have been polished to mirror surface and surface roughness has been reduced to 0.25 µm. Considering the two variables for D (40 and 60 µm), three variables for number of scans (1, 2 and 3 scans) and three variables for %overlap (0%, 33% and 66%), 18 experiments must be performed. Note that, more peening by increase in number of scan and percentage of overlap can create more probable plastic deformation on the surface. Hence, it is significant to create predictable curves for forecasting impact of % overlap and number of scans. For this, at least 3 sets of experiments are required and 1, 2 and 3 scans of peening have been proposed. Also, for % overlap 0% which is no overlap, 33% which equals 1/3rd of the spot size and 66% which equals 2/3^{rds} of the spot size were chosen. Hence, eighteen circular specimens (99.8%Mg-0.2%Ca) with 33 mm diameter and 6 mm thickness have been prepared for experiments as in table 3-2. In the first three experiments 1-3, the spot size is maintained at 40 µm, peening overlap at 0% and the effect of number of scans 1, 2, 3 are studied. In experiments 4-9 the overlap was increased to 33% and 66% by varying the scan speed. In the next 9 experiments, 10-18, the

spot size is changed to 60 μm and the effect of reduction in intensity by increasing spot size diameter, percentage of overlap and number of scans are studied. In order to evaluate the occurrence of HRLSP on magnesium, three approaches are proposed in this research.

a) Measurement depth of deformed rigions upon the specimen surface by *WYKO NT1100* interfrometer and comparison of theoretical and experimental magnitudes.

b) Measurement increasing hardness by *MVK-H1 Mitutoyo* micro-hadness tester.

c) Measurement of changed surface roughness by *WYKO NT1100* interfrometer and scanning electron microscopy (SEM).

Specimen number	Spot size(D)	%Overlap	Number of scans
1	40	0	1
2	40	0	2
3	40	0	3
4	40	33	1
5	40	33	2
6	40	33	3
7	40	66	1
8	40	66	2
9	40	66	3
10	60	0	1
11	60	0	2
12	60	0	3
13	60	33	1
14	60	33	2
15	60	33	3
16	60	66	1
17	60	66	2
18	60	66	3

Table 3-2 List of experiments

3.4 Results and Discussion

3.4.1 Peening depth evaluation

Plastic deformation by laser peening leads to change in surface topography. This issue has been presented by previous research on magnesium [42].

Measurement of depth of peened regions and comparison with theoretical magnitude that can be calculated by equation 10 is one of the reliable methods for assessing HRLSP occurrence [22].

$$\varepsilon_P = -\frac{2HEL}{2\mu+3\lambda}\left(\frac{P}{HEL}-1\right) \qquad (10)$$

Where, ε_P is depth of peening due to one laser shot, P is shock shock pressure, μ and λ are lama constants those are 15.4 and 36.3GPa respectively for magnesium. Figures 3-7 and 3-8, demonstrate the interfrometric line scan of samples peened with 40 and 60 μm laser spots in a single scanning pass and 0% overlap.

In the figures the X axis shows the width of the peened spots and the Y axis shows the depth of peening. Also the theoritical depth of peening calculated by equation 3-10, is shown as reference

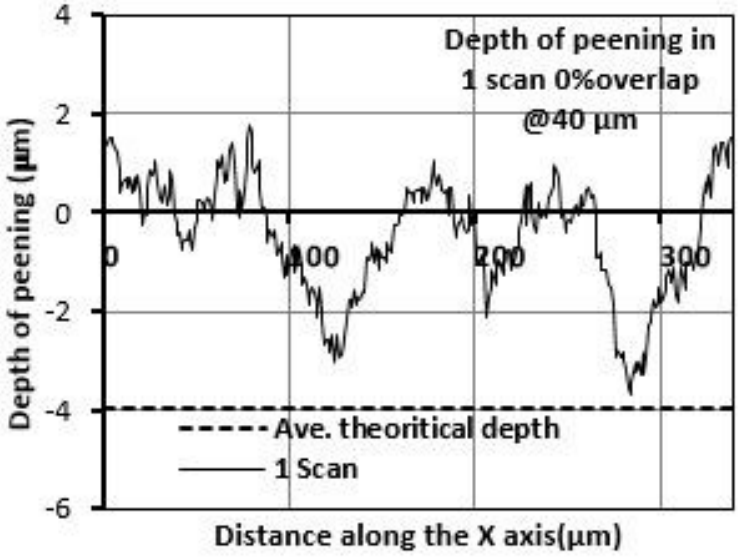

Figure 3-8 Fluctuations of peening depth at 40 μm

in the figure with a broken line (3.97μm for 40 μm spot and 2.24μm for 60 μm spot). It can be

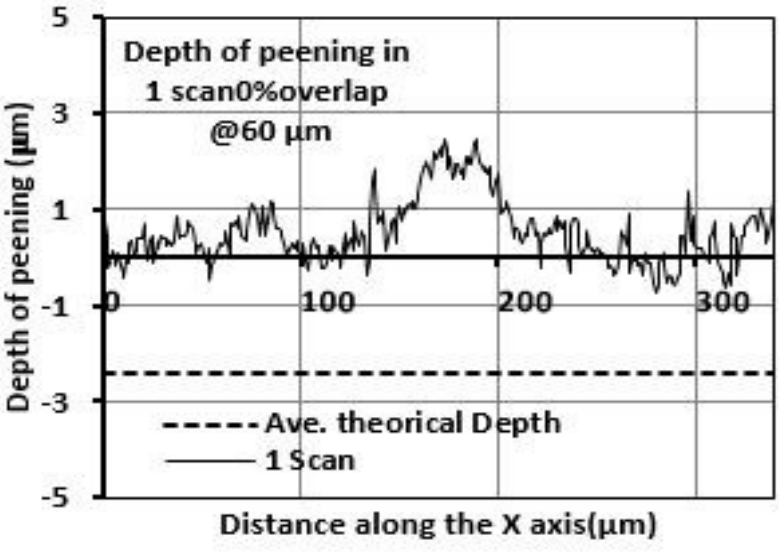

Figure 3-7 Fluctuations of peening depth at 60 μm

clearly seen that magnitude of peened depth 3 to 3.8µm from experiments is close to the theoritical magnitude with 3.97 µm. As the spot size increases to 60µm, this difference becomes 2 µm in figure 3-8.

The intensity has been reduced to 0.91 GW/cm^2. The notable difference in experimental and theoritical results at 60µm spot size is caused by reduction in laser intensity,which is not sufficient for effective LP. Regarding 60 µm experiments, it can state there is a combination of peening and machining (surface melting). Furthermore, in both figures theoritical depth in all experiments are more than experimental results.

Although, the measured laser power before the CM is 3.52W, hot plasma region reduces the CM transparancy. This means additional reduction in laser power after CM could be occurred and the real laser intensity is less than theory. In addition, oxidation of magnesium, forming a 5 µm thick layer [71] increases the hardness of magnesium which also increases the required pressure for peening. Therby, reducing the peening depth. This has been verified by conduction of micro hardness test immediately after polishing and the specimen that was used in experiment which shows increase in hardness from 38 to 45 HV due to oxidation. Though aforementioned reasons lead to reduction in shock pressure, the rest of the laser power has been adequate for peening at 40 µm spot size.

3.4.2 Hardness

Plastic deformation upon the specimen surface increases CRS [72]. The relation of hardness and CRS on magnesium has been observed in the literature [42]. Hence, notable change in hardness can be considered as an evidence to occurrence of HRLSP. Increasing laser intensity causes increase in plasma pressure resulting in higher CRS and hardness.

The effect of scanning parameters (percentage of overlap and number of scans) on hardness can be realized in figures 3-9 and 3-10, where the X-axis indicates % overlap and Y-axis specifies Vickers Hardness for various number of scans compared with unpeened specimens. Each of measurement has been repeated for three times and fluctuation of error bar indicate that, the percentage of error can be acceptable.

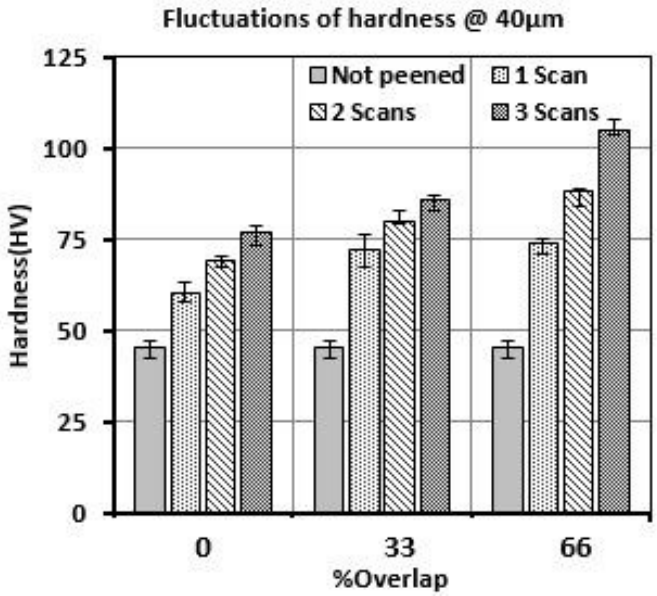

Figure 3-9 Fluctuations of hardness @ 40 µm

In Figure 3-9, it can be clearly seen that the hardness increases from 45 HV for unpeened sample to 60 HV for single scan at 0% overlap. This significant increase in hardness at single scan and 0%overlap can show the occurrence of laser peening. Note that, heat treatment (by laser heating) cannot be effective for enhancement of pure magnesium and it can be hardened by strain hardening that is created by cold working in laser shock peening [73].

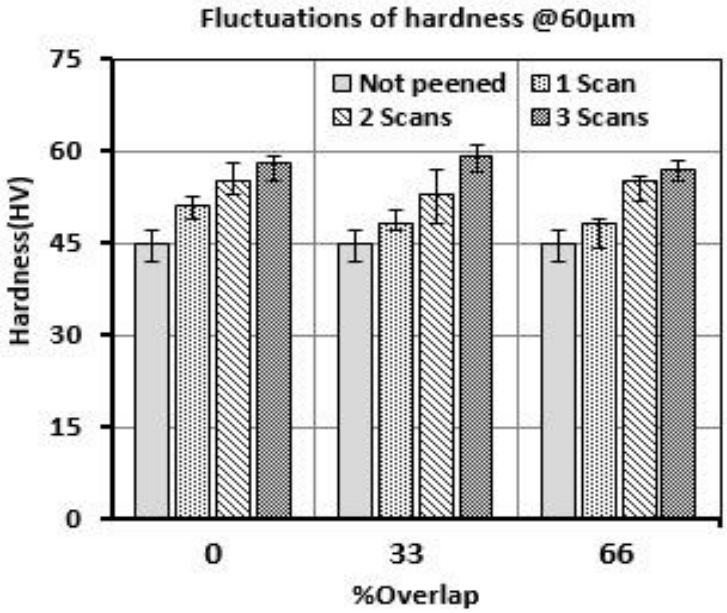

Figure 3-10 Fluctuations of hardness @ 60 µm

Furthermore, figure 3-9 demonstrates increase in number of scans and percentage of overlap leading to additional increase in hardness. This is similar to another reported work on laser peening [6]. From figure 3-9, the maximum achieved hardness is 103 HV that is 2.5 times higher than unpeened specimen. The comparable result has been reported in recent works on magnesium [42].

The Figure 3-9 indicates that the hardness of 3 scans, 0% overlap is 74 HV which is close to hardness of 71 HV at one scan, 66% overlap. This is due to equal energy magnitude has been applied to the identical area of specimens by the same numbers of laser shots. This shows that, the increase in hardness is correlated to the magnitude of applied energy used for laser peening. Figure 3-10 Fluctuations of hardness @ 60 **μ**mdemonstrates slight increase the hardness from 45 HV for unpeened specimen to 51 HV for single scan at 0% overlap. Additionally, increase in number of scans and percentage of overlap has a negligible effect, where the maximum achieved hardness is 59 HV that is just 1.25 times higher than unpeened specimen.

Referring Figure 3-4 Impact of confining medium (CM) on shock pressure, it can be seen that the increase in spot size from 40 to 60 μm, causes reduction in shock pressure. Consequently, the inferior shock pressure cannot create prominent cold working at 60 μm and lower hardness can be resulted. Therefore, even by increasing of number of scan and %overlap, enhancement of hardness in 60 μm experiments is not impressive.

3.4.3 Surface topography and roughness

A number of researches indicate that the controlled periodic shock pressure create uniform micro plastic deformation on the specimen surface [42][47]. Figures 3-11 and 3-12 show SEM of the specimen surface after HRLSP at 40 and 60 μm spot sizes, respectively (enlarged image shown as insert in the images for clarity). At 40 μm, there is no melting and solidified material remains on the peened region and the uniform surface is produced after laser irradiation, which can be seen in the SEM scan in figure 3-11. In lower laser intensity at 60 μm, it cannot see the same arrangement on the surface. The lower laser intensity cannot provide required energy to ablation and combination of LSP and laser surface melting (LSM) is created as shown in figure 3-12. Note that, in LSM, the laser energy is just adequate for converting surface specimen from solid to liquid stage.

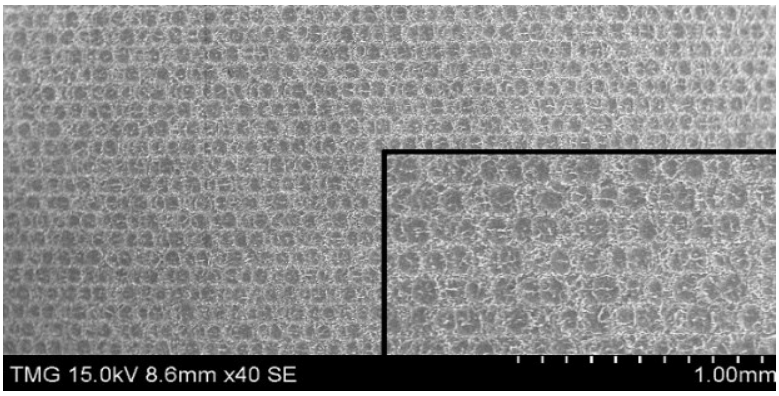

Figure 3-12 HRLSP of magnesium surface @40µm spot size

Closer inspection of figure 3-12, shows that the depth is shallower compared to peening at 40 µm and machined holes at the center of the spots could be observed. The melting that happens while machining causes solidified material to settle in the processed region which creates some disarrangement.

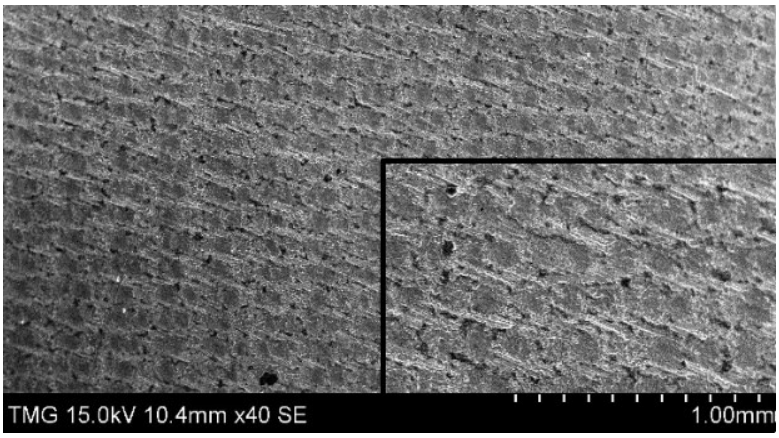

Figure 3-11 HRLSP of magnesium surface @ 60µm spot size

In order to more study the surface, average roughness (R_a) of all 18 specimens was measured with *WYKO NT1100* interfrometer. The results of these measurements are shown in figures 3-13 and 3-14 where the X-axis specify %overlap and Y-axis indicate the R_a value. In figure 3-13, it can be clearly seen that R_a increases with increase in number of scans. For instance in 0% overlap peening, the roughness has an important enhancement from 0.35 (not peened) up to 2.6 µm (3 scans). Correspondingly, for 33% overlap, the R_a enhances from 0.35 to 1.85 µm and for 66% overlap, it increases from 0.35 to 3.25 µm. It can also be seen that the R_a increases with increase in percentage of overlap, when using single scan, from 0.8 µm (single scan 0% overlap) to 1.8µm (single scan 66% overlap). However, at multiple scans peening there is a reduction while the overlap has been

33%. Increasing the % overlap eliminates some peaks from the previous scan. However, at higher overlap of 66% further plasticized material is being driven to peening sides and R_a increases.

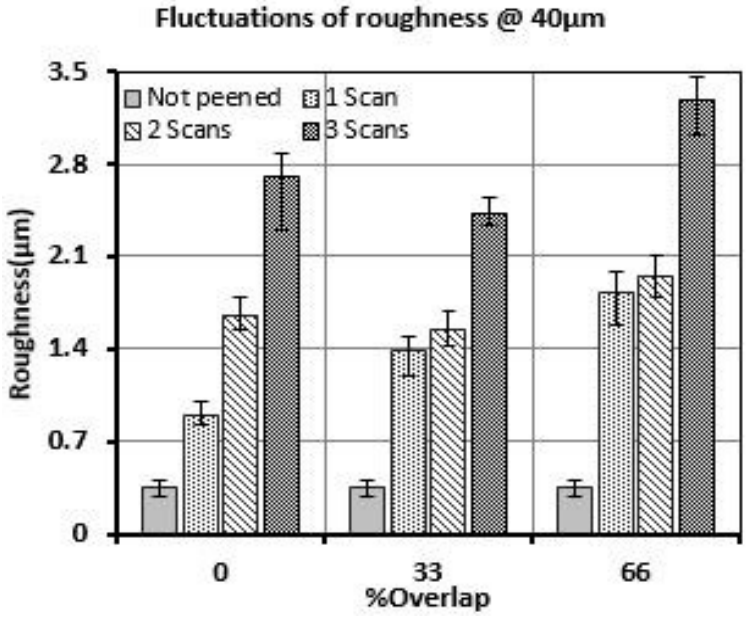

Figure 3-13 Fluctuations of roughness @ 40 µm

In figure 3-14, the increase in R_a is marginal for single scan regardless of the %overlap at 60 µm. The R_a increases from 0.35 to 1µm in case of 66% overlap and 2 scans. Highest increase in R_a

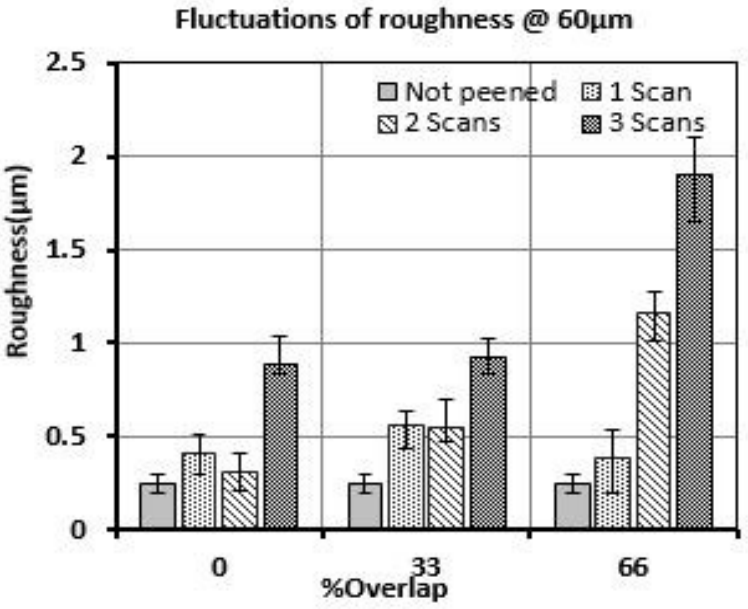

Figure 3-14 Fluctuation of roughness @ 60µm

from 0.35 to 1.8μm occurs at 3 scans, 66% overlap peening. At 66% overlap, 3 scans specimen this solidified material causes notable increase in R_a.

3.5 Conclusions

In this work, high repetition rate laser shock peening of magnesium is performed. To knowledge of the authors, this work is the first HRLSP on magnesium. The $NdYVO_4$ laser used for the experiments has a power of 3.52 W at 10 KHz repetition rate. The success of peening was evaluated by measuring depth of peening, change in micro hardness and surface roughness of peened samples in comparison to unpeened magnesium (each set of measurement of hardness has been performed for three times and results have been achieved from their average). Though at 60 μm spot size (I=0.91 GA/cm^2), the theoretical shock pressure is higher than the HEL of magnesium, evaluation of peening depth, hardness, and R_a show that there is no appreciable increase in any of these parameters when compared with unpeened magnesium. Furthermore, the SEM images clearly show evidence of machining and solidified material at 60 μm. However, at 40 μm laser spot size (I = 2 GW/Cm^2) there is appreciable increase in hardness, and R_a when compared with unpeened magnesium. This evidence shows effective laser peening at 40 μm. At one scan, 0%overlap, the depth of peening is calculated to be 3.97μm and the measured depth is 3.8 μm which is very close to theoretical value. The surface hardness increased from 45 to 103 HV which is very similar to the hardness achieved by other works on laser peening of magnesium. In addition, appreciable increase in R_a from 0.35 μm for unpeened specimen to 3.3μm for peened specimen with a 40μm spot size. Also the SEM images clearly show evidence of uniform peening without any trace of machining or solidified material at this intensity. Hence, the occurrence of HRLSP could be could be proved at 40 μm.

Subsequent to experimental verification of HRLSP, a Finite Element Analysis single shot HRLSP is presented in chapter 4. In this chapter, the occurrence of HRLSP will be evaluated by FEM results of surface displacement and CRS. To validate the results from FEM, experimental results of surface displacement have been compared with FEM. Analytical results of both surface displacement as well as Von Mises stress on peened magnesium samples are used for further validation.

CHAPTER 4. Finite Element Analysis of Residual Stress and Surface Displacement of a Single Shot in High Repetition Laser Shock Peening on Biodegradable Magnesium Implant

This chapter is based on an article under revision in Journal of Mechanical Science and Technology. Manuscript Number: MEST-D-15-00769R1 (Under revision) This chapter covers the objective '1b' of the "Objectives and Scope of the Thesis" in section 1.9

4.1 Introduction

Recently, a new generation of magnesium alloys have been introduced into manufacturing of bio-orthopedic implant with ability of absorption within the human body, subsequently eliminating surgery for implant removal. Avoiding bone asthenia and stress shielding phenomena [5] are the primary reasons in favor of magnesium based biodegradable ortho-implant. Hence, biodegradable magnesium alloys (Mg-Ca, Mg-Ca-Zn) [8] offer excellent advantages over conventional alloys (Ti or SS) for bio-implants. However, magnesium implants may corrode and rupture before the broken bones have cured completely, causing the bone to fail again. Thus, reduction of corrosion rate and improving mechanical strength assume significance in the implementation of these biodegradable implants [68]. The corrosion rate should be controlled at two different rates. The initial corrosion rate corresponds to period of bone treatment, during which corrosion needs to be minimized, and the next rate of corrosion relates to period after bone treatment. During this stage, the corrosion should accelerate to boost degradation of implant within the body. Increasing the Compressive Residual Stress (CRS) by laser shock peening has been proposed as a solution to reduce corrosion rates in previous empirical researches [8][42][74][75]. CRS prevents expansion of the nano/micro cracks upon the surface which is the main reason for premature corrosion and fatigue. After slow degradation of the region with CRS, the corrosion rate accelerates. Even though there are a number of conventional methods to add CRS, several reasons lead to LSP being superior when compared with conventional surface treatment methods such as burnishing [76] and shot peening [19]. With greater impact on surface owing to greater non-destructive power; good control over laser parameters in terms of energy; and precise relative movement on parts surface; lead to improved performance in the case of laser shock peening. In addition, improvement of surface topography

that is significant for biocompatibility [71] is also possible by laser peening [77]. To my knowledge, all of the research works are on the use of high energy and low repetition rate lasers for peening. The feasibility of high repetition rate laser shock peening (HRLSP) that requires lesser capital, particularly on low mechanical strength alloys like magnesium, has been evaluated in our previous research [30]. Since addition of CRS and control over surface topography are the anticipated results of laser peening, efficiency of the proposed HRLSP process can be evaluated by detection of CRS and surface displacement. This FEM is aimed to show the occurrence of HRLSP on Magnesium by modeling and predicting the CRS and plastic deformation on the peened area.

4.2 HRLSP theory and principles of induced CRS

Mechanisms of HRLSP and LSP are based on identical principles in most aspects. Whenever, absorption of laser energy exceeds the materials threshold, ablation happens. Consequently, the material transforms from solid state to vapor that result in plasma formation [24][22]. Plasma can generate extremely high pressure within the laser pulse duration [23]. As the shock pressure exceeds the Hugonoit Elastic Limit (HEL) [46], plastic deformation begins to take place along with elastic deformation. After relaxation, the interaction between the plastic strain and elastic strain results in development of CRS and tensile residual stress (TRS). Figure 4-1 demonstrates the sequence of residual stress generation. According to equation 4-1, the energy of each pulse (E_l) is equal to average laser power (P_w) divided repetition rate.

$$E_l = P_w / f \quad (4\text{-}1)$$

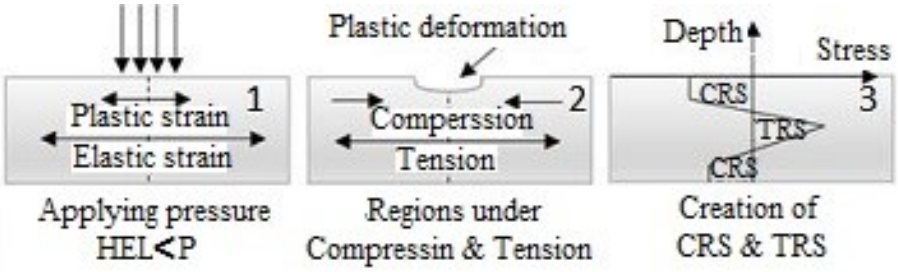

Figure 4-1 Generation of residual stress

When repetition rate increases from 10 Hz as in conventional LSP to 10000 KHz in the HRLSP, the energy of each pulse decreases. Hence, the laser must be tightly focused in the order of several microns to provide the required laser intensity for peening.

In addition, in HRLSP the laser frequency is very high, requiring the use of high speed scanning. The mechanism of HRLSP is shown in figure 4-2. According to Peyre et al. [78] the size of the laser spot, has an effect on the depth of residual stress, where they show that, smaller the spot, the closer to the surface is the accumulation of CRS. Owing to the reduction in depth of the CRS and the reduced time lag between successive peening pulses, new FEM is required to predict these parameters.

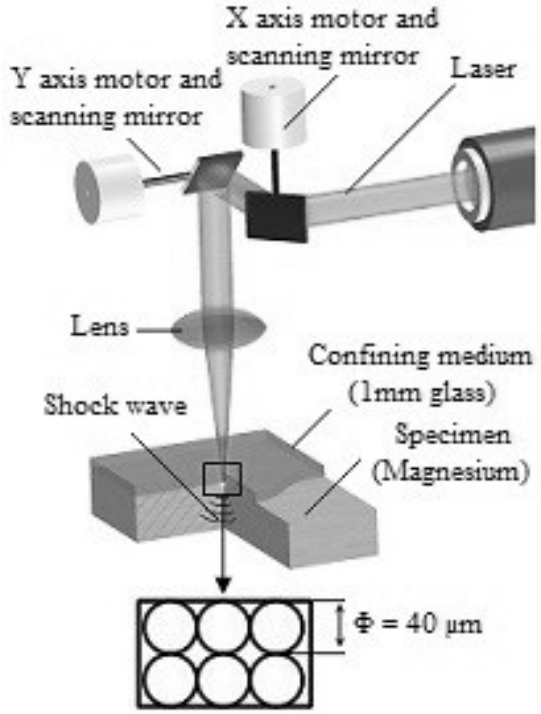

Figure 4-2 schematic of HRLSP

4.3 Proposition of the simulation diagram

Figure4-3 shows the flowchart of this research work. In pre-processing stage, based on laser and peening specifications, the appropriate pressure functions have been defined in the first stage. Also, the geometry and element sizes with proper boundary conditions have been designed and discussed. The required data has been input to the ABAQUS Dynamic Explicit (ADE) model for the determination of plastic deformation. The obtained results are served as input to ABAQUS Static Implicit (ASI) model to determine the CRS. Subsequently, the results from the FEM have been compared with analytical as well as experimental methods.

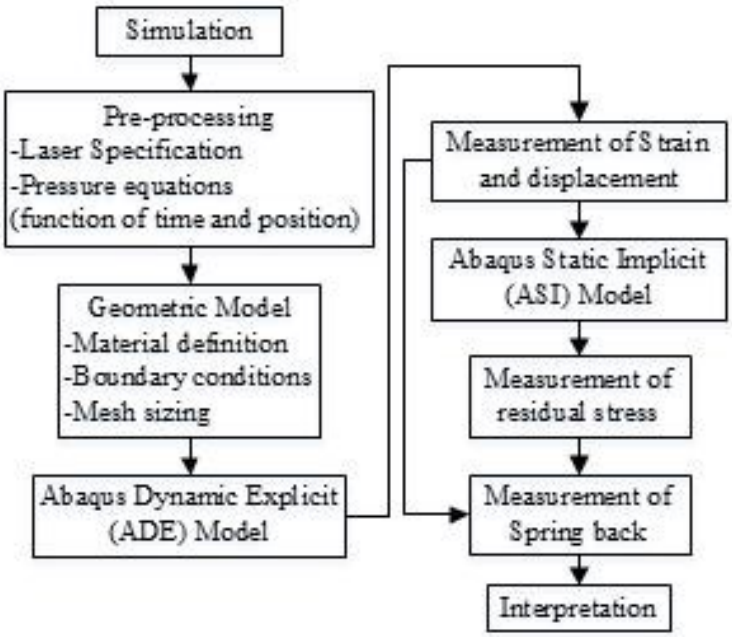

Figure 4-3 The flowchart of FEM

4.3.1 Pressure-Time-distance functions

The laser with specifications mentioned in table 4-1 was used for peening without overlay on magnesium specimen whose properties are tabulated in table 4-2. The peak shock pressure with the used laser can be calculated by equation 4-2 [22].

Laser Specifications

Laser power (P_W)	4 W
Pulse duration (τ)	14 ns
Wave length (λ)	1064 nm
Repetition rate (f)	10 kHz
Beam diameter (D)	40 μm

Table 4-1 Laser specifications

$$P(GPa) = 0.01\sqrt{\frac{\alpha}{2\alpha+3}}\sqrt{Z\left(\frac{gr}{cm^2 s}\right)}\sqrt{AI\left(\frac{GW}{cm^2}\right) - \frac{E_{vap}(\frac{J}{cm^2})}{\tau_p(ns)}} \quad (4\text{-}2)$$

$$Z = \rho U \quad (4\text{-}3)$$

Where Z is acoustic impedance, ρ is density and U is sound speed within material, P is the peak shock load, I is laser intensity, τ_p is duration of pulse pressure, A is coefficient of plasma absorption which is close to 1 at a laser wavelength of 1064 nm, E_{vap} is the required energy for vaporization

Specimen specification:

Specimen:	One pass extruded bar 99.8% Magnesium 0.02%Calcium
Yield stress:	100 MPa
Elastic modulus:	20 GPa
Density:	1800kg/m^3
Poisson ratio:	0.33
μ = 15.4 GPa	
λ = 36.3 GPa	

Table 4-2 Specimen specification

and α defined by equation 4-4 [22]:

$$\alpha = \frac{E_{th}}{E_{int}} \qquad (4\text{-}4)$$

Where E_{int} is internal energy of the plasma and E_{th} is thermal energy. Ignoring the light reflection at glass-plasma interface, the magnitude of α is 0.1. Since in HRLSP the spot size is in the micrometer range, the volume of ablated material is negligible when compared with conventional LSP. Hence, the magnitude of E_{vap}/τ_p is insignificant compared to I and equation 4-3 can be rewritten as equation 4-5 [46].

$$P(GPa) = 0.01\sqrt{\frac{\alpha}{2\alpha+3}}\sqrt{Z\left(\frac{gr}{cm^2 s}\right)}\sqrt{I\left(\frac{GW}{cm^2}\right)} \qquad (4\text{-}5)$$

The laser intensity I can be calculated using equation 4-6 [47].

$$I = \frac{E_l}{\tau A_S} = \frac{P_W}{\tau . f . A_S} = \frac{P_W/f}{0.78D^2.\tau} \qquad (4\text{-}6)$$

A_S is spot size area, E_l (J) is average energy of a pulse and D (mm) is the diameter of laser beam or spot size, τ is laser pulse duration that is constant at 14 ns in this research and *f* is the repetition rate in Hz. One of the prominent solutions to magnifying shock pressure in HRLSP is the addition of a confining medium (CM) and an overlay on the specimen surface. The equations 4-3 and 4-7 show the impact of CM on shock pressure.

$$\frac{2}{Z} = \frac{1}{Zs} + \frac{1}{Zc} \qquad (4\text{-}7)$$

Glass with 1 mm thickness has been chosen as the CM because of its high density and acoustic speed. The acoustic impedance (Z_C) of glass as CM is higher than Z_C of air. Increasing Z_C leads to increase in Z thereby magnifying the shock pressure.

However, magnification of shock pressure should be followed by mismatch theory as shown in equation 4-8 [63].

$$\frac{P_2}{P_1} = \frac{4\rho_2}{\left[(\rho_2)^{\frac{1}{2}}+(\rho_1)^{\frac{1}{2}}\right]^2} \qquad (4\text{-}8)$$

Where P_1 is shock pressure before the overlay that is calculated by equation 4-5, ρ_1 is density of overlay, ρ_2 is density of specimen and P_2 is resulted pressure (pressure after overlay within specimen surface).

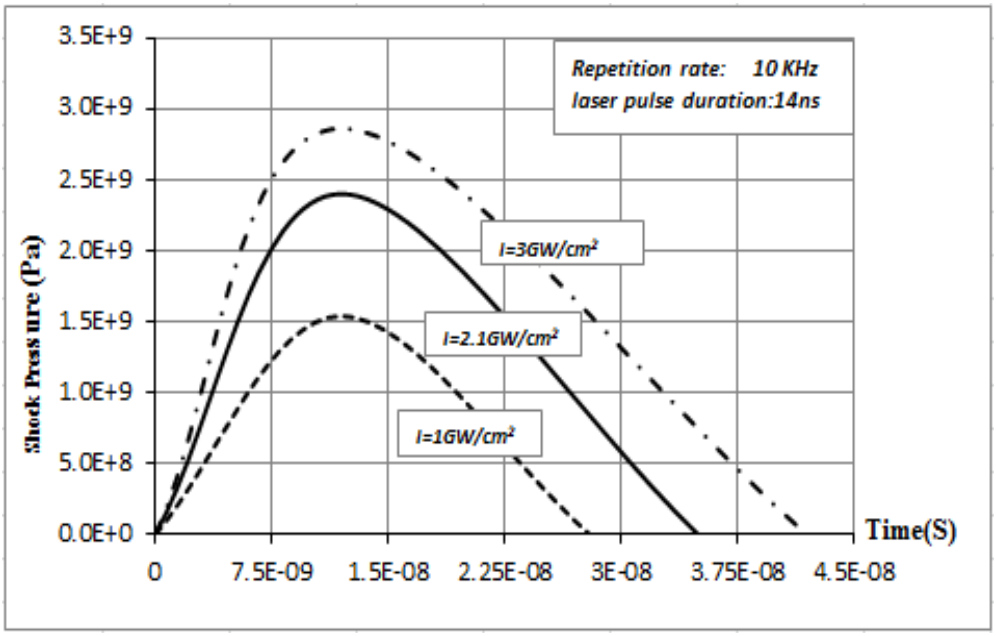

Figure 4-4 Fluctuation of shock load pulses

In order to obtain the figure 4-4, the amount of shock pressure has been calculated using equation 5. Furthermore, the previous researches indicate, regardless of laser intensities the required time to reach maximum shock pressure is close to the laser pulse duration [79][80]. Therefore, the peak of curve occurs at 14 ns. Subsequent to reaching the peak load, the shock pressure needs more time to reach zero depending on the magnitude of shock pressure. However, to input pressure-time in the model, the duration of pressure can be confined to 2-3 times longer than the laser pulse

duration [78][81][82] as the best effective time. Hence, it has been assumed that the pressure curve reaches 0 at 35 ns for 2.1GW/cm^2.

The shock pressure is a function of distance, as well. Equation 4-9 indicates the relation of shock pressure and the distance from the center of peened region [47].

$$P_p(r) = P\exp(-\frac{2r^2}{D^2}) \qquad (4\text{-}9)$$

Where, P was obtained by the equation 4-6, D is spot size diameter and r is radial distance from the center of peening. Figure 4-5 shows the impact of increasing distance from the center of peening zone on pressure propagation at three intensities. In figure 4-5, the X axis defines radial distance from the center of peening in meters and the Y axis defines the distribution of shock pressure in Pascals.

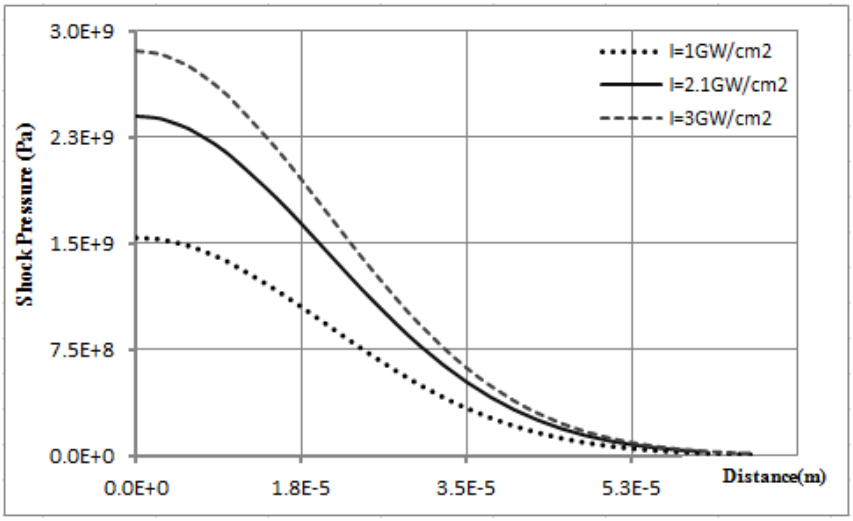

Figure 4-5 Relationship of pressure and radial distance

When the spot size diameter is constant at 40 μm, all pressure magnitudes reduce with different patterns and all curves tend to zero around 60 μm from the center of peening. While the pressure increases within the same spot size, the concentration of pressure is closer to surface. Hence, additional plastic deformation occurs closer to surface and accumulation of CRS occurs in this region [25][49].

4.3.2 Geometric model and material definition

At the initial stage, the geometric model with required dimension was created. In order to reduce calculation time, only the effective zone has been considered in this geometric model. From our

earlier work [30] and peening spot size is assumed as 40μm, the model is a cuboid of 400×400 μm with 300μm depth as illustrated in figure 4-6. The specimen is bounded at the bottom without any movement and rotation as in the case in experimentations. Mechanical constants of pure magnesium such as Poisson's ratio (υ), young's modulus (E), yield strength (σ_y), ultimate strength (σ_u) and lame's constants (μ, λ) were used as primary data of the model.

4.3.3 Element Sizes

The density and size of elements (meshes) have an undeniable role in the accuracy of FEM results [83]. The model has been divided into three main parts as shown in figure 6: coarse part 6(a), conical part 6(b) and cylindrical part or stem of model 6(c). Since the prediction of the depth is the primary aim, maximum density of 2×2×2 μm element size was allocated to top meshes. Owing to the spherical spreading of shock wave from the center of the peening zone, the second part was designed conically 6(b). In this part, the dimension of elements increases from 2×2×2 μm to 14×10×2 μm radially. An identical technique was used in the design of coarse part 6(a), where

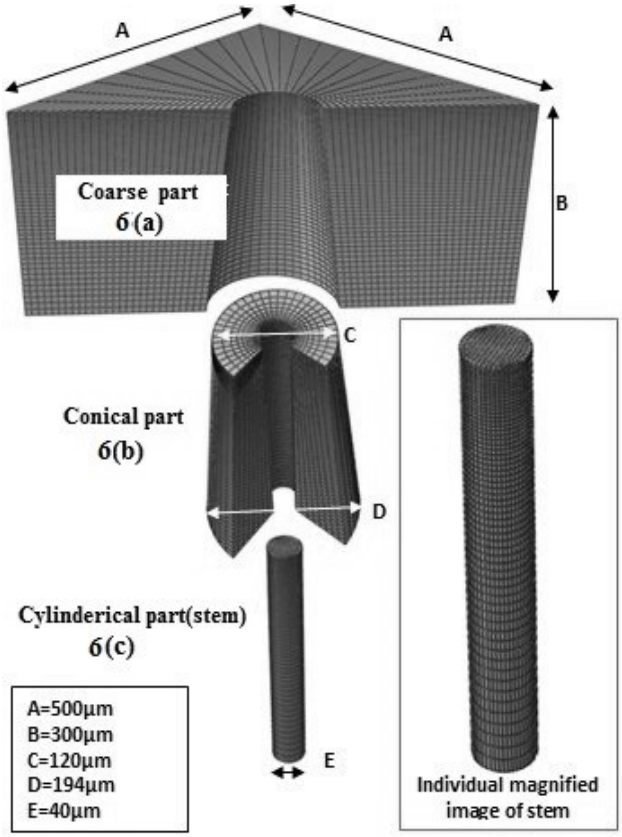

Figure 4-6 Design of elements

the size of elements increases from 14 µm to 42 µm with a height of 2 µm. The height of elements in all 3 sections increases from 2 µm at top surface to 10µm toward bottom of the model. Hence, the element sizes increase towards the bottom of the model. At the bottom, the element size of cylindrical part is 2×2×10 µm. The element size in the conical part increase toward the coarse part, radially up to15×10×10 µm, and element sizes varied from 15×10×10 µm to 42×10×10 µm in the coarse part. The model consists of a total number of 103560 linear hexahedral elements; which include 26500 elements in the stem, 35400 elements in the conical part and 41660 elements in the coarse part have allocated.

4.3.4 Solver tools

Over the course of application of laser shock pressure, the strain rate was found to be more than 10^6 S^{-1} in laser peening [84]. In this magnitude of strain rate, use of Johnson cook and elastic-perfect plastic rules are recommended, [85][86][87] and in this FEM the elastic perfect plastic rule is performed. It is significant to note that by increasing the strain rate, the magnitude of yield stress is increased. This corresponds to HEL and it needs to be used in high strain rate phase of simulation instead of static yield stress. The HEL can be calculated using equation 4-10 [88][89].

$$HEL = \frac{\rho_0 . C_{el} . u_{sv}}{2} = \frac{(1-\upsilon)(\sigma_y^{Dyn} - \sigma_0)}{1-2\upsilon} = \left(1 + \frac{\lambda}{2\mu}\right)(\sigma_y^{Dyn} - \sigma_0) \qquad (4\text{-}10)$$

$$C_{el} = \sqrt{\frac{(1-\upsilon)E}{(1+\upsilon)(1-2\upsilon)}\frac{1}{\rho_0}} = \sqrt{\frac{\lambda+2\mu}{\rho_0}} \qquad (4\text{-}11)$$

Where, ρ_0 is material density before applying of shock pressure, C_{el} is velocity of mechanical wave that can be calculated by equation 4-11 [90], E is young's modulus, υ is Poisson s ratio, U_{SV} is surface velocity during the peening, λ and μ are lame constants. In general, the average velocity is calculated by distance divided by time. Hence, by knowing the duration of applied pressure from figure 4-4 and depth of peening that has been characterized by experiment, U_{SV} that can be calculated. In the period of relaxation or spring back (subsequent to the applied pressure duration), the deformed material tends to recover to its initial phase. In this phase, owing to absence of external force and the strain rate is less than 10^2 S^{-1}, the hook rule must be used in relaxation phase. Hence, initially the high strain rate phase is simulated by ABAQUS/Dynamic-explicit (ADE) and in continue, low strain rate phase in relaxation period is simulated by ABAQUS/Static-implicit (ASI). The input data to ADE are pressure functions from figure 4-4 and equations 4-5 and 4-9.

The ASI is a copy of ADE with these differences all loads have been removed and the dynamic yield stress has been converted to static yield stress. The required laser specifications and characteristics of specimen are input as shown in tables 4-1 and 4-2.

4.3.5 Optimization period of ADE

The duration of peening in ADE has been divided into transient and steady state. The transient state is the duration in which the material response to shock pressure is dynamic and it changes as a function of time. Following the transient duration (TD), the material response is steady state and the results will be time independent. It is therefore essential to predict the TD. In order to predict the TD, it is necessary to monitor the kinetic and internal energies. Figures 4-7 and 4-8 illustrate the simulated fluctuations of internal and kinetic energies during impact of a laser shot.

In figures 4-7 and 4-8, the horizontal axis represents time and vertical axis defines energy, where the fluctuations of internal and kinetic energy are represented for duration of 200 ns. The analysis was performed at three different shock pressures 1.54, 2.4 and 2.86 GPa. Observing the energies in figures 4-7 and 4-8, at shock pressure of 2.4 GPa represented by solid black line, it can be clearly seen that in the first 35 ns, the internal energy increases from 0 to 28 μJ and the kinetic energy has

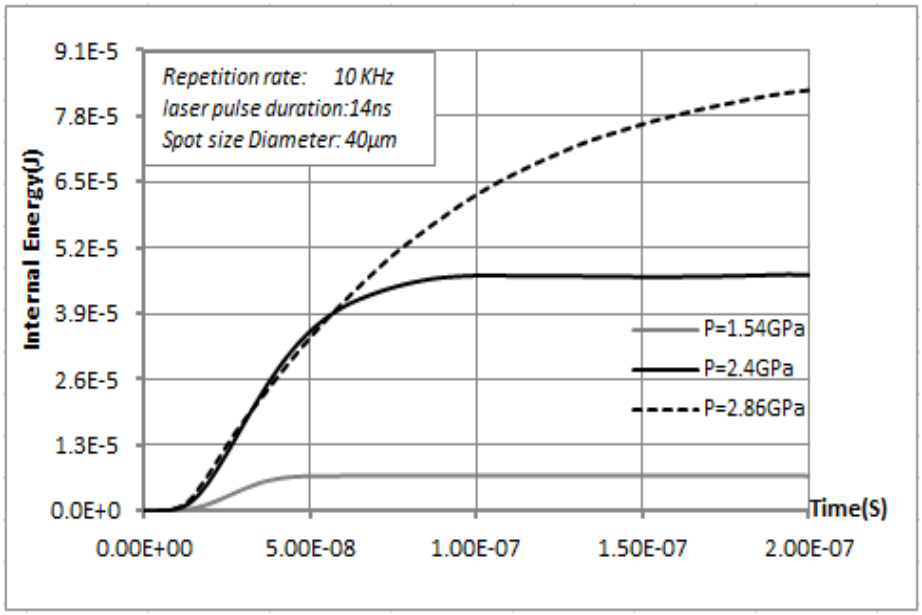

Figure 4-7 Fluctuations internal energy at three pressures

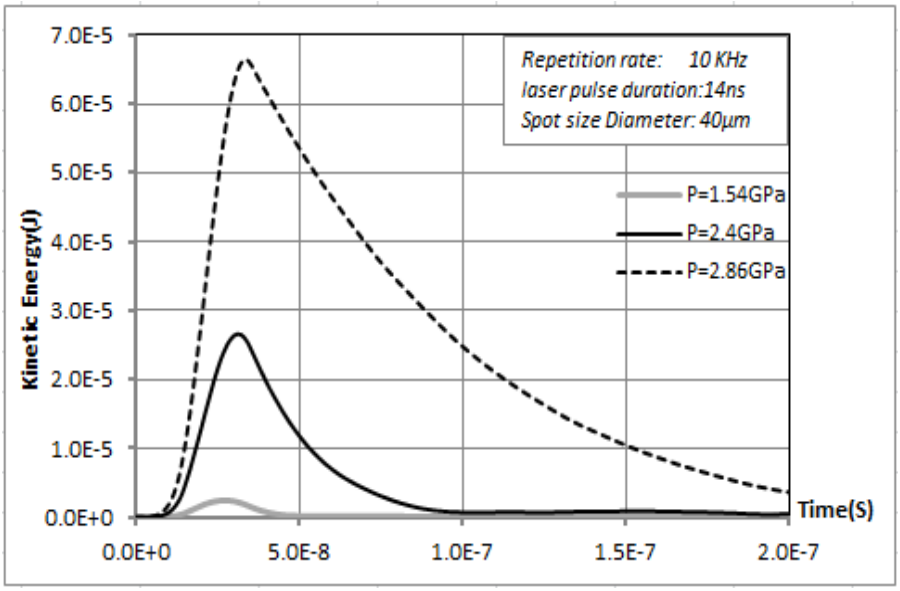

Figure 4-8 Fluctuations kinetic energy at three pressures

a peak magnitude of 26 µ. From 35 ns to 100 ns, owing to increase in mechanical strength by strain hardening [21], the rate of plastic deformation reduces and hence, the kinetic energy tends to zero. In this period, the rate of increase in internal energy reduces as shown in figure 4-7. After 100 ns, the kinetic energy remains 0 and the internal energy remains at 47 µJ, showing the end of TD and beginning of steady state. For the other energy profiles 1.54 and 2.86 GPa, it can be seen from the figures that the steady state begins at around 50 and 200 ns, respectively.

It can be seen that the increase in shockwave energy increases the TD time and for ADE analysis, a time span slightly longer than TD should be considered in order to make reliable measurements in the steady state. Especially in the case of HRLSP, it is also important to note that, the minimum interval between two sequential pulses cannot be less than TD. Although in conventional LSP [91] the TD is 4000ns, this is not a major cause of concern since the rate of pulse repetition is at 10 Hz. From the figure 4-7, the highest repetition rate that can be used without getting into the TD is 10 MHz in case of peak pressure at 2.4GPa.

4.4 Compressive residual stress (CRS)

In order to validate the results of simulation, a comparison between FEM and analytical results have performed. The analytical magnitude of residual stress is determined using equation 4-12[46][92].

$$\sigma_s = \sigma_0 - \left(\mu\varepsilon_P \frac{1+\vartheta}{1-\vartheta} + \sigma_0\right)\left(1 - 2.54(1+\vartheta)\frac{L_P}{D}\right) \quad (4\text{-}12)$$

In this equation σ_0 is initial residual stress on the specimen surface, σ_S is equal to von misses and L_p is plastically affected depth that could be obtained by equation 4-13 [46][92] and ε_p is plastic strain , that is achieved by equation 4-14 [46].

$$L_P = \frac{C_{el}C_{pl}\tau_P}{C_{el}-C_{pl}}\left(\frac{P-HEL}{2HEL}\right) \quad (4\text{-}13)$$

$$\varepsilon_P = \frac{-2HEL}{3\lambda+2\mu}\left(\frac{P}{HEL} - 1\right) \quad (4\text{-}14)$$

Where, C_{el} and C_{pl} are speeds of longitudinal elastic and plastic wave in the material, respectively. C_{el} is obtained by equation 4-11 and C_{pl} calculates by equations 15 [90].

$$C_{pl} = \sqrt{\frac{\lambda+\frac{2\mu}{3}}{\rho}} = \sqrt{\frac{E}{3(1-2\vartheta)}}\frac{1}{\rho} \quad (4\text{-}15)$$

The analytical von misses (σ_s) was found to be 31.5 MPa, which is closed to the result from FEM as shown in figure 4-9 indicating 30 MPa. In this Figure, distribution of von misses stress is shown up to a depth of 150 µm. Distribution of CRS from the FEM is illustrated in figures 4-10 a to d. Note while principal stresses ($S_{33}=\sigma_{zz}$ $S_{22}=\sigma_{yy}$ and $S_{11}=\sigma_{xx}$) are used for demonstrating CRS, magnesium being an isotropic material, S_{22} is removed from the results.

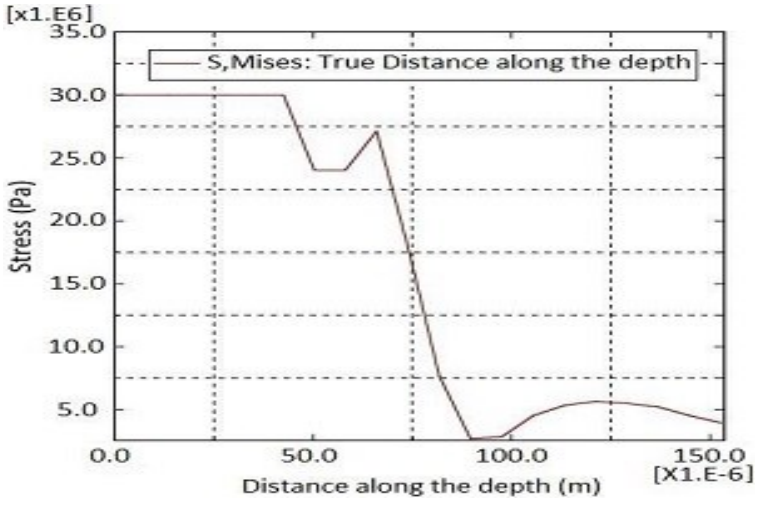

Figure 4-9 FEM Distribution of Von misses along the depth

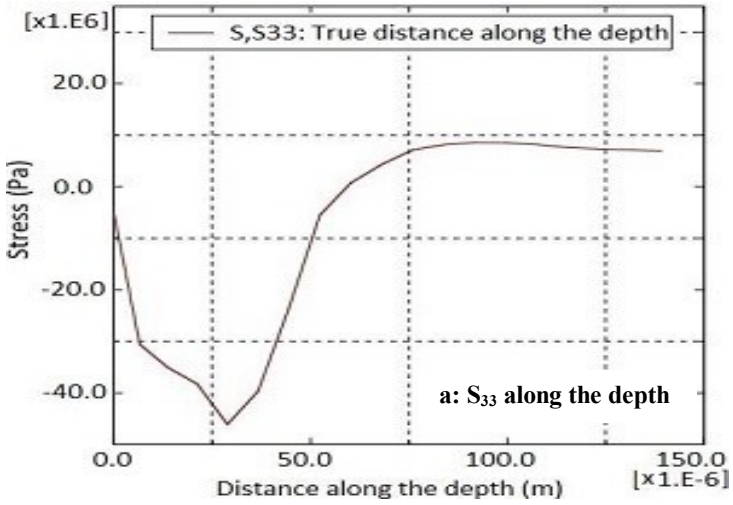

a: S_{33} along the depth

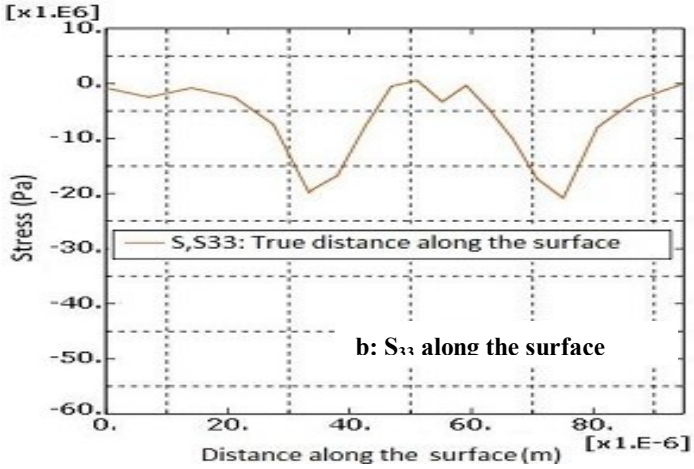

b: S_{33} along the surface

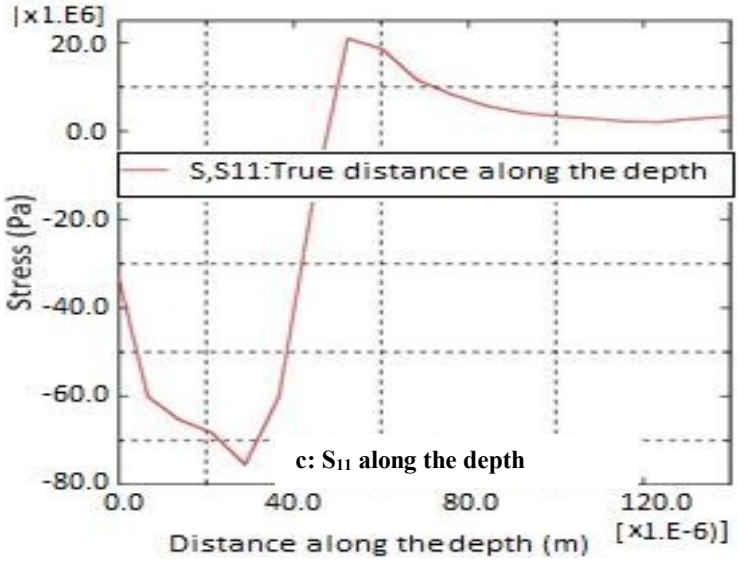

c: S_{11} along the depth

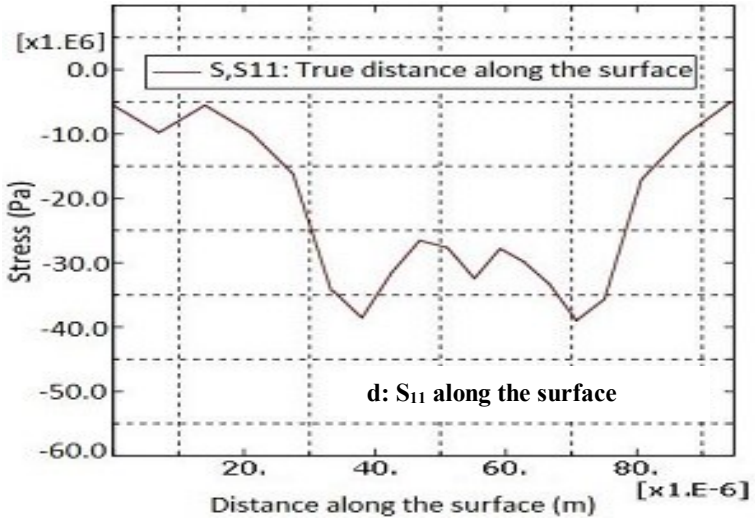

Figure 4-10 Stresses along the surface and Depth

In all graphs, the vertical axes indicate stress magnitudes and horizontal axes show direction of stress distributions. It can be observed that in figure 4-10-a, the peak of S33 is -48 MPa, which occurs at the depth of 28 μm. Whereas the maximum of S33 in surface direction is -21 MPa in figure 4-10-b. from figures 4-10-c and 4-10-d, the S11 magnitudes along the depth and surface are - 74 MPa and -40 MPa, respectively.

Guo et.al.[42] in laser peening of magnesium has reported that the maximum S_{33} occurred at 78 μm depth, where the laser intensity was 5.1 GW/cm^2 with laser beam diameter of 1 mm. By comparison of Guo et.al research and current work, it can be stated that by the reduction of laser beam diameter in HRLSP, CRS accumulates closer to peened surface, as mentioned by Pyre et al. [22]. However by increasing laser power intensity, the CRS can be stored with larger magnitude. For instance, in the Guo et.al research [42], the magnitudes of von misses has exceeded 40 MPa, whereas in current research by use of 2.1 GW/cm^2, the maximum deposited stress is 31.5 MPa. Although the laser power intensity of this simulation with 2.1GW/cm^2 is less than half in Guo et.al experimental research [42], the peak CRS has accumulated much closer to the surface, thereby providing greater protection against expansion of micro-cracks. This in turn provides further protection against corrosion. By performing multiple peening, the average magnitude of CRS created at the surface. Hence, it can enhance mechanical attributes, homogeneously. FEM study of multiple and overlapped HRLSP on magnesium, will be assessed in upcoming research of authors.

4.5 Surface displacement

Surface displacement has been calculated from the outcomes of plastic/elastic deformation by ADE in figure 4-11 and spring back can be achieved by ASI as shown in figure 4-12. The figure 4-11 shows plastic deformation (4.27 µm) exactly at the end of pressure duration and the figure 4-12 shows spring (0.25 µm) back after relaxation. Hence the final plastic deformation is the summation of both results which is 4.02 µm. The reason for low amount of spring back is due to high initial shock pressure, which leads to the material at peening zone becoming mostly plastic.

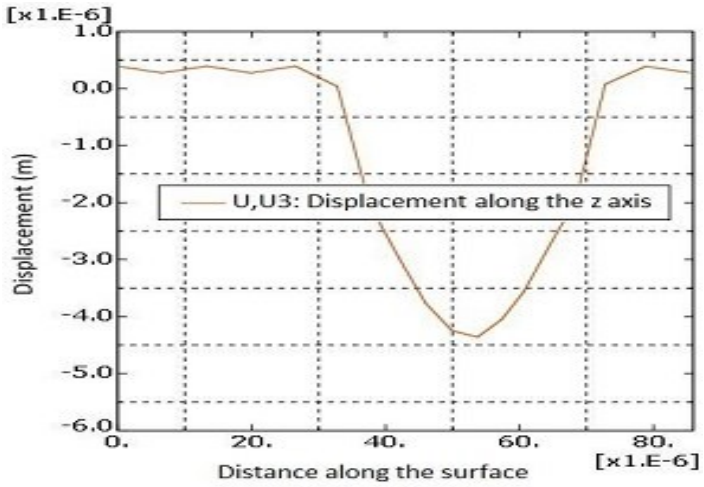

Figure 4-12 Plastic/elastic deformation by ADE

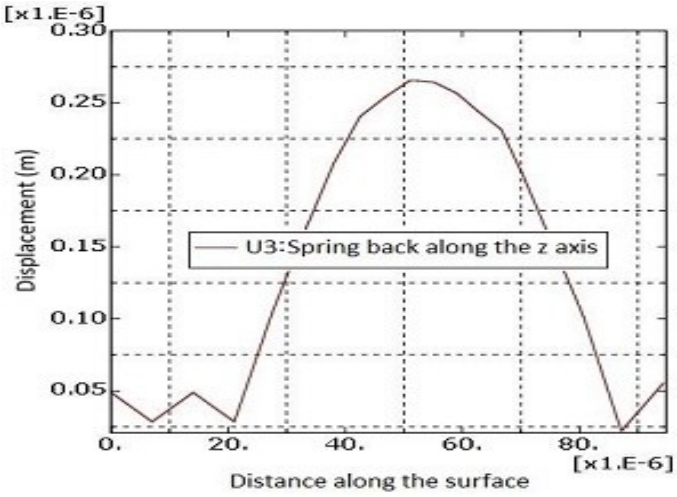

Figure 4-11 Spring back after ASI

WYKO NT1100 interferometer was utilized to obtain the profile of the peened area as indicated in the figure 4-13. The horizontal axis represents the peened area along the specimen surface and the

vertical axis shows the depth of peened region. From the experiment, the depth of peening at the center of the spot is 3.698 μm and from simulation it is found to be 4.02μm.

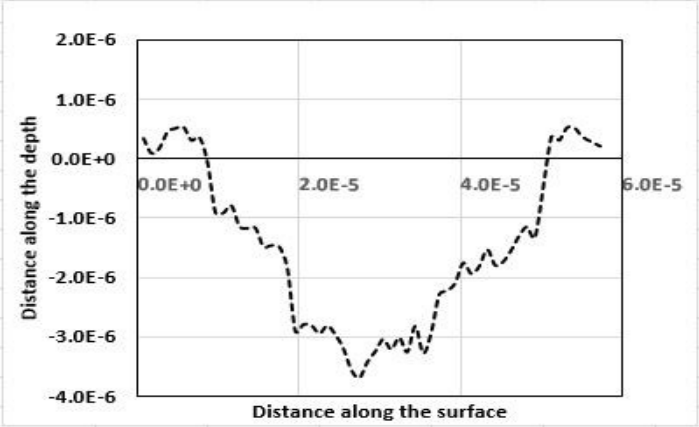

Figure 4-13 Measured depth profile of a laser shot

4.6 Conclusions

To the knowledge of the authors, this work represents the first FEM work of high repetition rate laser shock peening on magnesium. In this work, the transient time and steady state time for peening was modeled. Also the magnitude and depth of CRS in addition to change in surface topography by HRLSP of magnesium has been simulated. The simulated results have been validated by analytical and experimental work. The FEM was used to predict the residual stress caused by single laser shot. The maximum CRS (S_{33} along the depth) has been found to be at -48MPa and reaches to a depth of 28 μm below the peened surface. The FEM predicted the peening depth as 4.02 μm and this matches closely with the experimental calculation at 3.69 μm and analytical result at 4.01 μm. In addition, it has been shown that by reduction in spot size diameter, the CRS can be deposited closer to surface.

From the earlier chapters, the occurrence of HRLSP has been proved theoretically as well as experimentally. As an extension of this chapter, in Chapter 5, a real HRLSP finite element model with several shots at different percentage of overlap and number of scans have been simulated. In the proposed simulation, surface displacement has been compared with experimental measurements. Moreover, the effect of % overlap and number of scans on the magnitude and depth of CRS has been presented.

CHAPTER 5. Finite Element Analysis of high repetition rate laser shock peening on magnesium by multiple and overlapped techniques.

This chapter is based on an article submitted to Journal of Laser micro/Nanoeng., Manuscript number: JLMN-15-076(Under review). This chapter covers the objective '1c' of the "Objectives and Scope of the Thesis" in section 1.9

5.1 Introduction

Lot of research in the recent years have been performed on LSP by experimental, analytical and finite element methods. Recently, a novel method of LSP on biodegradable magnesium alloys [93] has been introduced by the authors [30]. This method has been named high repetition rate laser shock peening (HRLSP). The novelty of HRLSP is in utilizing high repetition rate pulsed laser instead of low repletion ones that has been used in conventional LSP. The main difference of LSP and HRLSP is the energy of each pulse. Depending on the pulse repetition rate (f), the pulse energy (E_p) in low repetition rate laser could be few orders of magnitude larger than the high repetition rate lasers. This is because of dividing the nominal laser power (P_w) by the pulse repetition rate as shown in equation 5-1

$$E_p = P_W/f \qquad 5\text{-}1$$

Hence, the required laser intensity (I) in equation 5-2 [30] could be achieved by reduction of laser beam diameter (D). Where, τ is pulse duration that is routinely constant in an experiment.

$$I = \frac{P_W/f}{0.78D^2.\tau} \qquad 5\text{-}2$$

Although tight focusing of laser beam by optical devices can increase laser intensity, it cannot provide adequate shock pressure for LSP on high strength materials. Hence, application of HRLSP is restricted to materials with low Hugonoit Elastic Limit (HEL) such as pure magnesium and its biodegradable alloys. Since, HRLSP has been introduced as a novel method of LSP, to the knowledge of authors there is no empirical, analytical or FEM research work on this subject. Owing to using extremely focused laser beam in a micrometer scale area, different behaviour of CRS accumulation is expected. Also the transient duration (TD), which is the time required for attaining steady state after application of each pressure pulse, assumes significance particularly in the case of HRLSP, as the minimum interval between the two pulses should be greater than the

TD, for effective peening. These factors are the primary motivators behind the FEM study proposed in this manuscript.

The most significant effect of laser peening is increasing compressive residual stress (CRS) under the peened surfaces. Cold working on the peened surface that is created by the plasma shock pressure is causes changes to surface topography and accumulation of CRS will be resulted [94]. Hence, by monitoring these two characteristics of HRLSP, the FEM can provide further information regarding behaviours of HRLSP on magnesium. In order to validate the results of proposed FEM, the FEM results of surface displacement have been compared with the experimental results of surface displacement measured by optical interfrometery. In addition the the accumalation of the CRS based on FEM results were compared with the increase in hardness on peened samples that were measured.

5.2 Theory of Multiple HRLSP and CRS induction

In HRLSP similar to LSP, while the plasma shock pressure exceeds the HEL [46], plastic deformation begins to take place along with elastic deformation. After elapsing the period of applying shock pressure, the interaction between the plastic strain and elastic strain results in development of CRS and tensile residual stress (TRS). During the application of laser shock load, the strain rate was found to be more than 10^6 S^{-1} in laser peening [84]. This high rate strain is resulted by extremely short pressure pulse duration of a few nanoseconds. In this magnitude of strain rate, use of elastic-perfect plastic rules [85][86][87] can be an appropriate method which is performed in this FEM. It is pertinent to note that by increasing the strain rate, the dynamic yield stress (σ_y^{Dyn}) which is proportional to HEL must be used instead of the static yield stress, over the period of shock pressure. The relationship between HEL and σ_y^{Dyn} is demonstrated by equation 5-3[88]:

$$HEL = \frac{\rho_0 C_e U_{sv}}{2} = \frac{(1-\upsilon)\sigma_y^{Dyn}}{1-2\upsilon} \qquad 5\text{-}3$$

$$C_e = \sqrt{\frac{(1-\upsilon)E}{(1+\upsilon)(1-2\upsilon)}\frac{1}{\rho_0}} = \sqrt{\frac{\lambda+2\mu}{\rho_0}} \qquad 5\text{-}4$$

Where, ρ_0 is material density before applying of shock pressure, C_e is longitude speed of elastic wave within specimen, that can be calculated by equation 5-4 [90], E is young s module, υ is Poisson ratio, λ and μ are lame constants. U_{sv} is surface velocity that can be calculated by knowing

duration of applied pressure from figures 5-6, 5-7 and the depth of peening measured by experiment. In the period of relaxation, which is the period subsequent to elapsing of applied pressure, the residual elastic deformed materials tend to rebound to its initial phase. In this phase, there are no external forces and the strain rate is less than 10^2 S^{-1}, hence, the Hook rule must be used.

5.3 Solver Tools

Initially the high strain rate phase (10^6 S^{-1}) is simulated by ABAQUS/Dynamic-explicit (ADE) in the transient duration, subsequently the low strain rate phase in relaxation period has been simulated by ABAQUS/Static-implicit (ASI). The input data to ADE are pressure functions, laser specifications and required characteristics of specimen as listed in the table 5-1.

Laser Specifications		Specimen specification:	
Laser power (p)	4 W	Specimen	99.8% Mg-0.02%Ca
Pulse duration (τ)	14 ns	Yield stress (σ_y)	100 MPa
Wave length (λ)	1064 nm	Elastic module(E)	200 GPa
Repetition rate (f)	10 KHz	Density(ρ)	1800kg/m³
Beam diameter (D)	40 μm	Poisson ratio(υ)	0.33

Table 5-1 Laser and Specimen Specifications

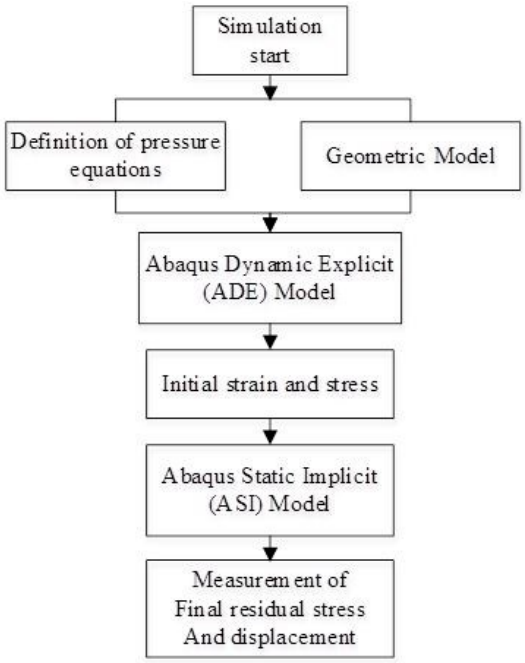

Figure 5-1 Flowchart of simulation

All the output data from ADE are then input into the ASI. Also the static yield stress of Magnesium at 100 MPa, is used instead of the dynamic yelled stress or HEL. Figure 5-1 shows the flowchart of this research work. In pre-processing stage, based on laser and peening specifications, the appropriate pressure functions have been defined in the first stage. Also, the geometry and element sizes with proper boundary conditions have been designed and discussed.

5.3.1 Shock pressure

In HRLSP, the shock pressure is created by resulted pressure plasma which is achieved by laser intensity in range of GW/cm^2 [22]. The shock pressure can be calculated by equation 5-5.

$$P(GPa) = 0.01\sqrt{\frac{\alpha}{2\alpha+3}}\sqrt{Z\left(\frac{gr}{cm^2 s}\right)}\sqrt{AI\left(\frac{GW}{cm^2}\right) - \frac{E_{vap}(\frac{J}{cm^2})}{\tau_p(ns)}} \quad 5\text{-}5$$

Where Z is acoustic impedance, ρ is density, P is the peak shock load, I is laser intensity, τ_p is duration of pressure pulse, α and A as laser absorption constant [22]. In HRLSP the spot size is in the micrometer range, the volume of ablated material is negligible when compared with conventional LSP. Hence, the magnitude of E_{vap}/τ_p is insignificant compared to I and equation 5-5 can be simplified as equation 5-6 [46].

$$P(GPa) = 0.01\sqrt{\frac{\alpha}{2\alpha+3}}\sqrt{Z(\frac{gr}{cm^2 s})}\sqrt{AI\left(\frac{GW}{cm^2}\right)} \qquad 5\text{-}6$$

In the case of wavelength at 1064 nm and high efficiency of laser absorption. [22], α and A are equal to 0.1 and 1, respectively. Hence, the equation 5 can be simplified as shown in equation 5-7

$$P(GPa) = 0.0014\sqrt{Z(\frac{gr}{cm^2 s})I\left(\frac{GW}{cm^2}\right)} \qquad 5\text{-}7$$

The effectiveness of laser peening can be improved by application of confining medium and protective coating. Glass with thickness of 1 mm has been employed as confining medium in this work. In order to increase magnitude of shock pressure, the protective coating must have less density compared to specimen [95]. Since Magnesium density is low at 1800 kg/cm^3, there is no economical choice as protective coating [30]. Hence, no protective coating has been utilized in this work. Previous research indicates the pressure reaches to maximum in a period equal to laser pulse duration [79][80].

In addition numerous researches have stated the effective length of pressure(τ_p) can continue over the course of 2 to 3 times further than laser pulse duration [81][82][78]. Therefore, considering the pulse duration (τ) as 14 ns, the pressure-time function can be illustrated by the figure 5-2.

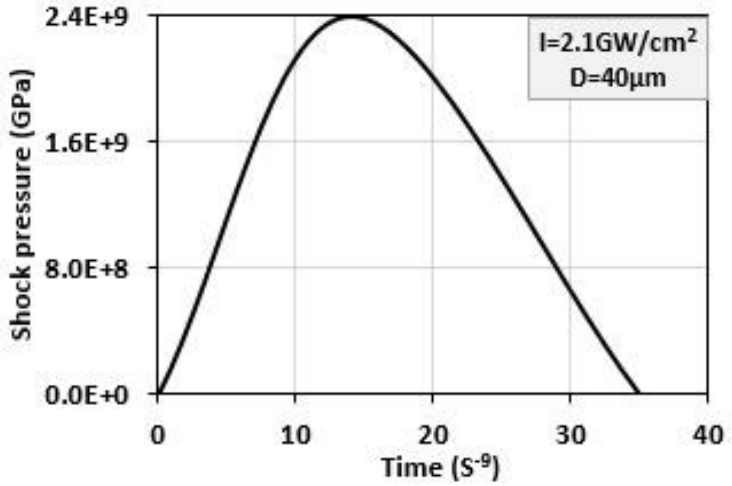

Figure 5-2 A pulse of shock pressure for a single laser shot

The shock pressure is also a function of distance from the center of the spot as shown in equation 5-8.

$$P_p(r) = P\exp(-\frac{2r^2}{D^2}) \qquad 5\text{-}8$$

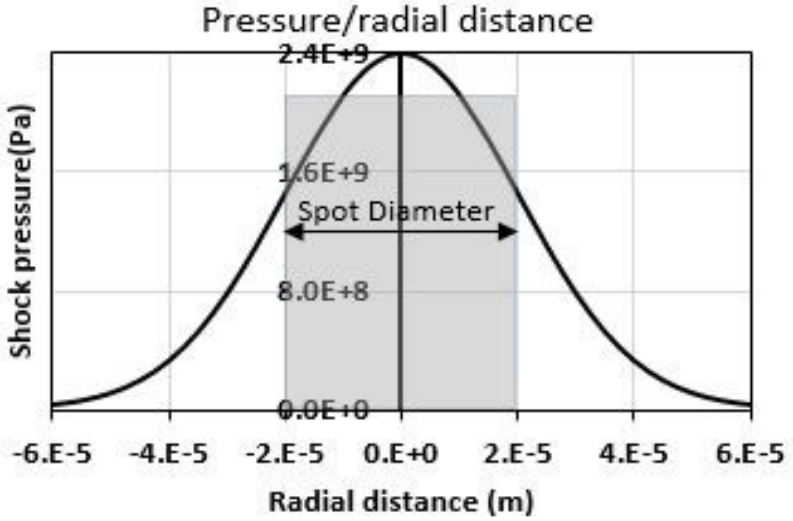

Figure 5-3 Radial propagation of shock pressure

Where, P is the shock pressure obtained by equation 1. D is spot size diameter and r is radial distance from the center of peening. It can be clearly seen that the peak pressure of magnitude 2.4 GPa is at the center of spot and it reduces exponentially to 1.48 GPa around the edge of the spot (r = 20 µm for a 40 µm laser spot).

5.3.2 Overlap calculation

Three spot overlap percentages at 0%, 33%, and 66% has been evaluated in this work. The overlap is just along the X axis as demonstrated in figure 5-4, and the Y axis overlap is always 0%. The figure 5-4 shows sequence of 9 laser shots which is used in model and in experiments. With the pulse repetition rate (f) used in this work at 10 KHz, the scan speed should be increased adequately to avoid repeated shots at the same position. On the other, for providing required laser intensity, the laser spot diameter must be 40 µm for effective peening [31].With respect to stated confinements; a Galvo Scanner (GS) has been used for scanning. As displayed in figure 5-4, the

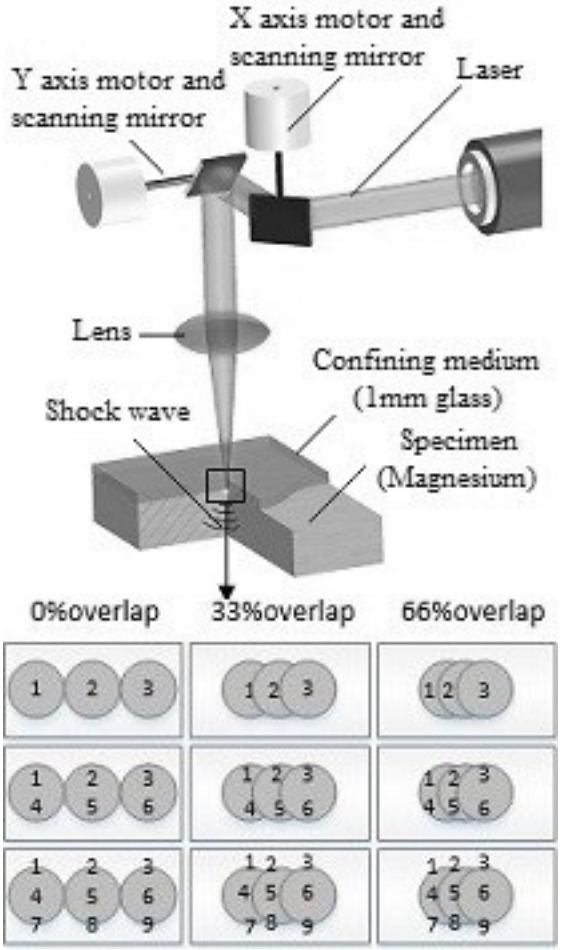

Figure 5-4 The schematic of HRLSP and Overlap in x-axis during laser shock peening

GS (*THORLABS GVS002*) has two DC servo motors. These motors are controlled with a NI6211 USB DAQ board controlled by program which is developed by LabVIEW. The peening scan speed (S_s) without overlap (O_P) along the y-axis, follow the equation 5-9.

$$S_s = D \times [1 + (1 - O_p)(f - 1)] \qquad 5\text{-}9$$

5.3.3 Element size

Since the work evaluates the HRLSP in 3 different types of overlap peening, three different models have been generated. However in all models an identical cuboid with dimension of 240×240×120 µm has been used. Defining the thickness of model (t_m) is significant and it must be follow equation 5-10 [96]. This is important to avoid mixing of the original wave and the wave that is reflected from the bottom of model.

$$t_m \geq U \times \tau_p \qquad 5\text{-}10$$

Where, U is speed of wave. Considering U~ 4500 m/s for magnesium, a t_m of 120 µm was used in the model. In the area where the shock pressure is applied, the size of the elements need to be less than the depth of deformation. From the measurement of deformation, the minimum deformation depth was found to be 3.5 µm and the smallest element size around this area is assumed at 1.7 µm.

In other part of the model, the mesh size can be increased to reduce the number of elements and the time of FEM calculations. The length and width of the elements in the fine portion is 160×90

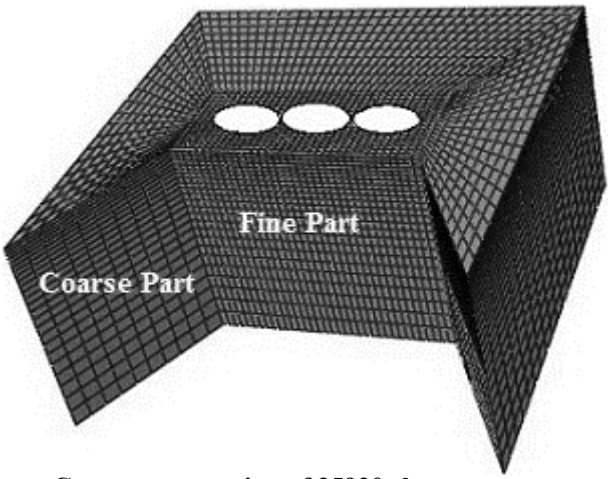

Coarse part consists of 25920 elements

Fine part consists of 15960 elements

Figure 5-5 Schematic of meshing technique

μm and surrounding the fine meshing area larger element sizes were allocated in the coarse part. The fine part of the model consists of 15960 elements and coarse part contains 25920 elements. A schematic of meshing model is displayed in figure 5-5.

5.3.4 Adjustment sequence of pressure pulse

In multiple LSP; the pressure pulses are repeated based on laser repetition rate. As the repetition rate is 10 KHz in the HRLSP work considered here, the pressure-time relationship could be illustrated as in figure 5-6. Owing to, the interval of two sequential pulses is few orders of magnitude larger than the pulse duration, the distance of two pressure pulses should be compressed, close to a time larger than TD, to reduce the computation time. Monitoring of internal energy after applying single laser shot is a reliable method to identify TD. After elapsing TD, due to absorption a certain amount of energy by the material, the internal energy of the material becomes steady state.

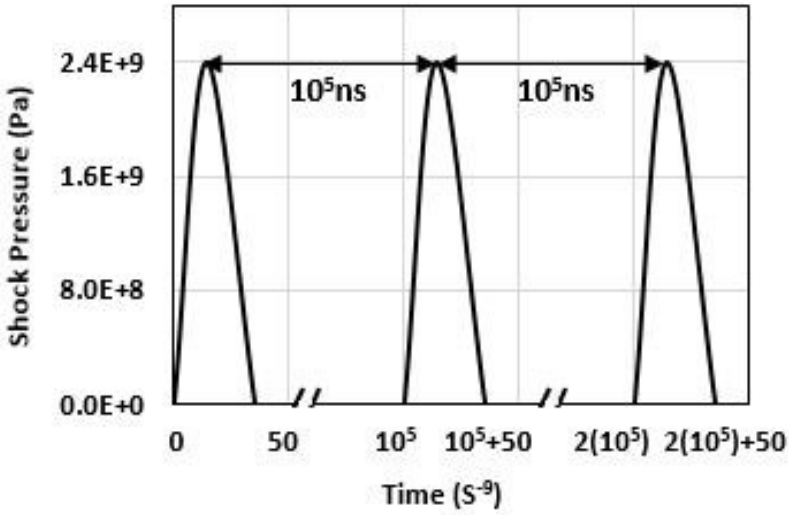

Figure 5-6 Real time sequential pressure pulses

The figure 5-7 shows internal energy in single laser shot at shock pressure of 2.4 GPa. It can be clearly seen that, the internal energy reaches steady state after elapsing TD at 40 ns[1]. In the model, the time between two successive pressure shocks should be greater than 40 ns. For further

[1] In the previous chapter on FEM of single shot HRLSP, the result shows TD of 98 ns required to achieve steady state. Considering the reduction in height of proposed model from 150 to 120 μm, the reflection of elastic and plastic wave from the boundary conditions caused the variation.

confidence, the interval of two sequential pulses has been increased to 100 ns as shown in figure 5-8 and input into the model.

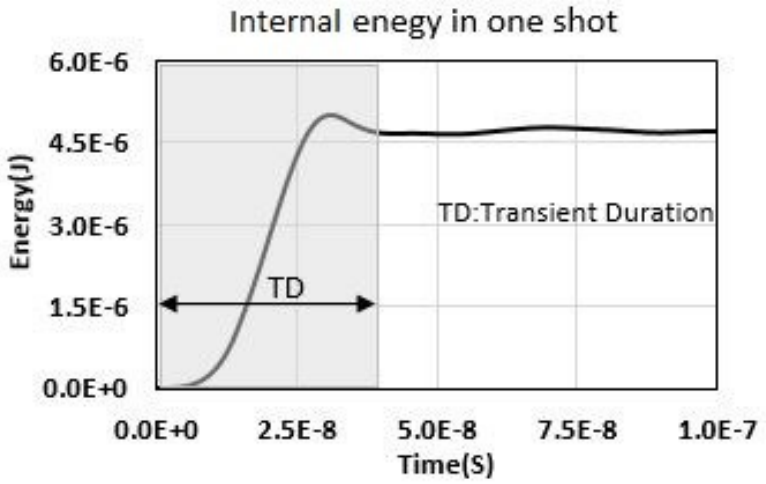

Figure 5-7 Internal energy at single laser shot

As mentioned earlier, 9 models are analyzed in this work, with 3 overlap percentages at 0%, 33% and 66% with one, two and three shots for each overlap. In each model the analysis was conducted to evaluate the depth of peening and to evaluate the magnitude and depth of CRS.

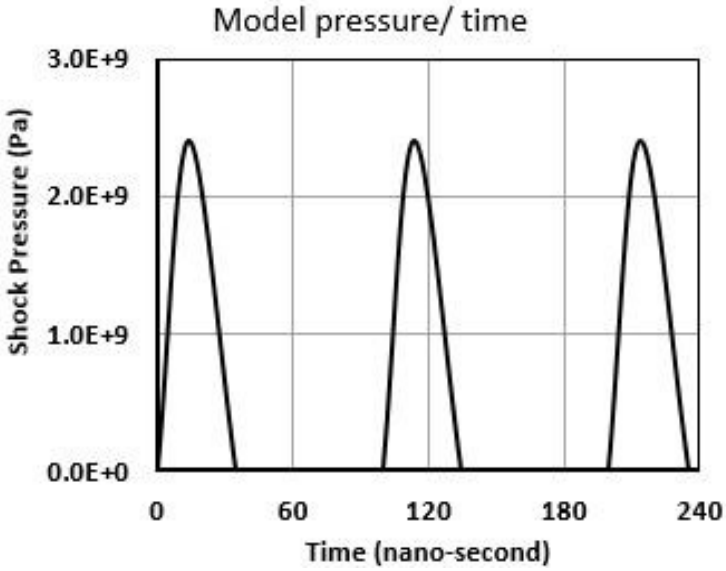

Figure 5-8 Modified pressure/time inputted in model

5.4 Results

5.4.1 Surface topography

Figure 5-9 indicates depth of peening (D_p) in 3 specimens at 0% overlap where the number of scans has increased from 1 to 3 scans. It can be clearly seen that increase in number of scans leads to increase in the depth of valleys. The maximum D_p at one, two and three scans are 4.1, 6.5 and 9.7 μm, respectively.

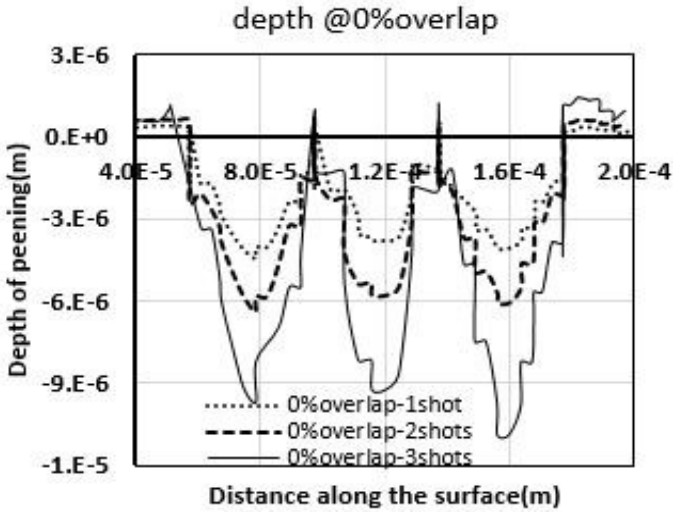

Figure 5-9 Depth of peening at 0%overlap

In figure 5-10, increasing overlap percentage of from 0 to 33% leads to eliminating rims between the edges due to overlap of laser shots, and similar to figure 5-10, increase in the number scans leads to increase in D_p which are 3.5, 5.9 and 8.2 μm for one, two and three scans respectively.

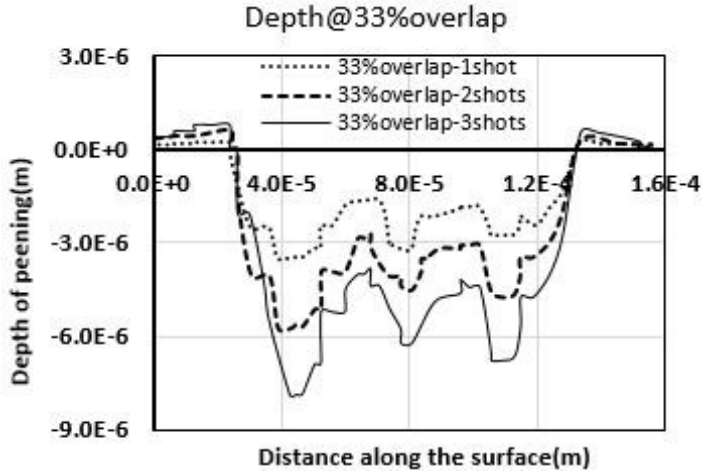

Figure 5-10 Depth of peening at 33%overlap

Figure 5-11 demostrates the D_p at 66% overlap where the maximum was 4.9, 7.8 and 11.2 µm at one, two and three shots 66%overlap, respectively. It can clearly be seen that the rims betweens laser shots are eliminated by increasing of overlap percentage.

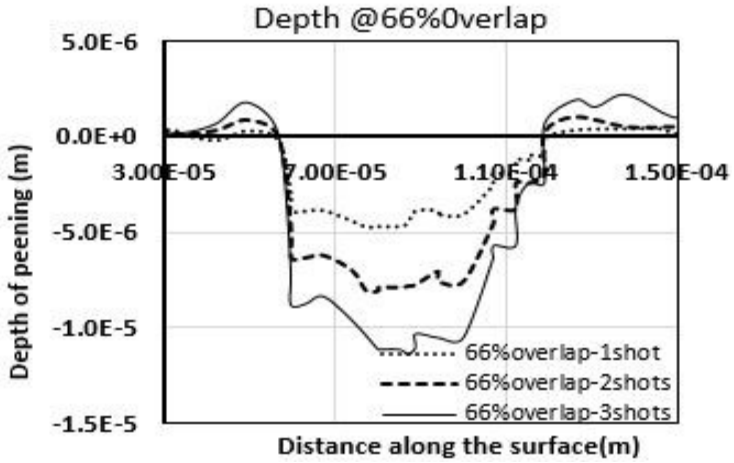

Figure 5-11 Depth of peening at 66%overlap

The SEM image with magnification of 300 times in figure 5-12 displays how the rims between shots in direction of overlap have been eliminated by increasing the overlap to 66%.

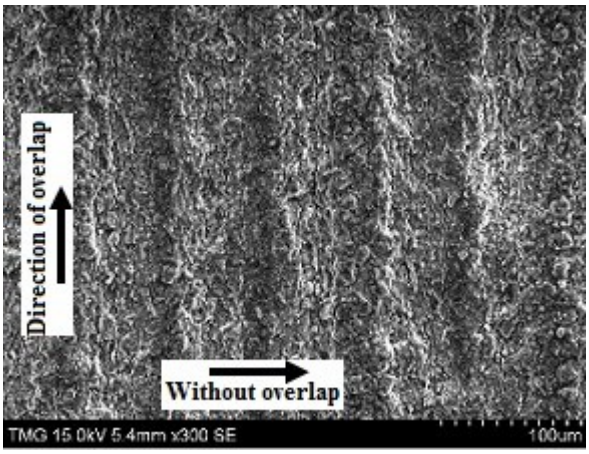

Figure 5-12 SEM of specimen surface at 66%overlap and 3 scans laser peening

Observing the figures 5-9 and 5-10 it can be seen that increasing the number of scans is more effective for enhancing the depth of plastic deformation at 0% overlap compared to 33%overlap. This can be interpreted by hardness magnitudes of specimen. The hardness of 3 specimens at figure 5-9 using *MVK-H1 Mitutoyo* micro-hardness tester, have been measured at 60, 69 and 77 HV,whereas hardness of three specimens at 33% overlap have been measured at 72, 80, 86 HV. The results indicate, increase in hardness creates additional strength on the surface and reduction

in depth of peening has been resulted. However, in 66%overlap despite increase in hardness of specimens 74, 87 and 105 HV, the maximum depth of peening has been achieved at 11.2 µm. Since, nine shots have been focused at a diameter of 67 µm; the focused shock pressure can create sharper plastic deformation. Furthermore, at 66%overlap, the area of walls are less than that in 33% and 0% overlap. Hence, allocated energy for wall removal is lesser than 33% and 0% overlap and more energy has been focused on to the surface.

5.4.2 Verification of FEM by experimental results

A comprative FEM and experimental results is illustrated in the figure 5-13. All peening depths of specimens have been measured by *WYKO NT1100* interfrometer with 10X magnification for all the samples measuring an area of 474×632 µm. The depths were measured for multiple holes and then averaged to get the results presented here. The experimental results of depth of peening in the proposed graph are close to predicted results by FEM in all the 9 models.

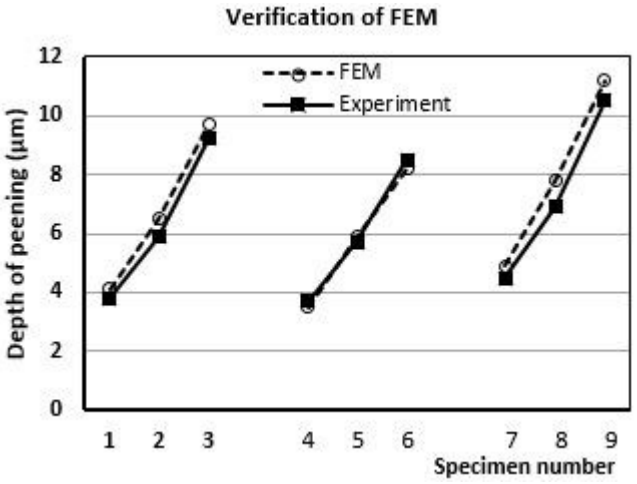

Figure 5-13 Comparison FEM and experimental results of peening depth

5.4.3 Compresive residual stress (CRS)

Evaluation of CRS, magnitudes and penetrated depth are the main objectives of this research. This aim is significant since the depth and magnitudes of CRS have undeniable influence on enhancement of mechanical attributes of specimen. In this research , S_{33} along the depth of 120 µm has been proposed as indicators for assessment of CRS. The FEM results of the magnitue and depth of CRS at one, two and three scans for 0% overlap is shown in Figure 5-14.

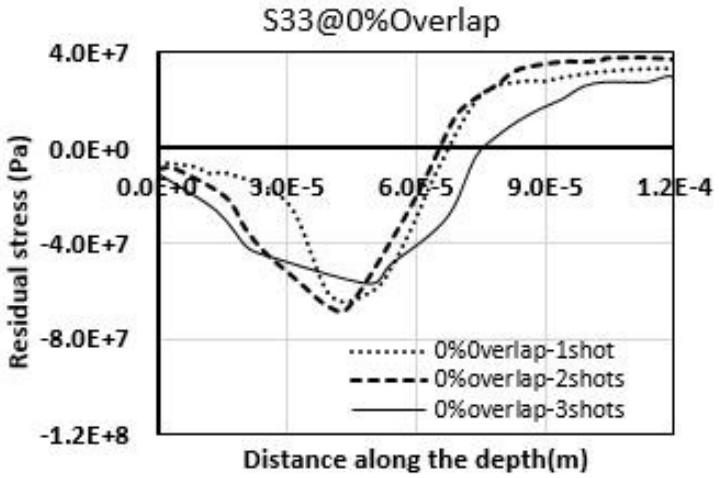

Figure 5-14 Residual stress at 0%overlap

The value of deposited CRS varies from 61 MPa at 40 μm below the specimen surface, 67 MPa at 44 μm below the specimen surface and 57 MPa at 49 μm below the specimen surface; for one shot, two shot and three shots respectively. Similarly the figures 5-15, and 5-16 show the FEM results for 33% and 66% overlap.

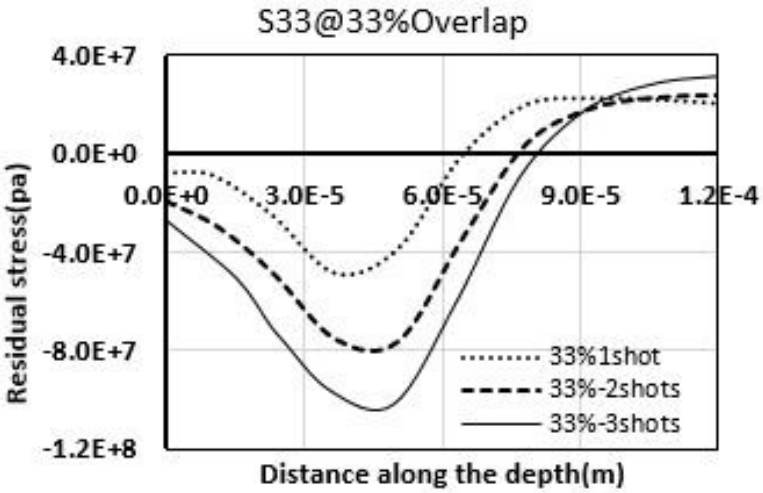

Figure 5-15 Residual stress at 33%overlap

From the figures it can be clearly seen that the maximum S_{33} is 109 MPa at 42.2 μm below the specimen surface for 66% overlap and three scans. The minimum S_{33} is 49 MPa at 37μm below the specimen surface for 33% overlap and one scan.

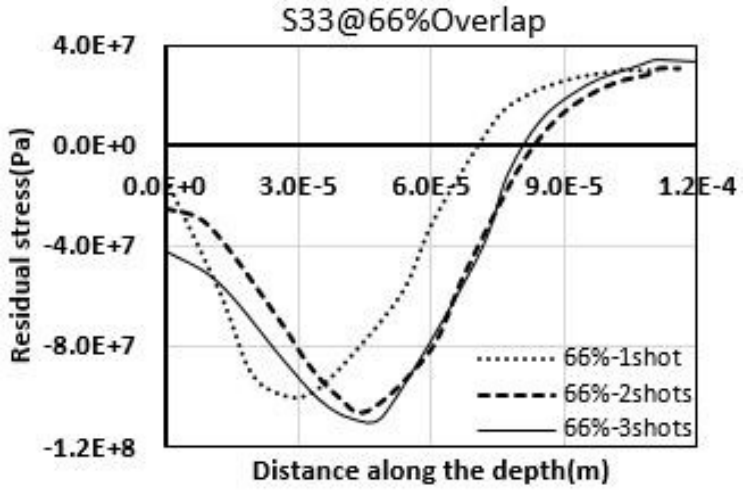

Figure 5-17 Residual stress at 66%overlap

Figure 5-17 provides comprative graph showing impact of percentage of overlap and number of scans on S_{33} in terms of magnitudes and depth of CRS accumulations. In the figure, the horizontal axis shows overlap percentage and the $-S_{33}$ magnitudes shown in vertical axis. Furthermore, the depth of occurrence of the maximum S_{33} have been labeled on each points. At 0%overlap for all specimens at 1, 2, and 3 scans; increase in number of scans from 1 to 2 increases the depth at which the maximum CRS is deposited and the 3 scan does not show major increase in the depth especially at higher overlaps.

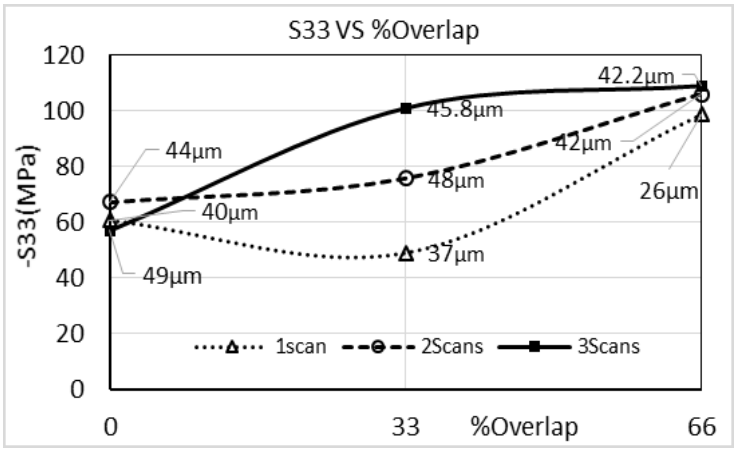

Figure 5-16 Impact of number of scans and %overlap on S_{33} magnitudes and depth

Theses figures 5-14, 5-15 and 5-16 also indicate increase in number of scans causes to increasing of area of S33 below the surface in all 9 models, which mean, more CRS has been accumulated by increasing the magnitude of peening by overlap and by number of scans. Guo et.al.[42] in laser

peening of magnesium has reported that the maximum measured S_{33} with 25 MPa has occurred at 78 μm depth, where the laser intensity was 5.1 GW/cm2 with laser beam diameter of 1 mm. By comparison, it can be stated that by the reduction of laser beam diameter in HRLSP, CRS accumulates closer to the peened surface. This trend is the one as mentioned in the work of Pyre et al. [22]. In order to verify the theoritical results of FEM, measured surface hardness is used to analyze the CRS.

Hardness can indicate accumulation of the compressive residual stress. However, Since in *MVK-H1 Mitutoyo* micro-hardness tester the penetration depth of indentor is less than 5 microns, accumulation of S_{33} in depth of more than 25 micron cannot be deteced by changes in hardness. Hence, the FEM results of S_{33} excactly on the surface has been used for showing correspondance of hardness and CRS. Figure 18 shows relation of measured hardness and S_{33} in all sets of FEM. In the fiugre, the horizontal and vertical axes indicate % overlap and S_{33} surface stress respectively for one two and three scans, totalling 9 specimens. The magnitudes of measured hardness have been labled on top of each specimen.

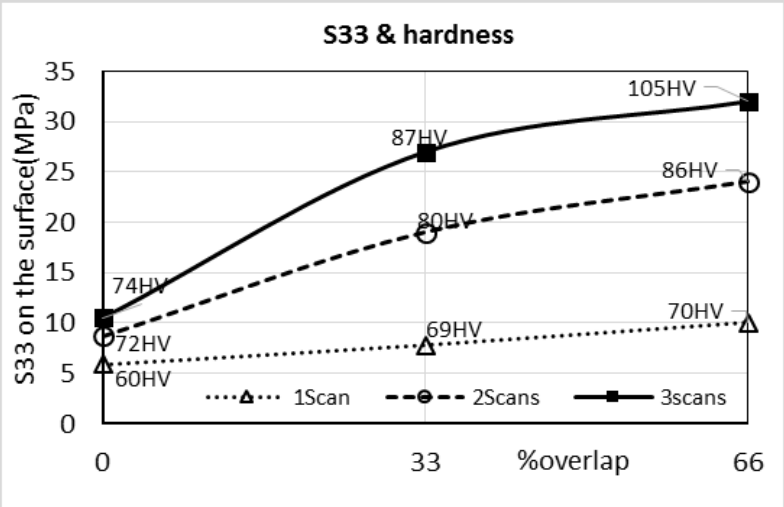

Figure 5-18 Relation of S33 on the surface and hardness

It can be clearly seen that, increase in peening by number of scans and overlap percentage lead to increase in S_{33}. Also it can be seen that the predicted surface S_{33} is accompanied by increasing hardness, where the maximum achieved CRS at the surface is 32 MPa at 66% overlap where the hardness is 105 HV. From the figure, it can be understood that increase in hardness by increase in

percentage of overlap cannot eceed over a value of around 110 HV. This also confirms the hardness increase in magnesium by LSP by Guo et. al. where the maximum achieved hardness was 107 HV.

5.5 Conclusion

The Finite Element Model presented in this work evaluates the impact of HRLSP on a number of magnesium attributes. In order to reduce time of FEM calculation, the interval sequential pressure pulse has been reduced from 10^5 to 10^2 ns. This duration has been calculated by measuring of TD. 9 models were created for 3 overlap percentages and 3 different number of scans. The FEM was executed for all the models and the prediction of CRS along the depth (S_{33}) was calculated, in addition to the depth of plastic deformation. The depth of plastic deformation from the measurement on peened samples showed good agreement with the results from FEM.

The magnitude of maximum deposited CRS and the depth at which the maximum CRS was deposited beneath the magnesium surface was calculated and the results showed that increase in CRS with increase in peening. However there was no significant increase in the depth of deposition when the number of scans were increased from 2 to 3 especially at higher overlaps. The surface CRS calculated from FEM was validated with the measured hardness of respective samples, and it was shown that the increase in surface CRS predicted by FEM accompanies an increase in measured hardness. Moreover, by comparison with earlier research on magnesium LSP with higher beam diameter at 1 mm, it can be stated that by the reduction of laser beam diameter in HRLSP, CRS accumulates closer to peened surface.

In chapter 4 and 5, a Finite Element Model for both single and multiple shot peening of magnesium was presented and the FE results compared favorably with both analytical and experimental results. For further proof of HRLSP, experimental verification of wear resistance and surface wettability, which are two significant parameters for biocompatibility of magnesium implant, have been ascertained in Chapter 6.

CHAPTER 6. Improvement in Attributes of Magnesium Surface by High Repetition Rate Laser Shock Peening

This chapter is based on an article submitted to Journal of Materials Engineering and Performance, Manuscript Number: JMEP-15-12-9637 (Under review)

This chapter covers the objective '2b' of the "Objectives and Scope of the Thesis" in section

6.1 Introduction

Wear resistance and wettability are essential attributes that should be modified for biodegradable magnesium implants [97]. Reduction of wear rate can be achieved by enhancement of hardness. Furthermore, increasing of wettability could be attained by increasing of surface roughness or decrease in grain size on the surface. Earlier, several methods of surface modification have been introduced: coating by biocompatible material such as particular polymer or hydroxyapatite (HA), implantation of oxide film [98], and laser shock peening (LSP) [99]. Inadequate adhesion of the coating with magnesium and possibility of detachment from the implant base is one of the limitations of using the HA or polymer for coating the magnesium. The LSP has been performed successfully to improve mechanical characteristics of magnesium [100]. The LSP creates an invisible coating of compressive residual stress (CRS) upon the magnesium surface. Owing to high capital investment of the LSP, its application is confined to expensive industries. Recently, a novel technique of laser shock peening by high repetition pulsed laser has been introduced by the authors of this study [30]. This novel method of laser peening is much faster and economical. However, insufficient laser intensity is the most significant challenge to perform high repetition rate laser shock peening (HRLSP). Since the number of shots in HRLSP is thousand times higher than LSP, the energy of each pulse in high repetition pulsed laser is less as compared to conventional laser peening. In addition, high number of pulses is another challenge of HRLSP that prerequisites to provide high speed/accuracy scanning system in order to prevent several laser shots at the same point. Use of high speed X-Y axis Galvo-scanner system have made HRLSP possible. This technique has been suggested in our earlier study [30].

6.2 High Repetition Laser Shock Peening (HRLSP)

Mechanisms of the LSP and HRLSP are based on the identical principles in many aspects and the main differences of HRLSP and LSP is laser pulses repetition rate. As long as absorption of laser energy exceeds the material threshold, ablation takes place for a short duration and the material is directly transformed from solid to gas state and plasma will be resulted [24].The plasma can generate an intense shock pressure in the order of few Giga Pascal. The peak of shock pressure and calculation of laser intensity are defined by the equations 6-1 and 6-2, respectively[30][101].

$$P(GPa) = 0.01\sqrt{\frac{\alpha}{2\alpha+3}}\sqrt{Z(\frac{gr}{cm^2 s})}\sqrt{I\left(\frac{GW}{cm^2}\right)} \quad (6\text{-}1)$$

$$I = \frac{P_w/f}{0.78t^2.\tau} \quad (6\text{-}2)$$

Where P stands for the peak shock load, Z represents the impedance of shock wave, α is a constant that is related to efficiency of laser absorption by the material (if most of laser energy absorbed by surface, α will be close to 0.1), I is laser intensity, τ is laser pulse duration, t is the diameter of laser beam or spot size, f is repetition rate and P_w is laser power.

When the shock pressure exceeds the Hugonoit Elastic Limit (HEL) [102], LSP is affected. The equation 2 shows the significance of repetition rate and laser beam diameter in laser peening. Since, in HRLSP the repetition rate is 1000 times greater than ordinary LSP, the laser intensity decreases drastically. Owing to P_w (is set at peak of laser power), f and τ are constant; reduction of beam diameter is the only solution to increase laser intensity that is required for laser peening to take place. Furthermore, avoiding repeated laser shots (10000 shots per second) at the same position is achieved by drastic increase in speed of laser scanning. The required scan speed along the X axis is attained by equation 6-3.

$$S_s = \mathrm{t} \times [1 + (1 - O_p)\,(f - 1)] \quad (6\text{-}3)$$

Where S_s is scan speed in mm and O_p is percentage overlap (shown in figure 6-1-b). This high scan speed (400 mm/s for 0%overlap at 40 µm) with the required accuracy in micrometer range has been provided by a Galvo-mirror *THORLABS GVS002*. The system consists of two Galvano mirrors attached to separate DC servo motors. By appropriate oscillation of the programmed DC motors, the X-Y plane can be properly scanned.

Figure 6-1(a) shows a schematic of the experiment. As figure 6-1-b shows, the overlap has been performed just in X axis. This is due to the fact that the minimum limitation of scanning angle in

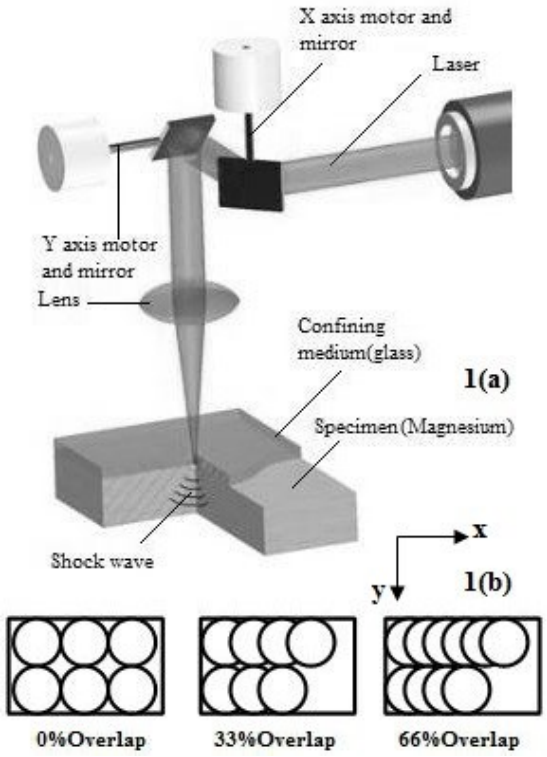

Figure 6-1 Schematic of HRLSP

Y axis direction cannot be less than 0.03º (diameter of one shots at 40 µm) in this Galvo-scanner. However, as long as the beam diameter reduces to micron scale, the unpeened area among the circular shots is negligible. Hence, it can be stated that the changes in mechanical attributes can be propagated homogeneously.

6.3 Setup and design of experiments

Tables 6-1 and 6-2, show the laser and peening specifications used for HRLSP of magnesium. Based on earlier research of the authors [30] and from table 6-1 and 6-2, the HRLSP of magnesium can be possible when laser beam diameter decreases to nearly 50 µm. Hence, by considering two close spot sizes at 40 and 60 µm, 18 experiments have been performed. Spot size, percentage of overlap and number of scans are the variable parameters as shown in table 6-3. The laser PRISMA TM1064-V diode pumped having an average power of 3.52 watts at 10 KHz repetition rate has been used.

Laser power (P_w)	Laser power (P_w)
Pulse duration (τ)	Pulse duration (τ)
Wave length (λ)	Wave length (λ)
Repetition rate (f)	Repetition rate (f)
Beam diameter	Beam diameter

Table 6-1 Laser Specifications

The applied confining medium is glass in all the experiments. The protective coating has not been used owing to the density of magnesium which is 1800 kg/cm^3, using protective coatings with higher density cannot be beneficial for magnification of shock pressure [30]. Specimens are 99.8% magnesium cuboids having 10×10 mm peened surface and 6 mm thickness.

Specimen	99.8% Mg – 0.02%Ca
Peening Area	10 X 10 mm
E and ν	200 GPa and 0.33
Density	1800 Kg/m^3
Confining Medium	Glass (1 mm thick)

Table 6-2 Peening Specifications

The first set of nine experiments has been presented having higher laser intensity of 2.1 GW/cm^2 at 40 µm spot size. These nine experiments has been conducted for evaluation of effectiveness of multiple laser scans (1-3 scans) and percentage of overlap (0 - 66%). Correspondingly, the second set of nine experiments have been performed with lower laser intensity of 0.91 GW/cm^2 at 60 µm spot size. In this study, the results of hardness and surface morphology have been used to investigate the wettability and wear results. Since wear examination was a destructive test, the wear test has been carried out at the end after measuring the hardness, roughness and wettability.

Specimen #	**1**	**2**	**3**	**4**	**5**	**6**	**7**	**8**	**9**	**10**	**11**	**12**	**13**	**14**	**15**	**16**	**17**	**18**
Spot size(µm)	40	40	40	40	40	40	40	40	40	60	60	60	60	60	60	60	60	60
%Overlap	0	0	0	33	33	33	66	66	66	0	0	0	33	33	33	66	66	66
Number of Scans	1	2	3	1	2	3	1	2	3	1	2	3	1	2	3	1	2	3
Hardness(HV)	60	69	77	72	80	86	74	87	105	51	55	58	48	53	59	48	55	57

Table 6-3 List of experiments and measured hardness

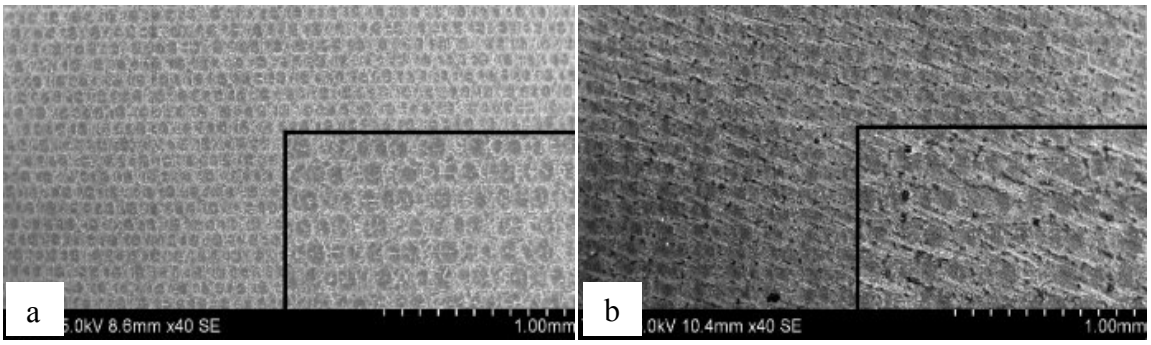

Figure 6-2 SEM of peened surface a) at 40 μm and b) at 60 μm

6.4 Results and discussions

6.4.1 Hardness

Significant increase in the hardness of magnesium is an indication of successful peening [42]. Plastic deformation of the specimen surface leads to enhancement of CRS on the peened surface [19] and increase in hardness will be resulted. MVK-H1 Mitutoyo micro-hardness tester has been used to measure the hardness. The measured hardness values have been tabulated in table 6-3. It must be noted that the hardness of unpeened specimen is 43 HV. The outcome displays that the increase in laser intensity (by reduction in spot size) leads to increasing in hardness. It is observed that the maximum hardness at 40 μm spot size is 105 HV having three scans and 66% overlap, whereas the hardness of three scans, 66% overlap at 60 μm spot size is 57 HV. Table 6-3 indicates that the HRLSP is more efficient at 40μm. Whereas at 60 μm spot size, the significant process can be laser surface melting (LSM). In order to convert the solid metal to gaseous state, the intensity of laser in peening region should be beyond the threshold magnitude. Otherwise the LSM can occur. In LSM, mostly heat treatment causes increase in hardness and surface roughness [103]. Whereas in LSP, increasing of hardness is based on strain-hardening [47]. The hardening of magnesium by the heat treatment is negligible compared to strain-hardening by the LSP[104]. Therefore, increase in hardness strongly proves occurrence of HRLSP on magnesium. To state greater reason for reality of the process at 40 and 60 μm, the figure 6-2 shows the images from the scanning electron microscope (SEM). The images correspond to two types of experiments performed at 33% overlap with shot peening done at 40 and 60 μm, respectively. It can be clearly seen that there are greater depth and arranged spots in figure 6-2-a at 40 μm. Each spot at 40 μm seems circular, whereas melting on the surface at 60 μm causes the expansion of places of the shots

in figure 6-2-b. In addition, in figure 6-2-b, some black tiny spots has been distributed on the surface and more darkness of the surface indicates higher oxidation has been occurred. These evidences indicate that the LSM can be a prominent process at 60 μm.

6.4.2 Surface topography

Kubiak et.al [105] showed that the wettability is a function of roughness depth (D) and surface roughness (R_a). They proposed that the contact angle (CA) as significant indicator for showing wettability; which is inversely proportional to R_a. The increase in the roughness depth can expand the area of the solid-liquid interaction by capillary phenomenon and a reduction in the CA will be resulted. To study the peened surfaces, measurements of R_a and D were performed by WYKO NT1100 interferometer over the scanned surface area of 632 μm×474 μm. Figure 6-3 demonstrates the influence of overlap percentage as well as the number of scans on roughness depth at 60 and 40 μm. The vertical axis displays roughness depth (D) and horizontal axis displays the overlap percentage while peening. The figure shows that increase in numbers of scan can enhance the

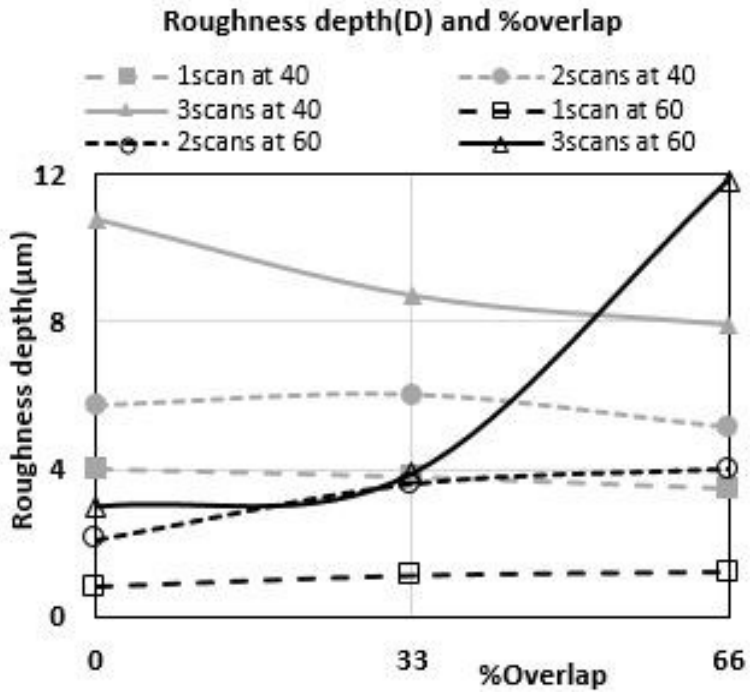

Figure 6-3 Influence of overlap % on fluctuations of roughness depth (D) at 60 and 40 μm

roughness depth at both 60 and 40 μm. While the percentage of overlap varied from 0% to 66%, the curves follow decreasing trend for 40 μm. But for 60 μm it is on the progressive side. This means at 40 μm, laser peening is increased by the number of scans and percentage of overlap leads

to further surface cold pressing. From table 6-3 at 40 μm experiments, significant increase in hardness proves that the major process could be LSP. It can see by increasing of percentage of overlap and number of scans the hardness has increased as well. However, negligible increase of hardness at 60 μm experiments (see table 6-3) indicates that the laser peening cannot be effective and the dominant process is LSM. The reason is that the laser peening (LP) results in reduction of D by additional plastic deformation as occurred in 40 μm experiments. Though in the LSM, each pulse of laser increases the depth of roughness by further surface melting. At higher overlap of 66%, further re-melted material is being driven to machining sides and a drastic increase of D up to 11.8μm is observed in figure 6-3. Equation 6-4 defines the relationship of plastic strain (ε_p) and shock pressure in HRLSP[106][107].

$$\varepsilon_P = -\frac{2HEL}{2\mu+3\lambda}\left(\frac{P}{HEL}-1\right) \qquad (6\text{-}4)$$

Where μ and λ are lama's constants. The equation 6-4 shows that increase in shock pressure enhances plastic deformation. From equations 6-1 and 6-2, amplifying of shock pressure occurs by reduction in laser beam diameter as this enhances the laser intensity (I). Hence, an increase in shock pressure results in higher cold working and strain hardening which in turn provides increased hardness. Figure 6-4 provides greater clarification for relationship between hardness and parameters of peening.

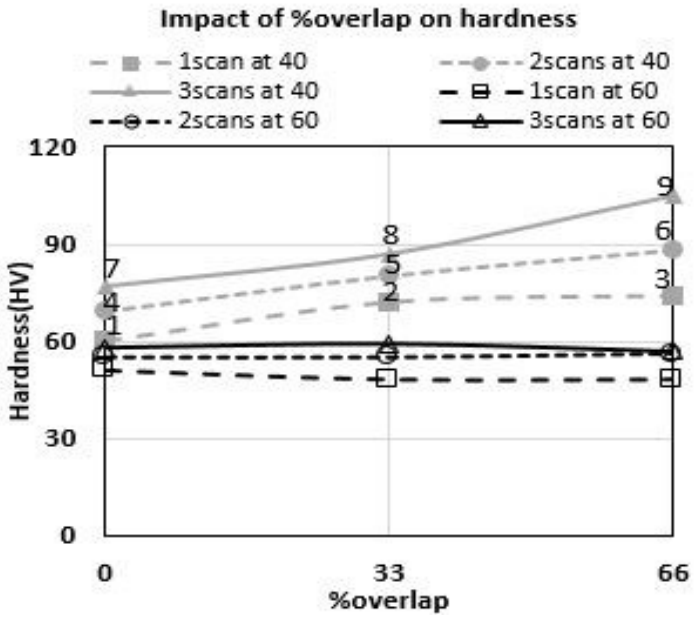

Figure 6-4 Impact of percentage of overlap on hardness at 60 and 40μm

At 60 μm experiments, increasing the percentage overlap and the number of scans does not have any significant effect in hardness. This shows that the laser peening has not occurred at 60 μm. However, at 40 μm experiments increasing the number of scans and overlap percentage leads to increase in hardness. For instance, the hardness at 1 scan increases from 60 HV to 74 HV, where the overlap percentage varies from 0 to 66% (specimens 1, 4, and 7). Also, the hardness increases from 77 HV to 105 HV at an overlap of 66%, where the number of scans is increased from 1 to 3 (specimens 3, 6 and 9).

Observing the results at 40 μm in figure 6-4, there is a significant effect of the time of applying the shock pressure on increasing hardness. Within range of experiments for 40 μm spot size, the total number of peening shots on the 10×10 mm area varies from 62500 peening shots for specimen 1 (0% overlap, 1 scan) to a maximum of 551500 peening shots for specimen 9 (66% overlap, 3 scans). It can also be seen that the number of peening shots is about 185000 for specimens 3, 5, and 7. Hence in figure 6-4, the hardness is lowest for specimen 1 at 60 HV; highest for specimen 9 at 105HV; and for specimens 3, 5, 7 the hardness is between 77±3HV, which further shows the effect of number of peening shots has a direct bearing on increasing the hardness.

6.4.3 Wettability

Enhancement of wettability plays a vital role in improvement of magnesium biocompatibility [108]. Measurement of contact angle (CA) is the method used to assess the wettability of the peened surface. The effectiveness of overlap on the CA at 60 μm has been demonstrated in figure 6-5. In this figure, the CA at the entire specimens has been reduced in comparison with un-peened specimen that is measured at 68.5^{o}. Overall, increase in roughness depth D, (see figure 6-3) has caused decrease in the CA. In 3 scans, even though there is a drastic increase in roughness depth from 3.9 to 11.8μm, the CA remains constant in figure 6-5. The reason is when D exceeds a critical value, further increase in the depth of valley creates a barrier to liquid expansion [109] and no further decrease is possible.

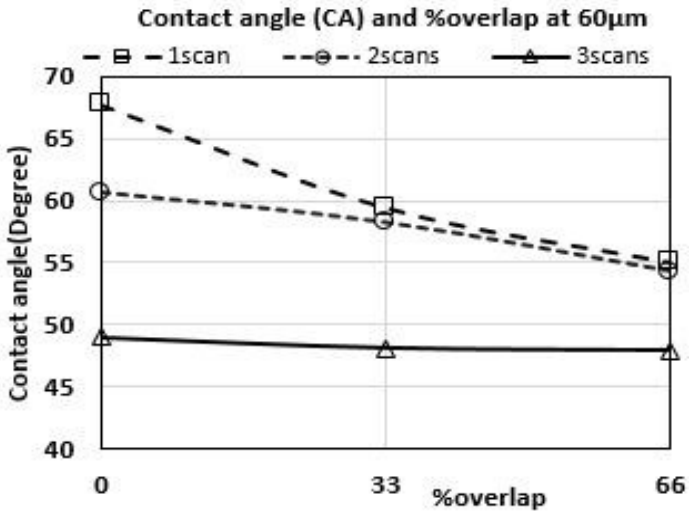

Figure 6-5 Impact of percentage of overlap and number of scans on contact angle at 60 µm

Figure 6-6 indicates fluctuations of the CA at 40 µm where the overlap varies from 0 to 66% and the number of scans from 1 to 3. In specimens 1, 2 and 3, where the number of scan is 1, reduction of roughness depth (see figure 6-3) leads to increase in CA.

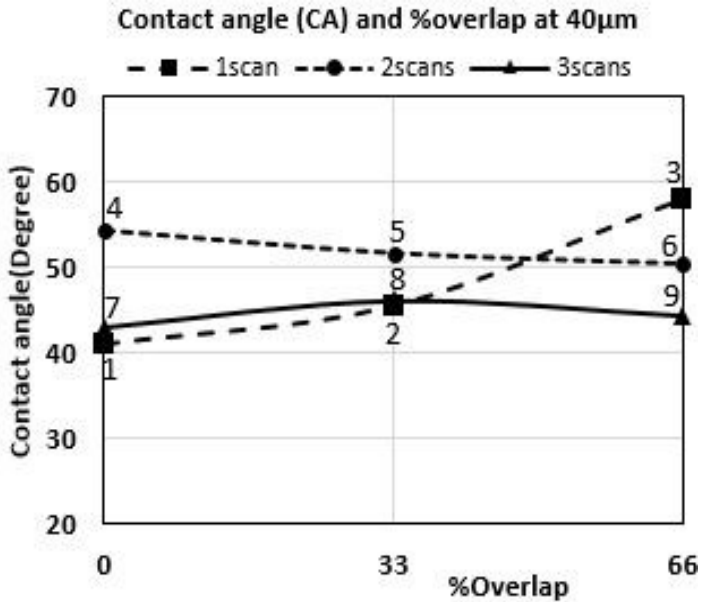

Figure 6-6 Impact of percentage of overlap and number of scans on contact angle

Where the number of scans is 2 (specimens 4, 5,6), owing to increase in D (see figure 6-3), reduction in the CA between specimens 4 and 5 is reasonable. However, between 5 and 6, regardless of the decrease in D, the reduction in CA is seen from 51.7º to 50.5º. This is repeated between specimens 8 and 9 at 3 scans where despite the reduction in D from 8.7 to 7.9 µm, the CA

reduces from 46.2º to 44.2º. These 2 anomalies in the relationship between D and CA is explained by the grain size reduction and grain distribution owing to significant increase in hardness of Magnesium [110]. Further peening (cold-working) due to increase in number of scans and overlap percentage increases the specimen hardness. This leads to reduction in grain size resulting in reduced CA (see specimen 5, 6 and 8, 9 in figure 6-6) [105] [107] [110]. Previous research indicate that as long as the hardness exceeds a critical value of around 80 HV for Magnesium [110], the propagation of grains starts to become more uniform and the reduction in CA is accelerated [111].

Though hardness does not have direct impact on the CA, it plays a significant role once the critical value is reached. This is shown in the figure 6-7 where the roughness depth is in horizontal axis, and the CA is in vertical axis. The hardness values in HV for each specimen is labeled on top of the points in the figure. It can be clearly seen that despite reduction of roughness depth from specimen 5 to 6 and 8 to 9, where the hardness of the specimens have exceeded 80 HV; there are reductions in CA.

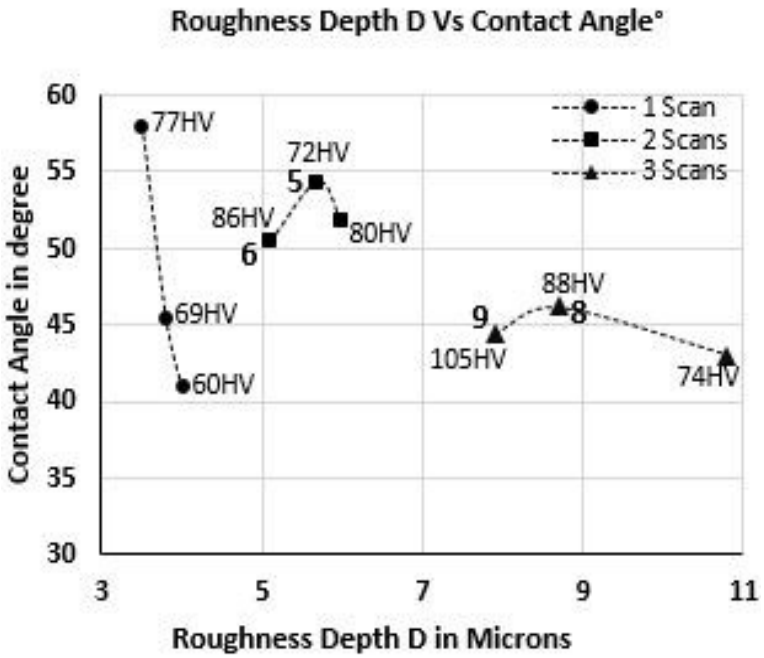

Figure 6-7 Impact of more peening (increasing in hardness) on contact angle

As mentioned earlier, the hardness is an indicator of further peening (cold working) causing reduction in grain size and increase in wettability. From the results, the best possible approach to improve both hardness and wettability within the experimental sets is to peen at three scans with

66% overlap and 40 μm spot size, where a minimum CA of 44.4° and the maximum hardness of 105 HV have been achieved.

6.4.4 Wear

Earlier research has reported decreasing of wear rate by conduction of LSP [112]. In this research, *Pin-On-Disc* method has been used for assessment of wear resistance. All the tests have been performed with a vertical force of 9.8 N. The area of attrition is 10×10 mm in all the experiments. The impacts of both hardness and roughness (R_a) on the wear rate have been evaluated in different stages. At the first stage, the initial weight of the specimen was recorded. Afterwards, 5 second attrition was used on the specimen, and weight of the specimen was measured again. This process was repeated two additional times for each attrition period of 10 seconds; making the overall attrition period to 25 seconds. This design of experiment provides beneficial data to evaluate wear rate in three layers. Hence, the wear rate can be measured in mass per time (gr/s) and thickness per time (t_i/s). This technique of wear measurement contributes to interpret a number of exceptions which will be discussed in figure 6-8 and 6-9.

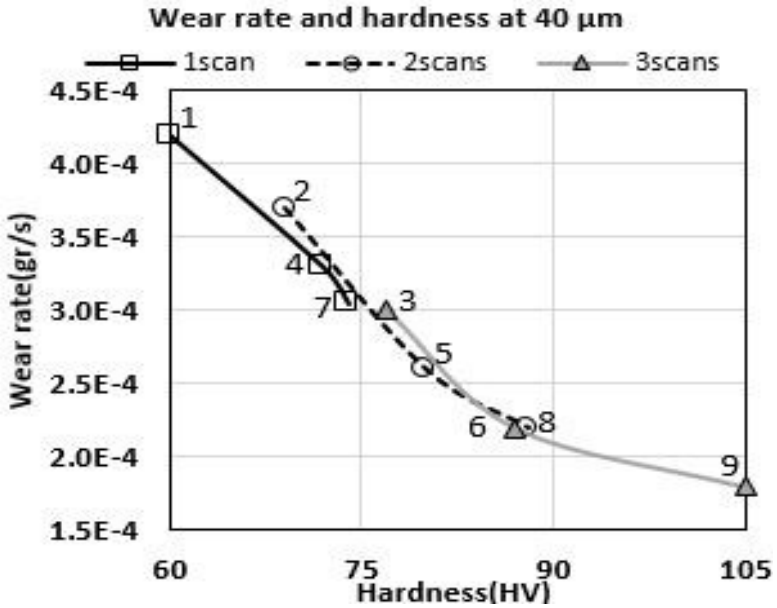

Figure 6-8 Impact of hardness on wear rate

At 60 µm spot experiments, there is no notable increase in hardness (see table 6-3). At 60 µm, the wear rates of specimens are extremely close to un-peened specimen which is 5.5E-4 gr/s. Dissimilar of 60 µm, significant improvement in wear rate have been recorded at 40 µm experiments as screening in figure 6-8. The horizontal axis shows hardness in HV and the vertical axis defines wear rate in gr/s over the course of 25 seconds attrition. It can be clearly seen that the reduction of wear rate has been occurred by enhancement of hardness. However, the specimens 3 and 7 demonstrate an exception in figure 6-8. Even though the hardness of 3 is greater than 7, the wear rates are equal at 0.0003 gr/s. This exception can be clarified by observing figure 6-3. Figure 6-3 indicates the corresponding D are 3.6 and 10.8 µm for specimens 3 and 7, respectively. It can assume that the attrition of rougher surface could be carried out at a higher rate. Therefore, despite high hardness of specimen 7, more roughness causes the wear rate to be equal to specimen 3. This issue can be explained by figure 6-9 which shows the sequences of wear rate for specimens 3 and 7.

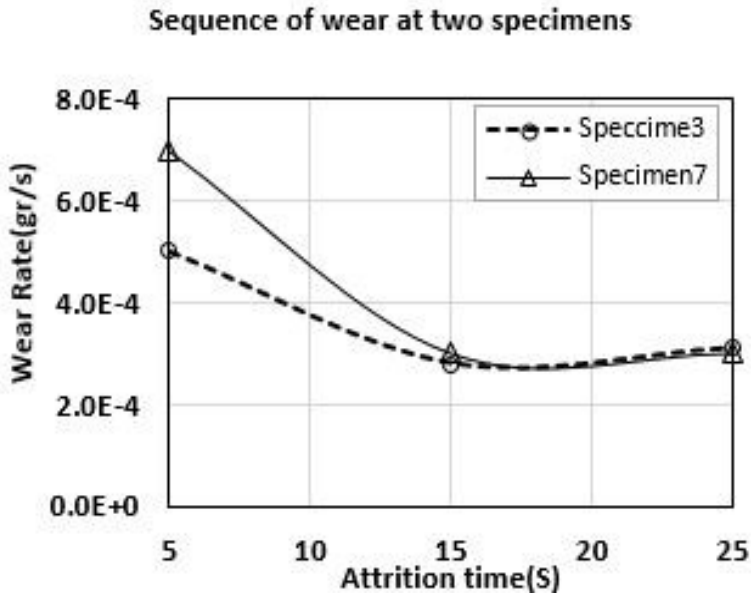

Figure 6-9 Wear rate of specimen 4 and 7 in 25(S) attrition

The figure 6-9 has been drawn by the data attrition at three stages 5, 15, and 25 seconds of attrition. During the first 5 seconds of attrition, the wear rate of specimen 7 (7.0E-4 gr/s) having more hardness is higher than specimen 5 (5.0E-4 gr/s). At 18 seconds of attrition, both specimens have the same wear rate at 3 E-4 gr/s and at 25 seconds, the wear rate of specimen 3 exceeds that of specimen 7. This trend is due to difference in D.

6.5 Conclusions

This study is an experimental attempt to prove the feasibility of high repetition rate laser shock peening (HRLSP) on magnesium. Significant increase in hardness from 45 HV for unpeened magnesium to 105 HV for peened magnesium at 40 μm is an evidence for the HRLSP occurrence. This is because of pure magnesium can be hardened just by strain-hardening that generated by laser peening. At 40 μm spot size, the dominant process is laser shock peening whereas laser surface melting is more dominant at 60 μm spot size. Hence, the maximum achieved hardness at 60μm peening is only 59 HV. The results indicate that increasing in amount of peening (through overlap percentage and number of scans) can reduce the contact angle from 68.5º for un-peened specimen to 44.4º for 3 scans-66% overlapped specimen. Furthermore, in high repetition rate, laser shock peening of magnesium, size of grains and roughness depth are effective parameters for variation in contact angle. At 40 μm, increasing the number of scans and percentage of overlap cause wettability and hardness to improve. The wear results indicate that enhancement of roughness can increase the wear rate. This research proposes the best possible approach to improve both hardness and wettability is at three scans, 66 % overlap with 40 μm spot size.

The feasibility, theoretical as well as experimental verification of HRLSP have been done in the preceding chapters. In Chapter 7, the conclusions of this thesis and possible future direction of research have been highlighted.

CHAPTER 7. Conclusions and Future Work

7.1 Conclusions

The primary objective of developing a High Repetition Rate Laser Shock Peening system for improving the surface attributes of biodegradable material like Magnesium has been achieved through this work. The feasibility study was done to understand if such a system will have positive impact on the surface attributes of Magnesium. Subsequently, the experimental system was setup and design of experiments was performed following which preliminary results on Magnesium surface were ascertained. Finite Element models were done to simulate the single shot as well as multiple shot peening considering the overlap and the number of scans to mirror the experimental conditions used. Further experiments were done on Magnesium to verify the model as well as measure improvements in surface attributes such as hardness, Roughness, Wettability and Wear Resistance. The summary of conclusions are highlighted below.

- From the critical review of literature, it is clear that, biodegradable metallic implants and application of LSP for tuning their properties is a novel area which needs lots of research work. Multiple works on Magnesium and LSP were reviewed and considering the low mechanical strength of magnesium use of High Repetition Rate Laser for Shock Peening was identified as the most efficient laser shock peening method.

- A feasibility study was done to identify the peening parameters to be able to modify the surface attributed to magnesium using the HRLSP process. Low cost equipment, fast performance, and accumulation of compressive residual stress closer to the surface providing better corrosion rate control are the main reasons for assessing the feasibility of HRLSP as a novel method instead of LSP. It has been recommended, in order to HRLSP Magnesium, the best choice could be: Magnesium foil as protective coating and quartz for flat and motor oil or any appropriate liquid with low chemical reaction and high acoustic impedance for complicated shapes as confining medium.

- Subsequent to the feasibility study, experiments were performed and the occurrence of peening was evaluated by measuring depth of peening, change in micro hardness and surface

roughness of peened samples in comparison to unpeened magnesium. Peening was performed with laser intensities of 0.91 GW/cm^2 and 2 GW/Cm^2. When the laser intensity is 0.91GW/cm^2, though the shock pressure is more than the HEL of mg, laser surface melting was more predominant compared to shock peening. This was evidenced by hardness measurements on the surface where no significant improvement was seen. Furthermore, the SEM images showed evidence of machining and solidified material. However, when the intensity was increased to 2 GW/Cm^2, effective peening was observed. At one scan, 0%overlap, the depth of peening was analytically found to be 3.97 μm and the measured depth was 3.8 μm which was very close to theoretical value. The surface hardness increased from 45 to 103 HV which is very similar to the hardness achieved by other works on laser peening of magnesium. In addition, increase in R_a from 0.35 μm for unpeened specimen to 3.3μm for peened specimen with laser intensity at 2 GW/Cm^2. Also the SEM images clearly show evidence of uniform peening without any trace of machining or solidified material at this intensity proving the occurrence of HRLSP.

- After the preliminary experimental work, Finite Element Analysis of the peening process with single laser shot was performed and the transient time and steady state time for peening was modeled. Also the magnitude and depth of CRS in addition to change in surface topography by HRLSP of magnesium has been simulated. The simulated results were validated by analytical and experimental work. The FEM was used to show occurrence of HRLSP by predicting the magnitude and depth of CRS. The maximum CRS along the depth has been found to be -48MPa at 28 μm beneath the peened surface. The FEM predicted the peening depth as 4.02 μm and this matches closely with the experimental and analytical results.

- Further FEM study on the impact of multiple shots was modeled to relate closely to experimental variations of HRLSP and 9 models were created for 3 overlap percentages and 3 different number of scans. This FEM evaluates the impact over an area of 3 subsequent spots on a number of magnesium attributes. The FEM was executed for all the models and the prediction of CRS along the depth (S_{33}) was calculated, in addition to the depth of plastic

deformation. The depth of plastic deformation from the measurement on peened samples showed good agreement with the results from FEM. The magnitude of maximum deposited CRS and the depth of deposition was calculated and the results showed increase in CRS with increase in peening. However there was no significant increase in the depth of deposition when the number of scans were increased from 2 to 3 especially at higher overlaps. The surface CRS calculated from FEM was validated with the measured hardness. By comparison with earlier research on magnesium LSP, it can be concluded that by the reduction of laser beam diameter in HRLSP, CRS accumulates closer to peened surface. This is one of the significant advantages of HRLSP that provide better prevention of nano cracks expansion on the surface which is the origin of corrosion.

- Finally, experiments were performed on the peened samples to understand the wear rate as well as the surface wettability at 2 GW/Cm^2 where the dominant process is laser shock peening. The results indicate peening parameters influence surface wettability which could be decreased from a contact angle of 68.5º for un-peened specimen to 44.4º for 3 scans-66% overlapped specimen. Furthermore, in high repetition rate, laser shock peening of magnesium, size of grains and roughness depth are effective parameters for variation in contact angle. In addition to change in wettability, wear resistance could also be improved by varying the peening parameters and the results indicate that enhancement of roughness can reduce the wear rate from $5.5X10^{-4}$ gr/s for unpeened mg samples to $1.8X10^{-4}$ gr/s for mg samples peened at 3 scans and 66% overlap.

7.2 Future Work

The primary objective of developing a High Repetition Rate Laser Shock Peening system for improving the surface attributes of biodegradable material like Magnesium has been achieved through this work. The occurrence of peening was analyzed both by FEM and by experiments. Improvement of mechanical attributes like R_a, hardness, wear resistance and wettability were proved experimentally. The possible future directions for continuance of this work are

- Experimentally verify the depth and magnitude of residual stress through XRD or by hole drilling methods

- Theoretically model the corrosion behaviour and magnesium
- Experimentally validate the theoretical corrosion prediction
- Assessing the impact of the laser peening mechanism at lower pulse width (Picosecond and Femtosecond laser) on hardness, surface topography, wear rate and wettability.
- More advanced peening techniques like warm laser peening where a pre-warmed specimen surface which is combined the thermal and the mechanical impact of shock pressure.
  This technique can provide a dynamic aging in the microstructure of the specimen surface. Sediments enclosed by compressed dislocation together with compressive residual stress cause significant increase the mechanical properties of the workpiece.

References:

[1] Y. K. Zhang, J. Z. Lu, X. D. Ren, H. B. Yao, and H. X. Yao, "Effect of laser shock processing on the mechanical properties and fatigue lives of the turbojet engine blades manufactured by LY2 aluminum alloy," *Mater. Des.*, vol. 30, no. 5, pp. 1697–1703, May 2009.

[2] X. P. Zhang, Z. P. Zhao, F. M. Wu, Y. L. Wang, and J. Wu, "Corrosion and wear resistance of AZ91D magnesium alloy with and without microarc oxidation coating in Hank's solution," *J. Mater. Sci.*, vol. 42, no. 20, pp. 8523–8528, Jun. 2007.

[3] M. P. Sealy and Y. B. Guo, "Fabrication and Characterization of Surface Texture for Bone Ingrowth by Sequential Laser Peening Biodegradable Orthopedic Magnesium-Calcium Implants," *J. Med. Device.*, vol. 5, no. 1, p. 011003, 2011.

[4] M. P. Staiger, A. M. Pietak, J. Huadmai, and G. Dias, "Magnesium and its alloys as orthopedic biomaterials: a review.," *Biomaterials*, vol. 27, no. 9, pp. 1728–34, Mar. 2006.

[5] C. Ruff, B. Holt, and E. Trinkaus, "Perspectives Who ' s Afraid of the Big Bad Wolff ? : '" Wolff " s Law '' and Bone Functional Adaptation," vol. 498, no. September 2005, pp. 484–498, 2006.

[6] J. C. Middleton and a J. Tipton, "Synthetic biodegradable polymers as orthopedic devices.," *Biomaterials*, vol. 21, no. 23, pp. 2335–46, Dec. 2000.

[7] D. Persaud-Sharma and A. McGoron, "Biodegradable Magnesium Alloys: A Review of Material Development and Applications.," *J. Biomim. Biomater. Tissue Eng.*, vol. 12, pp. 25–39, Feb. 2012.

[8] M. Salahshoor and Y. Guo, "Biodegradable orthopedic magnesium-calcium (mgca) alloys, processing, and corrosion performance," *Materials (Basel).*, vol. 5, no. 12, pp. 135–155, Jan. 2012.

[9] I. Nikitin and I. Altenberger, "Comparison of the fatigue behavior and residual stress stability of laser-shock peened and deep rolled austenitic stainless steel AISI 304 in the temperature range 25–600°C," *Mater. Sci. Eng. A*, vol. 465, no. 1–2, pp. 176–182, Sep. 2007.

[10] C. M. Gill, N. Fox, and P. J. Withers, "Shakedown of deep cold rolling residual stresses in titanium alloys," *J. Phys. D. Appl. Phys.*, vol. 41, no. 17, p. 174005, Sep. 2008.

[11] D. F. Williams, "On the mechanisms of biocompatibility.," *Biomaterials*, vol. 29, no. 20, pp. 2941–53, Jul. 2008.

[12] J. E. Gray and B. Luan, "Protective coatings on magnesium and its alloys — a critical review," *J. Alloys Compd.*, vol. 336, no. 1–2, pp. 88–113, Apr. 2002.

[13] P. Volovitch, J. E. Masse, a. Fabre, L. Barrallier, and W. Saikaly, "Microstructure and corrosion resistance of magnesium alloy ZE41 with laser surface cladding by Al–Si powder," *Surf. Coatings Technol.*, vol. 202, no. 20, pp. 4901–4914, Jul. 2008.

[14] B. Hadzima, M. Bukovina, and P. Doležal, "Shot Peening Influence on Corrosion Resistance Of Ae21 Magnesium Alloy," vol. 17, no. 4, pp. 14–19, 2010.

[15] Z. Pu, S. Yang, G.-L. Song, O. W. Dillon, D. a. Puleo, and I. S. Jawahir, "Ultrafine-grained surface layer on Mg–Al–Zn alloy produced by cryogenic burnishing for enhanced corrosion resistance," *Scr. Mater.*, vol. 65, no. 6, pp. 520–523, Sep. 2011.

[16] A. Abdal-hay, M. Dewidar, J. Lim, and J. K. Lim, "Enhanced biocorrosion resistance of surface modified magnesium alloys using inorganic/organic composite layer for biomedical applications," *Ceram. Int.*, vol. 40, no. 1, pp. 2237–2247, Jan. 2014.

[17] G. Wu, W. Dai, H. Zheng, and A. Wang, "Surface & Coatings Technology Improving wear resistance and corrosion resistance of AZ31 magnesium alloy by DLC / AlN / Al coating," *Surf. Coat. Technol.*, vol. 205, no. 7, pp. 2067–2073, 2010.

[18] T. M. Yue, Y. P. Su, and H. O. Yang, "Laser cladding of Zr 65 Al 7 . 5 Ni 10 Cu 17 . 5 amorphous alloy on magnesium," vol. 61, pp. 209–212, 2007.

[19] A. Gujba and M. Medraj, *Laser Peening Process and Its Impact on Materials Properties in Comparison with Shot Peening and Ultrasonic Impact Peening*, vol. 7, no. 12. 2014.

[20] M. Salahshoor and Y. B. Guo, "Process mechanics in ball burnishing biomedical magnesium–calcium alloy," *Int. J. Adv. Manuf. Technol.*, vol. 64, no. 1–4, pp. 133–144, Mar. 2012.

[21] H. Man, K. W. K. Yeung, K. On, V. Tam, P. K. Chu, K. D. K. Luk, and K. M. C. Cheung,

"Biomaterials A biodegradable polymer-based coating to control the performance of magnesium alloy orthopaedic implants," *Biomaterials*, vol. 31, no. 8, pp. 2084–2096, 2010.

[22] A. Kruusing, *Handbook of Liquids-Assisted Laser Processing*. Elsevier, 2007.

[23] Q.-Z. Luo, N. D'Angelo, and R. L. Merlino, "Shock formation in a negative ion plasma," *Phys. Plasmas*, vol. 5, no. 8, p. 2868, 1998.

[24] H. S. Niehoff, F. Vollertsen, and B. Institut, "Laser induced shock waves in deformation processing," *MJOM Metal. - J. Metall.*, 2007.

[25] H. Search, C. Journals, A. Contact, M. Iopscience, M. Simul, and I. P. Address, "FEM calculation of residual stresses induced by laser shock processing in stainless steels," vol. 205.

[26] Y. Hu, Z. Yao, and J. Hu, "3-D FEM simulation of laser shock processing," *Surf. Coatings Technol.*, vol. 201, no. 3–4, pp. 1426–1435, Oct. 2006.

[27] Y. Sano, M. Obata, and T. Yamamoto, "Residual stress improvement of weldment by laser peening Residual stress improvement of weldment by laser peening," vol. 7116, no. November, 2015.

[28] A. King, A. Steuwer, C. Woodward, and P. J. Withers, "Effects of fatigue and fretting on residual stresses introduced by laser shock peening," vol. 436, pp. 12–18, 2006.

[29] R. Peyre, P., Scherpereel, X., Berthe, L., & Fabbro, "Current trends in laser shock processing." Surface engineering, p. 377, 1998.

[30] H. Kamkarrad, S. Narayanswamy, and X. S. Tao, "Feasibility study of high-repetition rate laser shock peening of biodegradable magnesium alloys," *Int. J. Adv. Manuf. Technol.*, vol. 74, no. 9–12, pp. 1237–1245, Jun. 2014.

[31] H. Kamkarrad, S. Narayanswamy, and M. Keshmiri, "High Repetition Laser Shock Peening on Magnesium Based Biodegradable Alloys," *J. laser micro Nanoeng.*, pp. 1–7, 2015.

[32] J. K. A. Luft, "Microstructure Formed in Body Centred Cubic Metals by Laser Shock Processing," vol. 17, no. 5, pp. 379–383, 2001.

[33] G. Schmidt-Uhlig, T., Karlitschek, P., Yoda, M., Sano, Y., & Marowsky, "Laser shock processing with 20 MW laser pulses delivered by optical fibers," vol. 9, pp. 235–238, 2000.

[34] L. Berthe, A. Sollier, P. Peyre, R. Fabbro, and E. Bartnicki, "The generation of laser shock waves in a water-confinement regime with 50 ns and 150 ns XeCl excimer laser," vol. 2142.

[35] J. Masse and G. Barreau, "Laser generation of stress waves in metal," vol. 70, pp. 231–234, 1995.

[36] M. H. and H. N. P. M.Gerland, "Comparison of two new surface treatment processes, laser-induced shock waves and primary explosive: application to fatigue behaviour," vol. 56, pp. 175–182, 1992.

[37] A. B. V. D. GREVEY, L. MAIFFREDY, "Laser shock on a TRIP alloy : mechanical and metallurgical consequences," vol. 27, pp. 2110–2116, 1992.

[38] S. M. Toller, "Laser Peening Process and Apparatus with Uniform Pressure Pulse Confinement," 2000.

[39] "The world's most comprehensive materials database www.keytometals.com/Articles/Art146.htm." .

[40] M. Milad, N. Zreiba, F. Elhalouani, and C. Baradai, "The effect of cold work on structure and properties of AISI 304 stainless steel," *J. Mater. Process. Technol.*, vol. 203, no. 1–3, pp. 80–85, Jul. 2008.

[41] H. Carreón and J. L. González-carrasco, "Characterization of laser peening- induced effects on a biomedical Ti6Al4V alloy by thermoelectric means," 2015.

[42] Y. Guo, M. P. Sealy, and C. Guo, "Significant improvement of corrosion resistance of biodegradable metallic implants processed by laser shock peening," *CIRP Ann. - Manuf. Technol.*, vol. 61, no. 1, pp. 583–586, Jan. 2012.

[43] A. H. C. Fairand, B. P., "Laser generation of high-amplitude stress waves in materials.," *J. Appl. Phys.*, vol. 50, pp. 1497–1502, 1979.

[44] R. Berthe, L., Sollier, A., Peyre, P., Carboni, C., Bartnicki, E., & Fabbro, "Physics of shock-wave generation by laser plasma in water confinement regime.," *High-Power Laser Ablation*, pp. 511–520, 2000.

[45] R. F. P. PEYRE, “Laser shock processing : a review of the physics and applications,” vol. 27, pp. 1213–1229, 1995.

[46] H. P. L. b Peyre a R. Fabbro , P. Merrien, “Laser shock processing of aluminium alloys. Application to high cycle fatigue behaviour,” *Mater. Sci. Eng.*, vol. 210, pp. 102–113, 1996.

[47] M. P. Sealy and Y. B. Guo, “Surface integrity and process mechanics of laser shock peening of novel biodegradable magnesium-calcium (Mg-Ca) alloy.,” *J. Mech. Behav. Biomed. Mater.*, vol. 3, no. 7, pp. 488–96, Oct. 2010.

[48] W. Braisted and R. Brockman, “Finite element simulation of laser shock peening,” *Int. J. Fatigue*, vol. 21, pp. 719–724, 1999.

[49] K. D. and L.ye, *“Laser shock peening performance and process simulation.”* woodhead publishing limited, 2006.

[50] K. Kieswetter, Z. Schwartz, D. D. Dean, and B. D. Boyan, “in Oral Biology & Medicine The Role of Implant Surface Characteristics,” *Int. Am. Assoc. Dent. Res.*, 1996.

[51] B. Arifvianto, M. Mahardika, P. Dewo, P. T. Iswanto, and U. a. Salim, “Effect of surface mechanical attrition treatment (SMAT) on microhardness, surface roughness and wettability of AISI 316L,” *Mater. Chem. Phys.*, vol. 125, no. 3, pp. 418–426, Feb. 2011.

[52] A. Allen, C. Andreani, M. T. Hutchings, and C. G. Windsor, “Measurement of internal stress within bulk materials using neutron diffraction,” no. October, 1981.

[53] M. B. Ey, C. Electricity, G. Board, and B. N. Laboratories, “Accwrate measurement o f residual stress an any steel using the centre hole method,” no. July, pp. 99–106, 1976.

[54] G. S. Schajer and M. B. Prime, “Residual Stress Solution Extrapolation for the Slitting Method Using Equilibrium Constraints,” *J. Eng. Mater. Technol.*, vol. 129, no. 2, p. 227, 2007.

[55] E. Tanala, G. Bourse, M. Fremiot, and J. F. De Belleval, “Determination of near surface residual stresses on welded joints using ultrasonic methods,” *NDT E Int.*, vol. 28, no. 2, pp. 83–88, Apr. 1995.

[56] J. Gauthier, T. W. Krause, D. L. Atherton, M. T. Laboratories, and K. A. Og, "Measurement of residual stress in steel using the magnetic Barkhausen noise technique," *NDT E Int.*, vol. 31, no. 1, pp. 23–31, 1998.

[57] A. N. Measurement and G. P. Guide, "Determination of Residual Stresses by X-ray Diffraction - Issue 2," no. 52.

[58] G. Hammersley, L. a. Hackel, and F. Harris, "Surface prestressing to improve fatigue strength of components by laser shot peening," *Opt. Lasers Eng.*, vol. 34, no. 4–6, pp. 327–337, Oct. 2000.

[59] B. Wu, S. Tao, and S. Lei, "Numerical modeling of laser shock peening with femtosecond laser pulses and comparisons to experiments," *Appl. Surf. Sci.*, vol. 256, no. 13, pp. 4376–4382, Apr. 2010.

[60] R. . Nalla, I. Altenberger, U. Noster, G. . Liu, B. Scholtes, and R. . Ritchie, "On the influence of mechanical surface treatments—deep rolling and laser shock peening—on the fatigue behavior of Ti–6Al–4V at ambient and elevated temperatures," *Mater. Sci. Eng. A*, vol. 355, no. 1–2, pp. 216–230, Aug. 2003.

[61] H. Lim, P. Kim, H. Jeong, and S. Jeong, "Enhancement of abrasion and corrosion resistance of duplex stainless steel by laser shock peening," *J. Mater. Process. Technol.*, vol. 212, no. 6, pp. 1347–1354, Jun. 2012.

[62] M. K. Stanford and V. K. Jain, "Friction and wear characteristics of hard coatings," *Wear*, vol. 251, no. 1–12, pp. 990–996, Oct. 2001.

[63] M. Shukla, Y. Kashyap, P. . Sarkar, a Sinha, H. . Pant, R. . Rao, N. . Gupta, V. . Senecha, and B. . Godwal, "Laser induced shock pressure multiplication in multi layer thin foil targets," *Nucl. Fusion*, vol. 46, no. 4, pp. 419–431, Apr. 2006.

[64] G. Manivasagam, D. Dhinasekaran, and A. Rajamanickam, "Biomedical Implants : Corrosion and its Prevention - A Review," no. i, pp. 40–54, 2010.

[65] X. L. Zhang, Z. H. Jiang, Z. P. Yao, Y. Song, and Z. D. Wu, "Effects of scan rate on the potentiodynamic polarization curve obtained to determine the Tafel slopes and corrosion current density," *Corros. Sci.*, vol. 51, no. 3, pp. 581–587, Mar. 2009.

[66] J. a. Platt, A. Guzman, A. Zuccari, D. W. Thornburg, B. F. Rhodes, Y. Oshida, and B. K.

Moore, “Corrosion behavior of 2205 duplex stainless steel,” *Am. J. Orthod. Dentofac. Orthop.*, vol. 112, no. 1, pp. 69–79, Jul. 1997.

[67] et al 8. Ballard P, Fournier J, Fabbro R, “Residual stresses induced by laser-shocks." IV 1.C3 (1991): C3-487,” *J Phys IV*, vol. 3, p. 1991, 1991.

[68] G. Song, “Control of biodegradation of biocompatable magnesium alloys,” *Corros. Sci.*, vol. 49, no. 4, pp. 1696–1701, Apr. 2007.

[69] X. C. Zhang, Y. K. Zhang, J. Z. Lu, F. Z. Xuan, Z. D. Wang, and S. T. Tu, “Improvement of fatigue life of Ti–6Al–4V alloy by laser shock peening,” *Mater. Sci. Eng. A*, vol. 527, no. 15, pp. 3411–3415, Jun. 2010.

[70] P. Peyre, X. Scherpereel, L. Berthe, C. Carboni, R. Fabbro, G. Béranger, and C. Lemaitre, “Surface modifications induced in 316L steel by laser peening and shot-peening. Influence on pitting corrosion resistance,” *Mater. Sci. Eng. A*, vol. 280, no. 2, pp. 294–302, Mar. 2000.

[71] J. Yang, F. Cui, and I. S. Lee, “Surface modifications of magnesium alloys for biomedical applications.,” *Ann. Biomed. Eng.*, vol. 39, no. 7, pp. 1857–71, Jul. 2011.

[72] M. Turski, S. Clitheroe, A. D. Evans, C. Rodopoulos, D. J. Hughes, and P. J. Withers, “Engineering the residual stress state and microstructure of stainless steel with mechanical surface treatments,” *Appl. Phys. A*, vol. 99, no. 3, pp. 549–556, May 2010.

[73] C. H. Caceres and P. Lukac, “Strain hardening behaviour and the Taylor factor of pure magnesium,” *Philos. Mag.*, vol. 88, no. 7, pp. 977–989, Mar. 2008.

[74] G. Soares and Y. Garbatov, “Reliability of maintained, corrosion protected plates subjected to non-linear corrosion and compressive loads,” *Mar. Struct.*, vol. 12, pp. 425–445, 1999.

[75] I. Yakimets, C. Richard, G. Béranger, and P. Peyre, “Laser peening processing effect on mechanical and tribological properties of rolling steel 100Cr6,” vol. 256, pp. 311–320, 2004.

[76] M. Salahshoor and Y. B. Guo, “Surface integrity of magnesium-calcium implants processed by synergistic dry cutting-finish burnishing,” *Procedia Eng.*, vol. 19, pp. 288–293, Jan. 2011.

[77] R. Walter and M. B. Kannan, “Influence of surface roughness on the corrosion behaviour

of magnesium alloy," *Mater. Des.*, vol. 32, no. 4, pp. 2350–2354, Apr. 2011.

[78] R. Fabbro, P. Peyre, L. Berthe, and X. Scherpereel, "Physics and applications of laser-shock processing," *J. Laser Appl.*, vol. 10, no. 6, p. 265, 1998.

[79] W. Zhang, Y. L. Yao, and I. C. Noyan, "Microscale Laser Shock Peening of Thin Films, Part 1: Experiment, Modeling and Simulation," *J. Manuf. Sci. Eng.*, vol. 126, no. 1, p. 10, 2004.

[80] Y. Cao and Y. C. Shin, "Shock Wave Propagation and Spallation Study in Laser Shock Peening," *J. Eng. Mater. Technol.*, vol. 132, no. 4, p. 041005, 2010.

[81] H. K. Amarchinta, R. V Grandhi, K. Langer, and D. S. Stargel, "Material model validation for laser shock peening process simulation," *Model. Simul. Mater. Sci. Eng.*, vol. 17, no. 1, p. 015010, Jan. 2009.

[82] D. Devaux, "Generation of shock waves by laser-induced plasma in confined geometry," *J. Appl. Phys.*, vol. 74, no. 4, p. 2268, 1993.

[83] R. H. Macneai and R. L. Harder, "A proposed standard set of problem to test Finite Element accuracy," *Finite Elem. Anal. Des.*, vol. 1, pp. 3–20, 1985.

[84] M. a Meyers, *Dynamic Behavio r aterials*. Wiley & Sons,Inc., 1994.

[85] N. Duc-Toan, P. Jin-Gee, and K. Young-Suk, "Combined kinematic/isotropic hardening behavior study for magnesium alloy sheets to predict ductile fracture of rotational incremental forming," *Int. J. Mater. Form.*, vol. 3, pp. 939–942, 2010.

[86] Q. Y. Hou and J. T. Wang, "A modified Johnson-Cook constitutive model for Mg-Gd-Y alloy extended to a wide range of temperatures," *Comput. Mater. Sci.*, vol. 50, no. 1, pp. 147–152, 2010.

[87] a. W. Warren, Y. B. Guo, and S. C. Chen, "Massive parallel laser shock peening: Simulation, analysis, and validation," *Int. J. Fatigue*, vol. 30, pp. 188–197, 2008.

[88] S. V. Razorenov, G. I. Kanel, K. Bamming, and H. J. Bluhm, "Hugoniot elastic limit and spall strength of aluminum and copper single crystals over a wide range of strain rates and temperatures," *AIP Conf. Proc. 620*, pp. 503–506, 2002.

[89] G. Tani, L. Orazi, A. Fortunato, A. Ascari, and G. Campana, "CIRP Annals - Manufacturing Technology Warm Laser Shock Peening : New developments and process optimization," vol. 60, pp. 219–222, 2011.

[90] G. Singh, R. V. Grandhi, and D. S. Stargel, "Modeling and Parameter Design of a Laser Shock Peening Process," *Int. J. Comput. Methods Eng. Sci. Mech.*, vol. 12, no. 5, pp. 233–253, Sep. 2011.

[91] K. Ding and L. Ye, "Simulation of multiple laser shock peening of a 35CD4 steel alloy," *J. Mater. Process. Technol.*, vol. 178, no. 1–3, pp. 162–169, Sep. 2006.

[92] C. S. Montross, T. Wei, L. Ye, G. Clark, and Y. Mai, "Laser shock processing and its effects on microstructure and properties of metal alloys : a review," vol. 24, no. 2002, pp. 1021–1036, 2006.

[93] F. Witte, J. Fischer, J. Nellesen, H.-A. Crostack, V. Kaese, A. Pisch, F. Beckmann, and H. Windhagen, "In vitro and in vivo corrosion measurements of magnesium alloys.," *Biomaterials*, vol. 27, no. 7, pp. 1013–8, Mar. 2006.

[94] N. Hfaiedh, P. Peyre, H. Song, I. Popa, V. Ji, and V. Vignal, "Finite Element analysis of Laser Shock Peening of 2050-T8 aluminum alloy," *Int. J. Fatigue*, vol. 70, pp. 480–489, 2014.

[95] M. Shukla, Y. Kashyap, P. S. Sarkar, A. Sinha, H. C. Pant, and R. S. Rao, "IF / P7-36 Laser Induced Shock Pressure Multiplication in Multi Layer Thin Foil Targets IF / P7-36," pp. 1–8.

[96] B. Han, C. Xu, J. Shi, and H. Song, "Numerical Simulation and Experimental of Residual Stress Field of SAE1070 Spring Steel Induced by Laster Shock," vol. 5, no. 20, pp. 4869–4877, 2013.

[97] L. Pompa, Z. U. Rahman, E. Munoz, and W. Haider, "Surface characterization and cytotoxicity response of biodegradable magnesium alloys," *Mater. Sci. Eng. C*, vol. 49, pp. 761–768, 2015.

[98] X. Lin, X. Yang, L. Tan, M. Li, X. Wang, Y. Zhang, K. Yang, Z. Hu, and J. Qiu, "In vitro degradation and biocompatibility of a strontium-containing micro-arc oxidation coating on the biodegradable ZK60 magnesium alloy," *Appl. Surf. Sci.*, vol. 288, pp. 718–726, 2014.

[99] and M. C. L. de O. Antunes, R. A., *"Effect of surface treatments on the fatigue life of magnesium and its alloys for biomedical applications." Surface Modification of Magnesium and Its Alloys for Biomedical Applications: Volume 1: Biological Intera*, vol. 1. 2015.

[100] X. D. Ren, J. J. Huang, W. F. Zhou, S. D. Xu, and F. F. Liu, "Surface nano-crystallization of AZ91D magnesium alloy induced by laser shock processing," *Mater. Des.*, vol. 86, pp. 421–426, 2015.

[101] X. Zhang, J. She, S. Li, S. Duan, Y. Zhou, X. Yu, R. Zheng, and B. Zhang, "Simulation on deforming progress and stress evolution during laser shock forming with finite element method," *J. Mater. Process. Technol.*, vol. 220, pp. 27–35, 2015.

[102] K. Y. Luo, T. Lin, F. Z. Dai, X. M. Luo, and J. Z. Lu, "Effects of overlapping rate on the uniformities of surface profile of LY2 Al alloy during massive laser shock peening impacts," *Surf. Coatings Technol.*, vol. 266, pp. 49–56, 2015.

[103] Z. Zhang, P. Lin, and L. Ren, "Wear resistance of AZ91D magnesium alloy processed by improved laser surface remelting," *Opt. Lasers Eng.*, vol. 55, pp. 237–242, 2014.

[104] E. Mg-ai-zn, "Magnesium alloys and applications," *Mater. Sci. Technol.*, vol. 10, no. January, pp. 1–16, 1994.

[105] K. J. Kubiak, M. C. T. Wilson, T. G. Mathia, and P. Carval, "Wettability versus roughness of engineering surfaces," *Wear*, vol. 271, no. 3–4, pp. 523–528, Jun. 2011.

[106] M. Taro, T. Chaise, and D. Nelias, "Modeling of ultra-high-speed impact at the surface of an elastic half-space," *Wave Motion*, vol. 58, pp. 77–100, 2015.

[107] C. Liang, C. Li, X. X. Lv, and J. An, "Correlation between friction-induced microstructural evolution, strain hardening in subsurface and tribological properties of AZ31 magnesium alloy," *Wear*, vol. 312, no. 1–2, pp. 29–39, 2014.

[108] K. L. Menzies and L. Jones, "The impact of contact angle on the biocompatibility of biomaterials.," *Optom. Vis. Sci.*, vol. 87, no. 6, pp. 387–99, Jun. 2010.

[109] K. J. Kubiak, T. G. Mathia, and M. C. T. Wilson, "Methodology for metrology of wettability versus roughness of engineering surfaces," *Proceeding 14th Int. Congr. Metrol. Paris 22-25*, no. June, 2009.

[110] F. Akbaripanah, F. Fereshteh-Saniee, R. Mahmudi, and H. K. Kim, "Microstructural homogeneity, texture, tensile and shear behavior of AM60 magnesium alloy produced by extrusion and equal channel angular pressing," *Mater. Des.*, vol. 43, pp. 31–39, Jan. 2013.

[111] S. Fukumoto, D. Yamamoto, T. Tomita, K. Okita, H. Tsubakino, and a. Yamamoto, "Effect of Post Weld Heat Treatment on Microstructures and Mechanical Properties of AZ31B Friction Welded Joint," *Mater. Trans.*, vol. 48, no. 1, pp. 44–52, 2007.

[112] K. Y. Luo, C. Y. Wang, Y. M. Li, M. Luo, S. Huang, X. J. Hua, and J. Z. Lu, "Effects of laser shock peening and groove spacing on the wear behavior of non-smooth surface fabricated by laser surface texturing," *Appl. Surf. Sci.*, vol. 313, pp. 600–606, Sep. 2014.